Coastal marsh stratigraphy as an indicator of past earthquakes, Puget Lowland, Washington State

Maria Elizabeth Martin

A dissertation
submitted in partial fulfillment of the
requirements for the degree of

Doctor of Philosophy

University of Washington

2011

Program Authorized to Offer Degree:
Earth and Space Sciences

University of Washington
Graduate School

This is to certify that I have examined this copy of a doctoral dissertation by

Maria Elizabeth Martin

and have found that it is complete and satisfactory in all respects,
and that any and all revisions required by the final
examining committee have been made.

Chair of the Supervisory Committee:

_____
Joanne Bourgeois

Reading Committee:

_____
Joanne Bourgeois

_____
Brian F. Atwater

_____
Charles A. Nittrouer

Date:_____

In presenting this dissertation in partial fulfillment of the requirements
for the doctoral degree at the University of Washington, I agree that the Library shall make its copies freely available for inspection. I further agree that extensive copying of the dissertation is allowable only for scholarly purposes, consistent with "fair use" as prescribed in the U.S. Copyright Law. Requests for copying or reproduction of this dissertation may be referred to ProQuest Information and Learning, 300 North Zeeb Road, Ann Arbor, MI 48106-1346, 1-800-521-0600, to whom the author has granted "the right to reproduce and sell (a) copies of the manuscript in microform and/or (b) printed copies of the manuscript made from microform."

Signature _____

Date _____

University of Washington

Abstract

Coastal marsh stratigraphy as an indicator of past earthquakes,
Puget Lowland, Washington State

Maria Elizabeth Martin

Chair of the Supervisory Committee:
Professor Joanne Bourgeois
Earth and Space Sciences

In coastal wetlands fringing Puget Sound lies evidence for large earthquakes 1,100 years ago and subsequent subsidence. This study uses sedimentologic, stratigraphic, and geomorphic tools, as well as tsunami modeling, to determine the impact of these earthquakes and attendant processes. In five shoreline locations along the shores of Puget Sound and Lake Sammamish, sandy deposits record Holocene earthquake events. These records, deposited by tsunamis, sand blows, and debris flows, look similar in many areas but are distinguishable using criteria developed in this study by comparing modern analogs to ancient examples. Accompanying evidence for liquefaction, tsunami, and debris flows are sharp stratigraphic facies changes interpreted as coseismic land-level change. Detailed studies at Gorst and the Skokomish delta reveal over 3 m and 1 m respectively of uplift about 1,100 years ago. At Gorst, land-level change preceded a tsunami and a sandy debris flow,

both of which left deposits in the wetlands surrounding Sinclair Inlet, an arm of Puget Sound. These events coincide with an AD 900-930 Seattle fault-zone earthquake. At the Skokomish delta, uplift accompanies evidence for liquefaction and unusual delta morphology. The delta is tilted toward its eastern side, where the Skokomish River channel has remained for at least the last thousand years. Deposition from the stable river mouth has resulted in an eastern intertidal mudflat 2-km wider than the western mudflat. At the Skokomish delta it remains unclear which fault is responsible for abrupt stratigraphic changes and for tilting, but the most likely candidate is the Saddle Mountain fault zone. However there is also a hypothesized fault underlying the delta, expressed by a ridge; in this study, the ridge is interpreted as a paleoshoreline. Both Gorst and the Skokomish delta have experienced at least 1.5 m of submergence since the time of uplift. Eustatic sea-level rise, regional subsidence and possibly subduction-zone earthquakes may be underlying causes of the submergence. The newly mapped paleoseismologic features formed 1,100 years ago and the documented more recent submergence have implications for mapping the extent and estimating the magnitude of earthquakes on shallow crustal faults in this densely populated region.

Table of Contents

List of Figures:

List of Tables

ACKNOWLEDGEMENTS

This project was funded by USGS-NEHRP Award *07HQGR0009*, graduate student support from the University of Washington Department of Earth and Space Sciences and an ExxonMobil student grant. The USGS-NEHRP grant was written by Annaleise Eipert, Joanne Bourgeois and Brian Atwater. The USGS supported radiocarbon dating.

Thank you to Elizabeth Nesbitt for help with the identification of the shells and Megan Dethier for the ecology of the shells, and Brian Sherrod, Cynthia Updegrave and Estella Leopold for their expertise and lab space for the plant macrofossils identification. Brian Sherrod was of great assistance in learning diatom identification and analysis. Kyle Mandli and Breanyn MacInnes were of great assistance with the model. Bill McKinney of Bremerton Public Works facilitated access to land along Gorst Creek. The Skokomish tribe granted me access to tribal lands on the delta. Theler Wetlands granted access the lands at Lynch Cove. Numerous other landowners gave me access to their lands and many, many people volunteered to make sure I did not end up stuck in the mud. A special thanks to Jody and Brian, you taught me so much.

Thank you to my friends and family.

CHAPTER 1

Introduction

1.1 MOTIVATION AND FINDINGS

Since the first documentation in the 1970's of active faults in the Puget Lowland (Figure 1.1) the region has received considerable paleoseismological attention. The Puget Lowland is home to several million people and to critical infrastructure such as ports and military bases. Understanding the seismic hazard to the region necessitates the study of primary and secondary effects of paleoearthquakes, because there have been no historical, large, shallow earthquakes in the Puget Lowland. This dissertation looks at the record for four fault ruptures about 1,100 years ago in order to understand the impact of earthquakes in the region. It also examines evidence of submergence in the Puget Lowland and the implications for sea-level rise and for interpreting the record of past earthquakes.

The problems investigated in this study are:
What is the sedimentary record of earthquakes' secondary effects, and how are the sedimentary processes distinguished based on their deposits? In what way do these earthquakes deform the landscape? And, How do the earthquake events of about 1,100 years ago fit in with the longer-term tectonic regime in the Puget Lowland?

The goal of this project was to determine and refine estimates of the impact of late Holocene earthquakes on the Puget Lowland. Specific objectives were:

- to compile working criteria for distinguishing between tsunami deposits and vented sediments, then to apply these criteria to sandy deposits in the Puget Lowland;

- to trace to the west and south the extent of the AD 900-930 Seattle fault-zone rupture and the evidence for tsunami;
- to use sedimentologic, stratigraphic and geomorphologic evidence to study peculiar geomorphic features of the Skokomish delta; and
- to quantify submergence in coastal wetlands in the Puget Lowland in the last 1,100 years.

Addressing these objectives, my main findings include:

- Prior work misinterpreted vented sediments in the Puget Lowland as tsunami deposits.
- There are several criteria to aid in the distinction between tsunami and vented sediment deposits, which I compiled and used in the Puget Lowland.
- At least 3 m of coeseismic uplift from the AD 900-930 Seattle fault zone earthquake occurred at Gorst -- farther west than previously documented.
- At least 1 m of coseismic uplift occurred on the Skokomish delta prior to AD 780-990; I hypothesize this deformation was generated by rupture of the Saddle Mountain fault zone.
- Widespread submergence on the scale of 1-2 m occurred in the Puget Lowland over the last 1,100 years.

1.2 FIELD AREAS

This study focused on five main field sites in the Puget Lowland (Figure 1.1). Four of these sites, the Skokomish delta, Lynch Cove, Gorst, and the Snohomish delta are coastal wetlands. Issaquah Creek is a freshwater tributary of Lake Sammamish. Many of these areas

have been heavily modified by human activities. However, where undisturbed, these wetlands provide intriguing windows into the earthquake history of the Puget Lowland. While exploring several of sites, Chapter 2 focuses on Lynch Cove at the terminus of Hood Canal. Chapter 3 focuses on pocket coastal wetlands at Gorst and traces deposits upstream along Gorst Creek. Chapter 4 focuses on the Skokomish delta at the elbow of Hood Canal (Figure 1.1).

1.3 SYNOPSIS OF CHAPTERS

Chapter 2. In order to study past earthquakes' effects in the Puget Lowland, I needed to establish criteria for distinguishing between the most common sandy event layers encountered in the Lowland--tsunami deposits and vented sediment. In this chapter I use the application of modern analogs and understanding of depositional processes to determine characteristics useful in differentiating between tsunami deposits and vented sediments. Chapter 2 also includes a published-literature review of common characteristics of vented sediment and tsunami deposits. These characteristics then are used to identify paleo- "event deposits" in the Puget Lowland. Finally, I discuss the criteria identified as most useful to distinguish between vented sediment and tsunami deposits in the Puget Lowland environment.

Chapter 3. In my study of vented sediments and tsunami deposits, I found several locations with other indicators of past seismicity. Gorst is one such site. Chapter 3 discusses the effects of the AD 900-930 Seattle fault earthquake on the area surrounding the terminus of Sinclair Inlet. This chapter quantifies coseismic land-level change and identifies and analyzes deposits of tsunami and debris flows. I use modeling of tsunamis generated by the

AD 900-930 Seattle fault zone and by the Tacoma fault zone to determine the source and magnitude of the tsunami that generated the deposit in Gorst. I also examine and quantify post-earthquake submergence.

Chapter 4. Another site that shows intriguing coseismic uplift and deformation is the Skokomish delta. At the Skokomish delta I use stratigraphic, diatom, and geomorphic analysis to shed light on the relationship between uplift, submergence, and river migration patterns. I specifically examine the origin of strange geomorphic features including an eastward slope and a ridge that cuts the delta. Here I also quantify coseismic uplift, including likely tilting, and later submergence.

Chapter 5. Chapter 5 summarizes prior chapters and discusses the implications of this study for natural-hazards research and mitigation. In this chapter I also look at unanswered questions and areas for future work.

1.4 IMPORTANCE

First and foremost, the goal of this study is to assess the hazard posed by large crustal earthquakes in the Puget Lowland. Several million people, two large ports, two military shipyards and extensive coastal infrastructure in the Puget Lowland could be devastated by earthquakes and attendant events such as landslides and tsunamis. Understanding past events will aid in the mitigation of and planning for future earthquake events, thereby protecting the socio-economic livelihood of the Puget Lowland.

This study addresses the following critical needs: 1) to differentiate tsunami and vented sediment deposits to better assess the frequency and magnitude of earthquakes and their associated natural hazards, 2) to document and to understand the effects of past

earthquakes in the Puget Lowland, and 3) to quantify the late Holocene rate of submergence in the Puget Lowland.

Many shallow faults display evidence of Holocene rupture in the Puget Lowland, but no large crustal earthquakes have occurred in the region during historical times (Ludwin et al., 1991). However, geologists have uncovered conclusive evidence of large, shallow earthquakes about 1,100 years before present in this region. This evidence is particularly well displayed in tidal wetlands and deltas (Atwater and Moore, 1992; Bucknam et al., 1992; Bourgeois and Johnson, 2001; Sherrod et al., 2001; Sherrod et al., 2004).

This study establishes methodology to aid in distinguishing between tsunami deposits and vented-sediment deposits. Tsunamis are impulse-generated waves with the potential of both eroding and depositing sediment along coastlines. Vented sediments are fluidized sediments erupted onto a free surface. The deposits of sediment venting and tsunamis can appear very similar in the geological record, and the distinction between the two has been largely ignored in the published literature. This distinction is imperative because tsunami deposits and vented sediments have different implications for hazard mitigation and planning.

In areas such as the Puget Lowland where a potential for large earthquakes threatens but no historical events have occurred, paleoseismology is an important tool in mitigating the damages of future earthquakes. This dissertation builds on past paleoseismic studies in the Puget Lowland for a more comprehensive understanding of recent fault ruptures throughout the Lowland. This information is applicable to establishing hazard planning both for the communities in the vicinity of these studies and for the larger understanding of Holocene tectonics in the Puget Lowland.

1.5 GEOLOGICAL AND TECTONIC SETTING

Active tectonics and an ample sediment supply make the Puget Lowland an environment conducive to the study of sedimentary paleoseismology. Active faults cut across the Puget Lowland, and rupture on these faults can generate relative land-level change (Bucknam et al., 1992; Sherrod et al., 2004), tsunamis (Atwater and Moore, 1992; Bourgeois and Johnson, 2001), landslides (Karlin and Abella, 1992), and vented sediments (Bourgeois and Johnson, 2001; Sherrod et al., 2004; Kramer, 2010).

Pleistocene glaciation of the Puget Lowland produced large-scale sedimentation leading to geological hazards including slope failure, liquefaction, and tsunamis. The Puget Lowland is a glacially modified forearc basin between the Olympic Mountains to the west and Cascade Mountains to the east (Figure 1.1). The last glaciation, the Fraser glaciation, reached its peak in the Vashon stade ~15 ka (Booth, 1994) during which the Puget lobe of a continental ice sheet covered much of the Puget Lowland. After retreat of the Puget lobe, isostatic rebound occurred, ~100 m near Bellingham and less to the south where the ice sheet was thinner (Thorson, 1989). In the Puget Lowland land-level change due to isostatic rebound is thought to have been completed by ~8,000 years ago (Thorson, 1989). However, there is evidence of local changes in relative sea level since that time, more likely driven by tectonic processes, including co-seismic deformation.

Estimations of long-term land-level change in the Puget Lowland vary from ~2 mm/y uplift to 1 mm/yr submergence in different locations (Eronen et al., 1987; Holdahl, 1989; Beale, 1990; Verdonck, 2006). Values based on different methods have different results though there appears to be a trend of greater submergence in the south than in the north.

Understanding these rates is key to understanding the dynamics of the forearc basin and to predicting relative sea-level rise.

Associated with the Fraser glaciation are till, advance and outwash sediments, and lake deposits. These unconsolidated sediments drape much of the lowland and generate secondary hazards such as landslides and liquefaction (Kramer, 2009). For example, the 1949 Olympia earthquake was associated with a large landslide of glacial sediments, which in turn generated a 2 m tsunami (Chleborad, 1994). Also, liquefaction and venting sediments accompanied the 2001 Nisqually earthquake (Highland, 2003).

About 1,100 years ago, ruptures on four faults in the Puget Lowland and on the Cascadia subduction zone induced land-level change and strong shaking. The best studied of these earthquakes, estimated to be of magnitude 7+ (ten Brink et al., 2006), generated widespread uplift of up to 7 m along the Seattle fault zone (Bucknam et al., 1992; Ota et al., 2006). The Tacoma fault zone (Sherrod et al., 2004), the Saddle Mountain fault zone (Witter et al., 2008; Blakely et al., 2009), and Olympia fault zone (Sherrod, 2001) also show evidence for rupture about 1,100 years ago (Figure 1.1). These events generated liquefaction, at least one tsunami, and slope failures across the Puget Lowland.

While some of the sandy event deposits in the Puget Lowland represent local crustal earthquakes, some more likely represent other earthquake sources. In addition to shallow earthquakes, the Puget Lowland is subject to the effects of earthquakes from two other sources--the shallow Cascadia subduction zone and the deep Benioff zone (Atwater, 1987; Ludwin et al., 1991; Figure 1.1). For example, tsunami deposits near Admiralty Inlet are most likely from subduction-zone tsunamis and possibly from local faulting or landslides (Williams et al., 2000; Williams and Hutchinson, 2005; Figure 1.1). For the case of vented

sediments, it is more difficult to differentiate the location of the triggering mechanism unless the vented sediment is associated with other evidence of local faulting such as land-level change, because subduction and Benioff-zone earthquakes (Figure 1.1) can also induce liquefaction in the Puget Lowland (Frankel et al., 2002; Kramer, 2009).

1.6 PALEOSEISMIC INDICATORS

Coastal regions are ideal settings to study paleoseismology because seismic activity leaves behind a variety of geologic features that can be recorded there. The stratigraphy of marshes can record effects of earthquakes including strong shaking and land-level change. Land-level change generates change in relative sea level, which is recorded in marsh stratigraphy by facies change. Disturbances to the sea bottom or to lake floors as well as landsliding into water bodies can generate tsunamis that may both erode and leave sedimentary deposits in low-lying areas (Gelfenbaum and Jaffe, 1998; MacInnes et al., 2009). Cyclic seismic loading of saturated sediment can induce liquefaction and create a variety of liquefaction features including sand blows and injected dikes and sills (Obermeier, 1996). Shaking-induced slope failures can create a variety of deposits including rock falls, debris flows (Varnes, 1978), and also deposits resulting from the landslide-damming of streams.

Changes in stress and movement on a fault during rupture and also during the inter-seismic period can induce changes in land elevation relative to sea level. For example, uplift can strand wave-cut marine platforms creating marine terraces (Lajoie, 1986; Bucknam, et al., 1992). Also, salt-marsh environments are highly sensitive to relative sea level therefore land-level change can be recorded stratigraphically by changes in the assemblages of macro-

and microfossils. In the geological record, these changes when co-seismic are typically preserved as sharp stratigraphic changes in facies. This change can be lithologic—a change in grain size, e.g., or ecologic—a change in the assemblages of macro and/or microfossils. A variety of studies of relative sea-level change in the Puget Lowland have established vegetation and diatom zonations corresponding to various elevations relative to sea level (Bucknam et al., 1992; Sherrod, 1999).

Decades of research have established tsunami deposits as useful paleoseismological tools (Bourgeois, 2009). Tsunamis are long-period, shallow-water wave trains generated by an impulse, typically an undersea earthquake but also landslides, volcanic eruptions and bolide impacts. Tsunami deposits can consist of a variety of grain sizes from clay to boulders of which the most commonly studied deposits are sand layers. Though no specific criterion for distinguishing a tsunami deposit exists, in general the deposits thin and fine landward, are massive to upward fining, and contain evidence of being out of place, such as marine diatoms in a freshwater environment (e.g. Dawson and Shi, 2001). Because tsunami deposits indicate tsunami generation by a disturbance of the water column, the source of the tsunami can be indicated by mapping the distribution of deposits along a coastline, in association with modeling (Martin et al., 2008; MacInnes et al., 2010). In the Puget Lowland, Atwater and Moore (1992) gathered evidence for a about 1,100-year-old tsunami linked to the Seattle fault zone rupture. Bourgeois and Johnson (2001) linked evidence for a tsunami at the Snohomish delta to this event.

Strong shaking can generate liquefaction and sediment fluidization. In an earthquake, cyclic loading from seismic waves causes buildup of pore-water pressure in confined, saturated sediments, leading to the collapse of grain framework and flow of pore water (Seed,

1979). Liquefaction and fluidization features can present as a complex system of injected dikes and sills, as vented sediment onto a free surface, and as sediment-filled lateral-spreading cracks open to the surface (Audemard and Santis, 1991; Obermeier, 1996; Tuttle and Schweig, 1996). Sediment deposited within cracks forms dikes and sills, and erupted sediment deposited on the ground surface forms sand blows (Sims and Garvin, 1995; Obermeier, 1996; Tuttle and Schweig, 1996). Liquefaction features can be used to determine the minimum size and recurrence of large earthquakes (e.g., Tuttle et al., 1999; Obermeier and Dickenson, 2000; Castilla and Audemard, 2007). In the Puget Lowland, liquefaction has occurred during several historical earthquakes (Kramer, 2008), and paleoliquefaction features are reported from Burley, the Nisqually and Snohomish deltas, and several other locations (Sherrod et al., 2004; Barnhart and Sherrod, 2006; Bourgeois and Johnson, 2001).

Slope failures can occur in a variety of manners depending on lithology, slope, water content of rock or soil, and strength of initiator. Slope failures are classified based on the type of material involved and the way the material moves (Varnes, 1978). The distribution of temporally correlated landslides can be used to determine the source region for a paleoearthquake (Nikonov, 1988; Tibaldi et al., 1995). In the Puget Lowland synchronous dates for landslides on the Olympic Peninsula, including landslide-dammed lakes, are used to indicate a large earthquake about 1,100 years ago (Schuster et al., 1992). Landslides also dating to about 1,100 years ago are found in Lake Washington and Lake Sammamish (Jacoby et al., 1992; Logan et al., 1998).

In all of these cases careful consideration must be made to determine which of the processes occurred because they have different implications for understanding

paleoearthquakes and hazard analysis. Also, other processes not associated with earthquakes must be ruled as less likely.

1.7 SIGNIFICANCE OF DISSERTATION CONTRIBUTIONS

This dissertation uses a variety of methods to try to understand the story of Puget Lowland tectonics. By using sedimentology, stratigraphy, paleontology, geomorphology, and numerical modeling I am able to create a picture both of the events that occurred during fault ruptures 1,100 years ago and of submergence in the subsequent millennium. This work has implications both for understanding the fault structure underlying the Puget Lowland, and for hazard planning in the region.

The interpretation of tsunami- and vented-sediment deposits is imperative for interpreting seismic hazard. However, there have not been any previous studies detailing the differences and similarities. Chapter 2 examines in detail the sedimentological characteristics of well-exposed examples of tsunami deposits and vented-sediment structures in the Puget Lowland, and also reviews modern examples of vented sediments and tsunami deposits. Thus the study has broad applications for sedimentary paleoseismological studies both in other regions of the world and in the longer geological record.

Understanding the zone of deformation of past earthquakes facilitates the prediction of damages from future events. In chapter 3 and 4, I quantify uplift in two locations 8-10 km from the faults most likely to have generated the uplift. In chapter 3 the >3 m of uplift at Gorst in the AD 900-930 Seattle fault-zone earthquake doubles uplift predicted by previous fault models. This greater uplift indicates the structure of the Seattle fault zone or the slip distribution during the AD 900-930 earthquake may be different than previously

hypothesized. Fault structure and slip have implications for locations of strong shaking and tsunami generation and therefore are important for hazard mitigation. In chapter 4, I highlight differential uplift on the Skokomish delta. The uplift was likely generated by an AD 650-1050 earthquake on the Saddle Mountain fault zone. The variable uplift on the Skokomish delta may help indicate the underlying structure of the Saddle Mountain fault zone.

The implications of long-term submergence rates stretch from interpretations of coseismic deformation to projections of sea-level rise. Submergence as interpreted in chapter 3 and 4 from the stratigraphy indicates widespread land-level change in the southern Puget Lowland in the last 1,100 years. It is uncertain at this point if the submergence occurs relatively steadily or sporadically. This submergence indicates that marine terraces generated by uplift during the AD 900-930 Seattle fault zone earthquake may have been 1.5 m higher than their current elevation, and this increase would have implications for reconstructing the subsurface geometry of the fault zone. In addition, understanding the background rate of submergence is important for predicting rates of and planning for eustatic sea-level rise. The effects of submergence exacerbate the impacts of sea-level rise locally, so understanding and quantifying the rates lead to more effective hazard planning and mitigation.

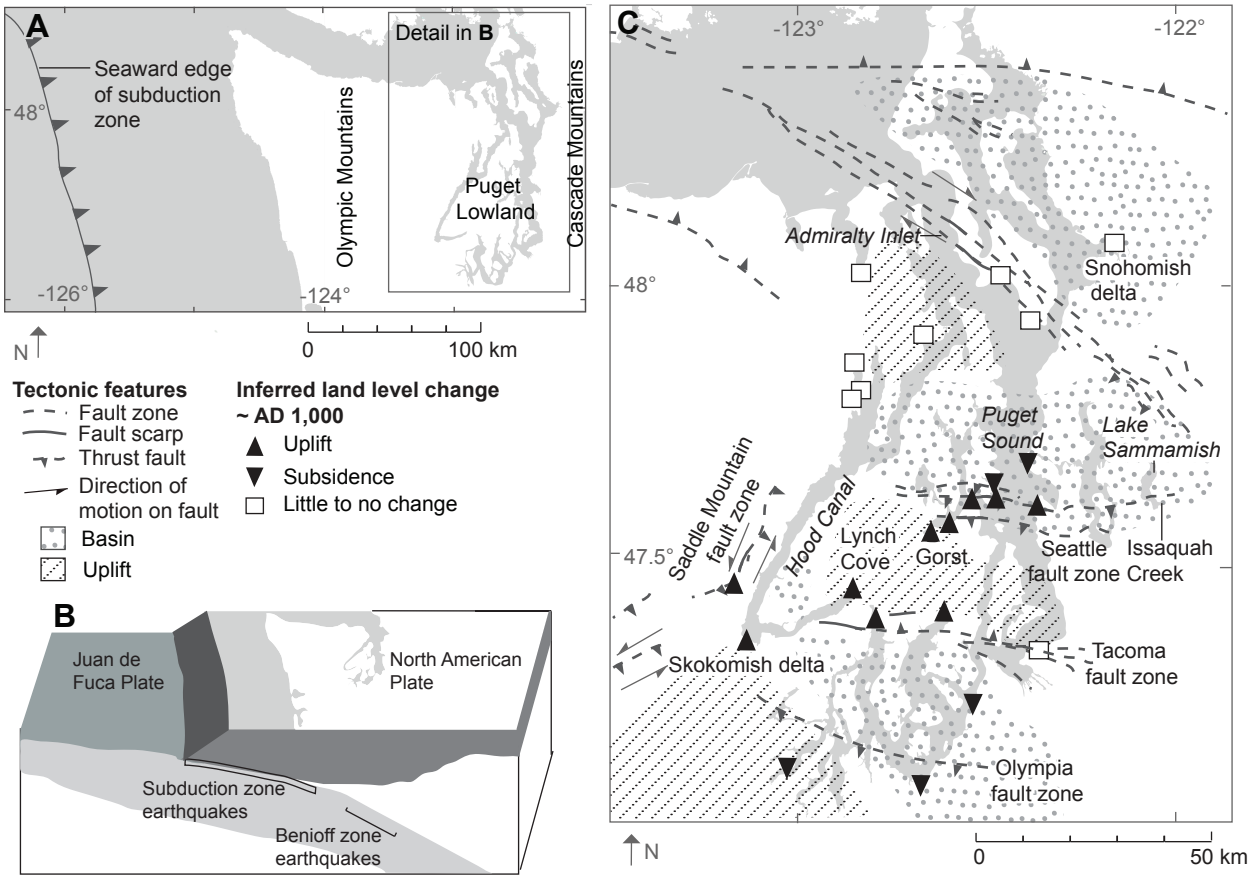

Figure 1.1 The tectonic setting of the Puget Lowland and crustal fault locations. A. Map of Cascadia subduction zone and coastline. B. Cartoon of the Cascadia subduction zone showing locations of subduction zone and Benioff zone earthquakes. C. Map of the Puget Lowland showing active faults and locations of paleoseismic studies. Modified from Blakely et al., 2009. Land level change information from Eronen et al., 1987; Beale, 1990; Bucknam et al., 1992; Sherrod, 2001; Bourgeois and Johnson, 2002; Blakely et al., 2009; Brian Sherrod, personal communication.

CHAPTER 2

Vented sediments and tsunami deposits in the Puget Lowland, Washington-- differentiating sedimentary processes

Disclaimer: This chapter was prepared as a manuscript submitted to the journal *Sedimentology*, currently accepted pending revision. The manuscript is co-authored with Joanne Bourgeois. She is responsible for most of the observations on the Snohomish delta. Joanne Bourgeois originally drafted figure 2.5. The remainder of the new work herein was accomplished by M.E. Martin as part of this dissertation project.

2.1 INTRODUCTION

In tsunami-susceptible coastal settings, not all sandy layers are tsunami deposits. Both tsunamis and sediment venting can occur in low-lying coastal areas, as can storms, floods, landslides, and debris flows, each with the potential to leave behind an "event deposit." Many of these processes can be earthquake-induced, and multiple depositional processes may occur in any location. This study in the Puget Lowland, the low region between the Olympic and Cascade Mountains in Washington State, demonstrates that vented-sediment deposits (known as *sand-blow* deposits when induced by seismic loading and *sand-boil* deposits when induced by other means of liquefaction) share many sedimentary characteristics with tsunami deposits, leading in some cases to the misinterpretation of vented sediments as tsunami deposits and potentially the reverse.

The underlying purpose of this study is to differentiate vented sediments from tsunami deposits in the Puget Lowland in order to expand understanding of

paleoearthquake(s) there about 1,100 years ago. In the process, we have developed some insights into general means for distinguishing the two deposits. Our approach has been to compare the sedimentary characteristics of known tsunami and vented-sediment deposits in the region and elsewhere, to develop depositional models for both types of deposits, and to apply lessons learned in order to identify and interpret these deposits. We studied deposits in five coastal marshes and swamps of the Puget Lowlands (Figure 2.1). In three of these locations--the Skokomish delta, Lynch Cove, and Gorst--the deposits are associated with evidence of coseismic land-level change. In two others--Issaquah Creek and the Snohomish delta--the mode of deposition indicates probable seismic origins though they are not noticeably associated with tectonic land-level change.

This study focuses in particular on a sandy deposit in the marsh at Lynch Cove previously identified primarily as a tsunami deposit (Hemphill-Haley, 1996; Jovanelly and Moore, 2009). We chose Lynch Cove as an area for detailed study because widespread outcrops allowed documentation of details in sedimentary characteristics of the deposit, and because our interpretation of the deposit as being generated solely by sediment venting (no tsunami evidence) counters previous work at this location.

2.1.1 Importance to hazard analysis

Liquefaction features and tsunami deposits indicate different hazards associated with earthquakes, so their distinction is important. For example, when found in only one location, liquefaction features indicate strong shaking, but not earthquake location or depth (e.g. Obermeier, 1996; Castilla and Audemard, 2007), whereas tsunami deposits indicate displacement of the water column (such as from a shallow earthquake or landslide) but not the source mechanism or location of displacement (e.g. Dawson and Shi, 2000; Bourgeois,

2009). When correlative tsunami or vented-sediment deposits are found across a wider geographic region, more information can gleaned about the source location especially when compared with historical events (e.g. Bourgeois et al., 2006; Tuttle, 2001).

In a variety of environments, tsunami deposits have been used to determine the size and recurrence of large earthquakes (e.g., Cisternas et al., 2005; Bourgeois et al., 2006; Jankaew et al., 2008; Sawai et al., 2009). In turn, the recurrence interval of tsunami deposits can be used to estimate earthquake and tsunami frequency and hazards for a region (Dawson et al., 2003; Geist and Parsons, 2006). Also, a minimum estimation of the size of a tsunami wave can be made from the elevation at farthest extent inland of a tsunami deposit. Then researchers using tsunami models can apply estimates of the size of the wave along a coast to test hypotheses about the source of the tsunami (Martin et al., 2008; MacInnes et al., 2010). However, these analyses are only effective if deposits are indeed of tsunami origin. If other types of coastal deposits are misidentified as tsunami deposits, tsunami frequency and thus hazard will be overstated. And if the extent of a tsunami deposit is mis-mapped by including vented sediment farther inland or at higher elevation, tsunami size will be overestimated.

Liquefaction features also have been used to determine the minimum size and recurrence of large earthquakes (e.g., Tuttle et al., 1999; Obermeier and Dickenson, 2000; Castilla and Audemard, 2007). Liquefaction features indicate a minimum amount of shaking a location experienced. When multiple episodes of sand blows are in the same stratigraphic sequence they can be used to estimate earthquake recurrence (Obermeier, 1996; Tuttle et al., 2002).

2.2 CHARACTERISTICS OF TSUNAMI DEPOSITS AND VENTED SEDIMENTS

The majority of recent work differentiating event beds in coastal environments has focused on distinguishing tsunami deposits from storm deposits (e.g. Goff et al., 2004; Tuttle et al., 2004; Switzer, et al., 2005; Morton et al., 2007; Komatsubura et al., 2008). Deposits from earthquake-linked processes other than tsunamis, however, have been treated in much less detail. Here we review the basics of tsunamis and sediment venting, and the resulting deposits.

2.2.1 Depositional processes

Tsunamis are long-period waves that both erode and deposit sediment on coastlines. Though tsunamis have several different initiators, the waves behave similarly. Tsunamis are impulse-driven, surface gravity waves generated by earthquakes, landslides, volcanic eruptions and bolide impacts. By disrupting the water column, these initiators typically generate a series of long-period (5-120 minutes) waves (Murty, 1977). This wave train can lead to multiple inundations of a coastal area, and as each wave comes onshore it erodes while accelerating and deposits while decelerating (e.g., Gelfenbaum and Jaffe, 2003). Different phases of tsunami flow can result in deposition, including slowing of flow, reversing of flow, and gravity-driven outflow (Paris et al., 2007).

Seismic or other types of loading can induce liquefaction and sediment fluidization (Lowe, 1975; Seed and Idriss, 1982). In an earthquake, cyclic loading from seismic waves causes buildup of pore-water pressure in confined, saturated sediments leading to the collapse of grain framework (*liquefaction*) and flow of pore water (Seed, 1979). In some cases, sediments are transported by entrainment in expelled pore water (*fluidization*), the

water typically flowing upward (down the pressure gradient), creating or exploiting cracks and in some cases erupting to the surface, forming fountains up to several meters high (Obermeier, 1996). In addition to earthquake-induced liquefaction, intergranular fluid flows can generate sediment fluidization, and the fluid may come from a layer other than the sediment layer that is fluidized. For example, the geometry of, and strain within, aquifers can change during earthquakes, potentially forcing water flow; this fluid can then entrain grains from other sedimentary layers (Wood et al., 1985). Also, artesian flow can generate fluidization (Holzer and Clark, 1993).

2.2.2 Depositional characteristics

While there is no single defining characteristic of tsunami deposits, many have characteristics in common. High-energy flow and grains falling out of suspension typically dominate tsunami deposition on a coastal plain, and suspended-load sedimentation leads to massive, planar-laminated, or fining-upward deposits (Bourgeois, 2009). Tsunami deposits are often described as thin (typically less than 25 cm thick), sheet-like, and thickening into depressions (Morton et al., 2007). Deposits can extend multiple kilometers inland (e.g. Paris et al., 2007) especially along rivers (Pinegina et al., 2003). The grains within deposits typically fine landward and upward (e.g. Dawson and Shi, 2000; Tuttle et al., 2004; Morton et al., 2007).

Tsunami deposits can contain sedimentary structures including laminae (Reinhart, 1991), rip-up clasts (Gelfenbaum and Jaffe, 2003), cross-stratification (Choowong et al., 2008), and soft-sediment deformation (Matsumoto et al., 2008). Muddy laminae or organic layers can represent evidence for multiple waves of the tsunami wave train (Reinhart, 1991; Bondevik et al., 2003). Sediment size can vary from mud to boulders; in many cases, grain-

size variation in tsunami deposits is controlled by the size of sediment available for transport, rather than by flow capacity (Bourgeois, 2009).

Liquefaction and fluidization features can present as a complex system of injected dikes and sills, as vented sediment onto a free surface, and as sediment-filled lateral-spreading cracks open to the surface (Audemard and Santis, 1991; Obermeier, 1996; Tuttle and Schweig, 1996). Fluidized sediment deposited within cracks forms dikes and sills, and erupted sediment deposited on the ground surface forms sand blows (Sims and Garvin, 1995; Obermeier, 1996; Tuttle and Schweig, 1996). Sediment dikes can extend more than ten vertical meters in the terrestrial environment (Obermeier, 1996) and hundreds of meters in the marine environment (Cartwright et al., 2008). Cracks can form above liquefied sediment layers, with spacing and width related to cap thickness and proximity to slopes or stream banks (Obermeier, 1996).

Our study focuses on deposits of sediment venting because these features emerge onto a surface and thus share some characteristics with tsunami deposits. Vented sediments typically form dome-like morphologic structures or coalesced domes above and along a crack or fissure (Audemard and Santis, 1991; Obermeier, 1996). In some areas where these structures are closely spaced or very large, they can run together, forming complex, interfingering deposits (Sims and Garvin, 1995). Discontinuous vented sediments in the New Madrid seismic zone vary in thickness from over a meter to zero, are present over several square kilometers, and are detectable in aerial photographs (Obermeier, 1989; Tuttle, 1999). In recent events such as the M 7.1 Loma Prieta earthquake and aftershocks (Sims and Garvin, 1995) and the 1988 M 5.8 Saguenay, Quebec earthquake (Tuttle et al., 1990), sand blows were generally less than 30 cm thick.

Vented sediments can contain sedimentary structures including intraclasts, laminae, soft-sediment deformation, and fluid-escape features (e.g. Lowe, 1975; Audemard and Santis, 1991; Tuttle, 1999). Vented sediments typically consist of coarse silt to pebbles and fine upward and away from the vent or injected dike (Tuttle, 1999). Intraclasts tend to be larger and in higher concentration closer to dikes (Obermeier, 1996). Laminae or organic layers can indicate time lapse, possibly pointing to multiple episodes of liquefaction during a sequence of earthquakes or aftershocks over months or years (Saucier, 1989; Tuttle et al., 2002) or to multiple phases of increased pore pressure (Sims and Garvin, 1995).

2.2.3 Comparison of tsunami deposits and vented sediments

We have found only a few studies that have examined both tsunami deposits and vented sediments in the same environment (Atwater, 1992; Bourgeois and Johnson, 2001; de Martini et al., 2003). In these case studies with both tsunami deposits and vented sediments present, sedimentary dikes were an important clue for the presence of vented sediments.

Some sedimentary characteristics are better than others for distinguishing between vented sediments and tsunami deposits. We found no single characteristic could distinguish between tsunami deposits and vented sediments, though multiple characteristics can help distinguish between the two. Where possible we used surveys of modern events in similar environments (coastal and terrestrial) to the Puget Lowland and of comparable earthquake magnitudes (M 7-7.5) to postulated paleo-events studied in the Puget Lowland.

The distinguishing criteria we have compiled, from most to least useful, are summarized below.

Map-scale architecture

On a map scale, tsunami deposits are more widespread and show less variation in thickness than vented sediments (Figure 2.2). Because tsunamis affect large areas with similar hydraulic conditions, widespread consistencies in structure are to be expected. For example, tsunami deposits tend to fine and thin landward (e.g. Dawson and Shi, 2000; Tuttle et al., 2004; Morton et al., 2007). In contrast, during sediment venting, different sedimentary dikes may be sourcing different layers and may flow for different durations. Also, sediment from different dikes can interfinger or mix, creating potentially much more variable structures across a field location. The distribution of vented-sediment deposits depends on the location of sediments that liquefy and on the fluidized sediment reaching the surface (Tuttle, 1999). Facilitated flow along cracks and lateral spreads can lead to clumped and linear zones of deposition (Sims and Garvin, 1995).

Outcrop-scale morphology

At outcrop scale (1-10 horizontal meters), tsunami deposits are less variable in thickness and internal sedimentary structure than vented-sediment deposits. Over this scale, tsunami deposits maintain consistent thickness unless there is underlying topographic variation to fill; that is, the top of a tsunami deposit will tend to be flat. The thickness of vented sediments, however, can be highly variable on this scale, and vented sediments tend to create positive, dome- or cone-like structures (Obermeier, 1996). In the particular cases where tsunamis transport sediment as bedload and generate positive-relief bed forms (e.g. Choowong et al., 2006), it is important to use observation to distinguish these regularly spaced and oriented features from vented sediments.

Presence of feeder dikes

Injected dikes connected to a sediment unit deposited at the surface indicate sediment venting, but the mere presence of sediment-filled cracks and cavities is not a reliable criterion because earthquakes trigger both sand venting and tsunamis. Also, while injected dikes and sills are indicators of fluidized sediment and potential liquefaction, care should be taken in distinguishing injected dikes from passively filled cracks and spreads. Tsunamis can deposit sediment into cracks, lateral spreads and burrows (e.g., Higman and Bourgeois, 2008) creating vertical, sediment-filled structures resembling injected dikes. Fluidized sediment often exploits cracks and burrows on its path to the surface (Audemard and Santis, 1991). Injected and filled dikes can be difficult to distinguish (Aspler and Donaldson, 1985). However, injected dikes are more likely to have laminae parallel to dike walls, to bifurcate upward and to be associated with sills (Aspler and Donaldson, 1985).

Thickness and thickness variability

Even in large tsunamis such as the 2004 Indian Ocean tsunami in Sumatra and Thailand, tsunami deposits average less than 25 cm thick, whereas vented sediment deposits are on average much thicker (Figure 2.3). Though tsunami deposits may be greater than 25 cm thick near the shoreline, they usually thin landward and are typically less than 25 cm thick (Morton et al., 2007). However, smaller earthquakes and earthquakes in areas less prone to liquefaction can generate sand blows of the same average thickness as a tsunami (Tuttle et al., 1990; Audemard and Santis, 1991; Sims and Garvin, 1995). Therefore, while a thin deposit may not be a defining characteristic of the tsunami case, a deposit that is on average greater than 25 cm thick (on an outcrop scale, <10 m) may indicate sediment venting.

Grain size

Tsunamis have the potential to deposit larger grains than sediment venting, but the grain size in a deposit is not only a factor of the energy available to transport the grains but also of the sediments available to be moved. Therefore, if only sand and silt are available in the environment available for transport, only those grain-size classes will be deposited. Along a depositional surface, tsunamis are typically higher energy than the flow from fluid-sediment expulsion and have the potential to transport larger grains up to boulders, such large clasts also being more readily available to a tsunami. Nevertheless, the majority of described tsunami deposits are sandy (Bourgeois, 2009), and vented sediments typically consist of sand but can contain grain sizes from silt to pebbles (Obermeier, 1996).

Location of deposit

Tsunami deposits are tied to coastlines, and vented sediments are tied to earthquake shaking combined with settings susceptible to liquefaction. Thus tsunamis can create deposits on distant shores, far from the earthquake source, but rarely more than a few kilometers inland from a coastline, and usually much less (Bourgeois, 2009). Seismically induced liquefaction typically occurs close to the rupture zone, typically less than 200 km for a M 7.5 earthquake (Wang et al., 2006), and vented sediments are not tied to the coastline. However, coastal settings such as deltas are particularly susceptible to liquefaction, and thus coastal wetlands close to shallow faults can be expected to exhibit deposits from both tsunamis and sediment venting.

Erosional base

Tsunamis have more potential to erode and do so at a larger scale than venting sediments. Tsunami inundation and outflow can generate small-scale erosion around

structures and in zones of weak soil as well as large-scale erosion of landforms such as beach ridges (e.g. MacInnes et al., 2009). During sediment venting and the formation of sand-blow craters, only laterally small-scale (<1 m) erosion of land surfaces occurs, typically centered on a vent (Tuttle et al., 2002).

Thickening into depressions

Deposits of both tsunamis and sediment venting can be thicker in depressions, but tsunami deposits tend to drape and fill topography whereas vented sediments can create new topography. Tsunami deposits are often thicker in low-lying areas (Bourgeois et al., 2006; Jankaew, 2008), but the same may be said of vented-sediment deposits. The process of venting sediments originates with expulsion of water and fluidized sediment from the subsurface, and thus can result in local subsidence of tens of centimeters (Tuttle, 1999; Clague et al., 1992). Because the greatest amount of subsidence and sedimentation typically occurs near the vent, the deposit is often thickest in these depressions. The difference between tsunami infill and vented-sediment infill is that in the case of venting the depression is created as it is being filled.

Marine microfossils

Marine and brackish microfossils are common in tsunami deposits but also can be present in vented sediments. In tsunami deposits the presence of salt-tolerant microfossils indicates the marine origin of sediments and water (Dawson et al., 1996; Hemphill-Haley, 1996). In vented sediments, microfossils can indicate either marine origin of the sediment that fluidized or marine origin of strata the fluidized sediment passed through. In the latter case, diatoms can be ripped from dike walls and mixed into the fluidized sediment during the breakdown of intraclasts.

Association with land-level change

Both tsunamis and sediment venting can be associated with coseismic land-level change (Walsh et al., 1995; Cisternas et al., 2005). Earthquake-driven cyclic loading can trigger liquefaction in saturated, confined sediments, and tectonic displacement of the seafloor can generate tsunamis. The process of venting can also generate local subsidence, as can earthquake-induced compaction, which on a map scale will be less regular than co-seismic subsidence.

Intraclasts

An accelerating tsunami can rip clasts from any exposed surface; sediment venting typically tears material from dike walls or from the vent mouth**.** In general, then, intraclasts in vented sediments can come from a deeper stratigraphic source than in tsunami deposits. Intraclasts in general are not indicative of any particular event, however, and are common in deposits not only from tsunamis (e.g., Bondevik, 2003, Goff et al., 2004) and sediment venting (e.g. Tuttle, 2001), but also from other events such as storms.

Rapid deposition, fining upward

Both sediment venting and tsunami deposition occur on the time scale of hours (or less) to days—rapid sedimentation relative to most other depositional processes common in coastal settings. Evidence for rapid deposition includes massive to graded bedding, sharp basal contacts, burial of in-situ plants, and soft-sediment deformation. Thus though not diagnostic, upward fining is expected in and described from both tsunami deposits (e.g., Gelfenbaum and Jaffe, 2003) and vented sediments (Tuttle, 1999).

2.2.4 Preservation potential of tsunami and vented-sediment deposits

The preservation potential of tsunami deposits and vented sediments will partly

depend on the morphology of the deposit. In general, thicker deposits are more likely to be preserved, and widespread deposits are more likely to be preserved and also discovered by scientists. Because tsunami deposits typically are more continuous than vented sediments, preserved deposits are more likely to be evident in cores and outcrops. Post-depositional reworking of either type of deposit may remove many of their distinguishing characteristics. The dome-like morphology of some vented sediments makes them susceptible to erosion of positive topography so that the preserved deposit becomes more sheetlike.

Environmental factors that influence the preservation of deposits include bioturbation, coseismic land-level change, and reworking and erosion of the deposit. Bioturbation is variable and dependent on climate, environment and ecology. These factors being equal in a given case, deposits are less likely to be obliterated by bioturbation if they are thick or rapidly buried. Coseismic land-level change can both help and hinder event-deposit preservation. While (co-seismic) subsidence may lead to protective burial (e.g. Atwater, 1987; Atwater, 1992, Cisternas et al., 2005), it can also subject tsunami and vented-sand deposits to erosion by storms and tides (e.g., Walsh et al., 1995). Uplift can elevate deposits out of the zone of storms and tides but also can expose the deposits to reworking and erosion via wind and runoff if they are not anchored by vegetation. Vented sediments are more likely than tsunami sediments to be deposited in environments where they may be preserved, out of the zone of coastal erosion and reworking. Subsequent exploitation of either type of deposit by later fluidization will complicate the sedimentary structures (Clague et al., 1992).

2.3 PUGET LOWLAND CASE STUDY

2.3.1 Geological setting

Pleistocene glaciation generated conditions leading to high liquefaction potential and high rates of slope failure in many areas of the Puget Lowland (Kramer, 2009), a glacially modified lowland between the Olympic Mountains to the west and Cascade Range to the east (Figure 2.1). The last glaciation, the Fraser glaciation, reached its peak in the Vashon stade ~15,000 years ago (Booth, 1994). Associated with the Fraser glaciation are till, advance and outwash sediments, and lake deposits. These sediments drape much of the lowland and are exposed in many unstable escarpments that may fail in earthquakes; for example, the 1949 Olympia earthquake is associated with a large landslide of glacial sediments that generated a 2 m tsunami (Chleborad, 1994). Moreover, outwash sediments buried by lacustrine and marine clays and muds are prone to liquefaction (Kramer, 2009).

In addition to shallow crustal earthquakes, the Puget Lowland is subject to the effects of earthquakes from two other sources, the shallow Cascadia subduction zone and the deeper Benioff zone (Figure 1.1; Ludwin et al., 1991; Bourgeois and Johnson, 2001). The focus of this study will be on evidence for large crustal earthquakes such as the ruptures on four shallow faults in the Puget Lowland about 1,100 years ago, which induced strong shaking and land-level change. One earthquake, estimated to be of magnitude 7+ and dated to AD 900-930, occurred on the Seattle fault zone (Bucknam et al., 1992; Atwater, 1999; ten Brink et al., 2006). At around the same time, the Tacoma fault zone (Sherrod et al., 2004), the Saddle Mountain fault zone (Witter et al., 2008; Blakely et al., 2009), Olympia fault zone

(Sherrod, 2001) and Cascadia subduction zone (Atwater et al., 2004) also appear to have ruptured (Figure 2.1).

2.3.2 Sedimentary evidence of earthquakes

Active tectonics and an ample sediment supply make the Puget Lowland an ideal environment for the study of sedimentary paleoseismology. Pre-historic deposits from tsunamis and vented sediments have been studied in several locations around the Puget Lowland (Figure 2.1). A tsunami associated with the Seattle earthquake of about 1,100 years ago best explains sediment sheets documented from coastal lowlands in localities near the Seattle fault (Atwater and Moore, 1992) and on the Snohomish delta near Everett (Bourgeois and Johnson, 2001). Vented sediments are documented in primarily deltaic settings around the lowland (Bourgeois and Johnson, 2001; Sherrod, 2001). A sediment deposit in Lynch Cove on Hood Canal previously was interpreted primarily as a tsunami deposit with local sand venting (Hemphill-Haley, 1996; Jovanelly and Moore, 2009), but herein we reinterpret it to be solely vented sediment.

While most of the sandy tsunami deposits in the Puget Lowland represent local crustal earthquakes, some more likely represent other earthquake sources, and these other sources may also be the triggers of sand venting in the Lowland. For example, some tsunami deposits north of Puget Sound are probably from Cascadia subduction-zone generated tsunamis (Williams and Hutchinson, 2000; Williams et al., 2005; Figure 2.1). And because subduction and Benioff zone earthquakes can also induce liquefaction in the Puget Lowland (Frankel et al., 2002; Kramer, 2009), attributing vented sediment to local crustal faults requires association with other evidence of local faulting such as co-seismic land-level change.

2.4 METHODS

The goal of fieldwork was to map the deposits in question, to describe them stratigraphically and sedimentologically, and to take samples for lab analysis. The majority of the fieldwork took place in the summers of 2007-2009 though many of the Snohomish-delta data are taken from unpublished work by Bourgeois from 1996 to 1998. Sites required foot and canoe access, and all coastal sites required a low tide to work outcrops. Field methods varied depending on the thickness of the sediment deposit and permit limitations. Each site was located with a GPS and plotted onto a georeferenced map except for the Snohomish delta where sites were located on a topographic map.

To map deposit thickness and examine sedimentary structures, we used hand-dug pits, backhoe trenches, outcrops, gouge cores, vibracores, and soil-auger holes. For most locations, the preferred method was to clean and examine cutbanks along tidal creeks and streams using shovels and scraping tools to examine variability in thickness and sedimentary structures. The majority of cleaned sections were ~0.5 m in width, but in some areas we cleaned long (3-5 m) sections of banks or cleaned sections spaced 1-5 m apart for up to 40 m length.

In each outcrop and core, we measured stratigraphy and noted lateral and vertical changes in lithology and sedimentary structures. For about 30 sites where the stratigraphy was exposed by outcrop or trenching, we took monoliths and/or made sedimentary peels, which bring out details of the sedimentary structure.

Laboratory methods included cleaning sediment for diatoms and foraminifera analysis and examining sediment samples. Diatom samples of 2 cc were cleaned in 30%

hydrogen peroxide and then rinsed seven times in filtered water. Samples were settled onto coverslips through evaporation and mounted on microscope slides using Naphrax (refractive index D=1.7). Slides were then checked for the presence/absence of diatoms. Foraminifera were picked under a microscope and identified. Clay and mud samples were examined as wet mounts under the microscope for grain size, rounding and sorting. We examined clay samples (from intraclasts) by x-ray diffraction to determine potential sources, but results were inconclusive.

2.5 DEPOSIT DESCRIPTION AND BASIC INTERPRETATION

We chose sites based either on previous publications or on reconnaissance work indicating the presence of tsunami or vented sediments; all are located on stream banks, coastal marshes, and deltas. In this section, for each field location – Issaquah Creek, Snohomish delta, Gorst, Skokomish delta, and Lynch Cove -- the ecologic and stratigraphic setting of the sediment deposit is described followed by a description of the structure and morphology of the sediment deposit and associated features such as sediment dikes. In the section following this site-by-site interpretation, we combine and summarize our criteria for making those interpretations.

2.5.1 Issaquah Creek

Issaquah Creek flows from the foothills of the Cascade Mountains into Lake Sammamish in the eastern Puget Lowland (Figure 2.4), forming a small delta. Though the delta is heavily modified by people, a swamp fringes the shoreline where undisturbed. The modern channel contains mud to cobbles, and the banks comprise a range of facies discussed below.

Prior work has documented seismically triggered features at and near this site. Large paleo-landslides in Lake Sammamish are linked to the AD 900-930 Seattle fault earthquake (Logan et al., 1998; Prunier, 1998). Though the details of how these landslides failed are not established, they could have been tsunamigenic. In a site on Issaquah Creek, now inaccessible due to bank failure, Whistler et al. (2002) observed a sediment dike. Furthermore, this area generated sand blows during the 2001 M 6.8 Nisqually earthquake (Nisqually Clearinghouse).

The banks of this creek reveal a willow swamp facies abruptly overlain by more than 1 m of sand and mud (Figure 2.4). Above this package is a thin, <10 cm thick, peat overlain by several meters of fluvial sand and mud (Figure 2.4). The elevation of the willow peat falls within the range of modern lake level. Leaves entrained in the base of the sand unit date to AD 640-980.

The sand deposit overlying the willow swamp facies contains a variety of sedimentary features. The deposit thickens and thins from >100 cm to <20 cm thick over 15 m laterally, with an average thickness of 35 cm. The sand is often capped gradationally by up to 60 cm of gray mud, which fills topography created by the sand (Figure 2.4). The sand deposit contains mud laminae, peat and mud intraclasts, soft-sediment deformation, and fluid-escape structures (Figure 2.4B and D). In a few sites the deposit includes coal clasts up to 2 cm in the long axis and well-preserved entrained leaves in the basal 10 cm of sand. The deposits fill in the space between *in situ* willow and other woody vegetation.

Whistler et al. (2002) interpret this deposit to be vented sediment, and we agree. The basic criteria are sediment thickness and thickness variability, presence of a sand dike, and historical record of susceptibility to liquefaction.

2.5.2 Snohomish delta

The Snohomish River empties into Possession Sound creating a large Holocene delta (Figure 5) between the municipalities of Everett and Marysville. Much of the modern delta has been diked and drained and converted for agricultural and industrial use (Collins et al., 2003). The modern distributary channels contain mud to pebbles, and the banks primarily comprise accumulated point-bar and marsh facies.

In a previously published study of the Snohomish delta, Bourgeois and Johnson (2001) examine several sedimentary deposits in the delta stratigraphy, primarily as exposed in cut banks at low tide. Along the banks of the distributaries, a distinctive sand layer (part of their Unit B) interrupts muddy marsh sediment, and the layer below dates to AD 800-980 (Bourgeois and Johnson, 2001; Figure 2.5). Locally, 50-75 cm of subsidence is associated with the sediment deposit, and sediment-filled dikes and lateral spreads are also present. Bourgeois and Johnson (2001) interpret the subsidence to be due to local compaction by shaking during an earthquake that also generated the dikes and lateral spreads.

In this paper we present more detailed analysis of Unit B of Bourgeois and Johnson (2001). The Unit B sand layer (0.5-10 cm thick), coupled with a gray mud (0-12 cm thick), can be traced in distributary cutbanks for several kilometers inland. Fining and thinning landward (Bourgeois and Johnson, 2001, their Figure 7), the sand deposit has consistent structure and general thickness over several square kilometers (Figure 2.5A). The sediment fines upward from medium or rarely coarse sand to fine sand (and silt), and it is typically capped by two to three sand and mud laminae (Figure 2.5B). In a few outcrops, there are positive domes where the sand layer more than doubles in thickness for less than a meter laterally (Figure 2.5C). Dikes of mud and sand are also present in some outcrops; some

terminate at Unit A, others cut through it, or their termination points are not clear. The sand layer and sediment dikes consist of similar grain sizes and brackish diatom assemblages (Bourgeois and Johnson, 2001).

Bourgeois and Johnson (2001) interpret the sand deposit to be primarily a tsunami deposit with local presence of small sand volcanoes. We agree with this interpretation and present additional data to contrast the tsunami deposit with the vented sediment bodies (Figure 2.3, 2.5C). The basic tsunami-interpretation criteria are the thin yet consistent thickness of the layer (thinning and also fining landward), and its lateral extent. The vented sediment bodies have positive topography or locally thick and variable geometry.

2.5.3 Gorst

Gorst Creek empties into upper Sinclair Inlet, generating a small delta (Figure 2.6A and B). Most of the surface has been covered with roads, buildings and parking lots, leaving remnants of salt marsh and alder swamp. The creek discharges sand and gravel onto muddy tidal flats. There is no prior published work on this site.

Outcrops, pits, and cores in the remnant wetlands reveal an abrupt upward change from shell-bearing tidal-flat facies to freshwater forest peat (Figure 2.6), evidence for Holocene uplift about 1,100 years ago. This forest peat is in turn overlain by salt-marsh peat of the modern depositional environment, indicating more recent subsidence. A complex silty sand unit up to 1.6 m thick lies between the shelly tidal-flat deposits and the forest peat, and is present along 0.5 km of the upper inlet's shoreline. It has a sharp lower contact and a sharp to gradational upper contact. The silty sand unit typically contains three layers: a lower sand (typically 5-7 cm thick) that fines upward; a thin (< 1 cm thick), discontinuous mud lamina, in one site with flame structures; and an upper silty sand (up to 50-cm thick), with massive

structure and faint grading (Figure 2.6B and C). The lower sand layer is only present in the marsh and swamp excavations near the shoreline, but the upper silty sand was found 2 km up Gorst Creek. (A detailed discussion of the upper sand and its interpretation as a sandy debris flow deposit is in Chapter 3.)

The lower sandy layer is typically 5-7 cm thick, and ranges from 0 to 24 cm, thickening into local depressions while maintaining a horizontal upper surface. It is characterized by normally graded, medium- to fine-grained sand; pebbles and coarse sand are locally present at the base, and the uppermost zone is silty very fine sand. In some sites the sediment fills burrows into the underlying shelly mud unit. Pebbles consist of lithics and rounded mud clasts similar to those in the modern stream channel and the paleo-tidal-flat deposits, respectively. All of the sampled sandy sedimentary layers in the marsh area contain marine and brackish diatoms (Yuki Sawai, personal communication).

We interpret the lower sediment layer to be a tsunami deposit, showing typical features. It is simply and normally graded, only present near the shoreline, and sheet-like overall. It is relatively thick compared to the Snohomish-delta tsunami deposit because (we reason) it is a proximal deposit onto an unvegetated tidal flat. We infer that the generating tsunami was from the Seattle fault rupture about AD 900-930 (Chapter 3).

2.5.4 Skokomish delta

The Skokomish River forms a delta at the “elbow” of the Hood Canal fjord (Figure 2.1B). The delta (Figure 2.7) consists of salt- and freshwater marshes and swamp, which are pristine in some areas while other portions of the delta have been diked and used for farming, of which some parts are under restoration. The main channel is currently restricted to the eastern delta and has only one small distributary. Modern channel bottoms contain mud to

pebbles, and channel banks primarily comprise accumulated point-bar and marsh facies. There is no prior work on the stratigraphy of this delta.

Cores, outcrops and pits on the delta reveal evidence for uplift from a tidal flat to a forested environment about 1,100 years ago. This forest environment has reverted to salt marsh at the seaward end of the delta, indicating subsidence since about 1,100 years ago (Polenz et al., 2010). Of 73 excavations and cores on the Skokomish delta, eight contained a sandy unit between the underlying tidal flat deposits and overlying forest peat. Where present, the sand overlies a muddy facies.

The eight sand occurrences are concentrated into two local sand bodies (Figure 2.7A) with sedimentary characteristics including intraclasts and laminae. In both places mapped, the deposit reaches a maximum thickness of >30 cm and thins to zero within 10 m of the thickest point. One of these deposits is associated with a branching sediment dike ~2-cm-wide (Figure 2.7D). The sediment in the sandy deposits consists of mostly coarse sand but contains some granules; the internal structure is massive, with a faint indication of fining near the top, but also coarse grains throughout. The deposit contains mud intraclasts, and in one sediment body there is a discontinuous muddy lamina associated with the intraclasts (Figure 2.7C). Foraminifera are present in the sand, dominated by *Trochammina* sp. with rare *Elphidium* sp. Both of these genera are shallow-marine dwellers, typically intertidal marsh and inter- to subtidal respectively.

The sand bodies mapped within the Skokomish delta we interpret to be vented-sediment deposits. Basic criteria for this interpretation are the limited extent of these sand bodies and their pronounced variation in thickness.

2.5.5 Lynch Cove

The Union River flows westward into the terminus of Hood Canal forming a small delta at Lynch Cove. Agricultural lands and artificial fill segment remnant woodlands and marsh. Some portions of the delta are being preserved and restored. The modern extensive tidal flat consists of primarily sandy mud with some pebbles (Figure 2.8).

Early paleoseismological studies at Lynch Cove focused on evidence for coseismic land-level change (Bucknam et al., 1992). Marsh stratigraphy shows muddy tidal-flat facies abruptly overlain by forest peat, in turn overlain by salt-marsh peat. The mud-to-forest peat contact is interpreted as evidence for coseismic uplift dated to AD 680-1020 (Bucknam et al., 1992). Commonly, there is a sandy layer up to 100-cm thick between the tidal-flat mud and forest peat. Two prior published studies examined aspects of this sandy layer (Hemphill-Haley, 1996; Jovanelly and Moore, 2009)

Thickness of this sandy unit in Lynch Cove is highly variable, with no discernable trends of thinning landward or seaward (Figure 2.8B). Of our 182 cores and excavations in this locality, about 50% contain no sandy deposit (96 sites). Of the 96 sites with sandy deposit, the average thickness is ~24 cm. The thickest deposit we found was 84 cm thick; Jovanelly and Moore (2009) reported sand up to 1 m thick. The thickest sandy deposits are not at the seaward end of the marsh but farther inland (Figure 2.8B).

Our investigation found more sand dikes than Jovanelly and Moore (2009), who reported only two dikes out of almost 350 core sites (<1%). We found that of 135 sites where outcrop along tidal creeks was cleaned, 23 contained sand dikes (~17%) (Figure 2.8B). Moreover, when we disregard outcrops without a sandy layer (81), the percent of outcrops with sand dikes is ~39% (21/54; two sediment dikes contacted the peat/mud contact where no

sediment deposit was present). The discrepancy between the two studies in the ratio of dikes to data points is almost certainly due to our use of excavations rather than cores. The dikes are typically 1-2 cm wide and are similar in grain size to the deposit above, thus difficult to identify in core.

Sedimentary structures within the sandy deposit are variable, resulting in no consistent stratigraphy over the field-area scale of 100s of m (Figure 2.9) or the outcrop scale of less than 10s of meters (Figure 2.10). The deposit contains many sedimentary structures (Figure 2.11) including multiple units, cross stratification, intraclasts, mud laminae, microfaults, and soft-sediment deformation. Sediment also fills burrows into the basal mud terminating at the sediment deposit. The most common structures are intraclasts and laminae. Convoluted laminae and flame structures in silt laminae and are the most common soft-sediment deformation features (Figure 2.9).

The sand unit contains two kinds of intraclasts: soft olive mud that ranges from rounded to angular, and firmer gray mud that is typically angular (Figure 2.9D). Where present, both types of intraclast are typically high in concentration, particularly the blue-gray clasts. Higher concentrations of intraclasts are typically but not always near dikes (Figure 2.10). The olive mud in intraclasts is similar in grain size and diatom assemblage to the underlying tidal-flat deposits (Yuki Sawai, personal communication). The blue-gray mud clasts contain no diatoms.

The sandy deposit contains marine and brackish diatoms (Hemphill-Haley, 1996), and dike sediment contains brackish diatoms (Yuki Sawai, personal communication, 10/9/2009).

While the olive mud intraclasts are likely derived from the underlying tidal-flat facies, the source or source depth of the blue-gray intraclasts is unknown. Coring over 3.5

meters through marsh stratigraphy (~2 m below the sediment layer) did not reveal the lower contact of the tidal-flat facies. We found an outcrop of similar material to the blue-gray intraclasts in one site at the edge of the marsh; this outcrop is interpreted as Pleistocene glacial mud, which we infer also to underlie Lynch Cove. It may be at shallower depths in places not cored.

Jovanelly and Moore (2009) conclude the sandy deposit is of tsunami origin, with augmentation by liquefaction where the deposit is thickest. They base their interpretation on a general landward trend of grain-size fining and deposit thinning, over a more limited field area than our study, and a trend we could not reproduce. They invoke a tsunami that was generated either by coseismic deformation of the seafloor or by the nearby Alderwood landslide (Sarikhan et al., 2007; Figure 2.8A).

We interpret the sandy deposit to be vented sediment. We base our interpretation on lateral variation in thickness on both small and large scales, on absence of sand bodies at many sites, on high average thickness of the deposit, and on inclusion of intraclasts from what is likely a lower stratigraphic level. Although the abundance of sediment dikes is not diagnostic, it supports the sand-venting interpretation. Our interpretation differs from that of other workers (Hemphill-Haley, 1996; Jovanelly and Moore, 2009).

2.6 GENERAL CRITERIA FOR INTERPRETATION OF DEPOSITS

In sum, we interpret the primary sand deposit at the Snohomish delta and the lower sand layer at Gorst to be deposited by tsunamis (with some vented sediment bodies in Snohomish outcrops), whereas we interpret the sediment bodies at Lynch Cove, Skokomish delta and Issaquah Creek to be vented sediments. We use the deposit characteristics as

introduced above and enhanced by our study—architecture and morphology, sedimentary structures, (filling of) dikes and burrows, intraclasts, diatoms and foraminifera, and grain size—to determine the more likely mode of deposition.

Tsunami deposits and vented sediments are not the only potential sources for sandy sediment layers in coastal marshes. In the case at hand, we have ruled as unlikely alternative processes—storms, landslides, debris flows and floods—to be generators of the deposits in question. The short fetch associated with these field localities minimizes the impact of storms. The sediment layers do not thicken and coarsen toward landward slopes, as would be expected for deposits of landslides and debris flows. The lateral distribution of deposits, their lack of mud, and their singular occurrence in the record make floods an unlikely source of the deposits.

We focus below on what sedimentary characteristics from these study sites are most consistent with deposition by tsunami or by sediment venting or both.

2.6.1 Architecture and morphology

Overall thickness of deposits, lateral variation of thickness and sedimentary structures, and landward thinning trends are different in tsunami and vented-sediment deposition (Figure 2.2 and 2.3). Thickness variations are present on two scales--over entire field areas (map scale), and over meters (outcrop scale). For example, the deposit at the Snohomish delta thins landward on map scale, is thin overall (Figure 2.3), and has little variability in thickness on map and outcrop scale (Figure 2.12), typical of tsunami deposits. However, there are sites where the sediment thickens and exhibits mound-like morphology on the lateral scale of a meter or so, most likely the local deposits of vented sediments (Figure 2.5C). At Gorst, there is not enough discernable geographic extent to make

conclusions about thinning trends, but in general, the lower sand layer has consistent thickness, similar to tsunami deposits (Figure 2.12).

The deposits at Issaquah Creek, the Skokomish delta and Lynch Cove thicken and thin on outcrop scale (Figure 2.12), create positive dome-like structures, have high mean thicknesses, and are not present in most areas, typical of deposition by vented sediment. However, based on thickness alone, in some cases at outcrop scale, the Lynch Cove sediment layer resembles a tsunami deposit (Figure 2.12, compare with Gorst).

2.6.2 Sedimentary structures

At the localities studied, the main distinction in sedimentary structures between interpreted tsunami deposits and vented sediments is variability of sedimentary structure across a field area, with higher consistency associated with tsunami deposition. For example, sediment deposits at Gorst and the Snohomish delta have consistent grading and lamination traceable across the field area and at outcrop scale. At Lynch Cove, the Skokomish delta, and Issaquah Creek, sedimentary structures in the deposits are rarely consistent over more than 10 m laterally.

Only Lynch Cove and Issaquah Creek sandy layers contain distinct soft-sediment deformation features, but both tsunami and vented-sediment deposits represent rapid deposition and thus soft-sediment deformation would not be unexpected in either (Choowong et al., 2008; Tuttle, 1999). Also, the deposits containing soft-sediment deformation features are typically greater than 20 cm thick, indicating that deposit thickness rather than mode of deposition may be the controlling factor for the presence of these features.

2.6.3 Sediment filling -- dikes and burrows

Sediment dikes and sediment-filled burrows can have ambiguous origins. Cracks, lateral spreads and burrows can be filled from above during a depositional event or exploited by fluidized sediment from below. The majority of dikes in this study (including those at the Snohomish delta, Skokomish delta, and Lynch Cove) exhibit characteristics of injected dikes, including upward bifurcation and high angle relative to horizontal. We were not able to determine the depositional mechanism of sediment-filled burrows. The mere presence of dikes is not indicative of vented origin of an overlying sediment body without a clear relationship showing the dike feeding the sediment body. We interpret the majority of the Snohomish delta sediment layer (Figure 2.5C and D) to have been deposited by a tsunami. In this and other cases, it is possible that a tsunami reworked some vented sediment.

2.6.4 Intraclasts

Intraclasts are present both within the sandy deposits and/or within dikes at all locations. Only in the case of Lynch Cove is intraclast origin distinctive enough to support a vented-sediment interpretation over tsunami. At that locality, the blue-gray-clay clasts appear to be from deeper stratigraphy, whereas the olive clasts are similar in grain size and diatom assemblage to the mud underlying the sandy deposit. In all of the other locations, all intraclasts consisted of material similar to that found within the top 10 cm of the underlying unit. Such clasts are inconclusive evidence because they could have been torn up by tsunami flow or ripped from dike walls as fluidized sediment pushed its way to the surface.

At Lynch Cove, not only the presence of the blue-gray clay but also high concentrations of intraclasts near dikes (Figure 2.10) indicate vented-sediment deposition. The blue-gray intraclasts indicate a watery sediment source below the glacial mud, with the

fluidized sediment entraining clasts as it flowed to the surface. The high concentrations of intraclasts over short lateral distances, typically near dikes (Figure 2.10) is another example of lateral variability in sedimentary structure, as discussed above.

2.6.5 Diatoms and foraminifera

In this study of Puget Sound sediment bodies, the presence of marine and brackish diatoms and foraminifera was not useful in distinguishing between tsunami and vented-sediment deposits. The potential sources for these microfossils, both from modern surfaces and from underlying stratigraphy, are too similar.

2.6.6 Grain size

The range in grain size of all deposits falls in the range of potential grain sizes for both tsunami and vented-sediment deposits. In general, all the event deposits in all studied locations consist of coarse silt to sand. All deposits except the Snohomish delta case also contain pebbles.

2.7 DISCUSSION

2.7.1 Implications

This paper calls to the attention of tsunami geologists the necessity to consider sediment venting as a possible and likely source of deposition associated with earthquakes and tsunamis in coastal regions. Because both tsunamis and sediment venting can occur at the same location and during the same earthquake, such as is the case at the Snohomish delta, care should be taken to distinguish the two. Confounding vented-sediment deposits with tsunami deposits could lead researchers to draw incorrect conclusions regarding tsunami run-up and inundation.

The differentiation of tsunami deposits and vented sediments is also important because the deposits help us understand different processes. Tsunami deposits typically indicate shallow faulting, and with modeling the distribution of tsunami deposits can be used to test differential slip on faults (e.g. MacInnes et al., 2010) or to differentiate fault sources (Chapter 3). Vented sediments indicate strong shaking, and the source depth and the distribution of vented sediments can be used to map zones of this strong shaking and to help locate earthquake sources (Tuttle, 1999).

In outcrops, sedimentary features can be used to distinguish tsunami deposits from vented sediments, but cores make the distinction more difficult. In outcrop one can describe and map sediment thickness and internal sedimentary structures, and sediment dikes can be obvious. Sediment dikes are rarely captured in cores, and where they are, they may be mistaken as sediment layers. In many coastal areas, however, high water tables and legal protection of wetlands prohibit excavations. Studies using wider cores and slicers show more detail in sedimentary structure and have better chance of revealing dikes (e.g. Takada and Atwater, 2004). Where outcrop is not available and excavation not possible, wider cores or a closely spaced coring strategy may be necessary for distinguishing between tsunami and vented-sediment deposition.

2.7.2 Potential sources of tsunami and shaking

The wide geographic distribution of faults with ruptures dating to about 1,100 years ago in the Puget Lowland makes it difficult to determine which fault rupture is related to deposition at each site. None of the sites is more than 50 km from a fault dated to have ruptured ~1,100 years ago and all are within 300 km of the subduction zone.

Tsunami deposits at Gorst and on the Snohomish delta are most likely related to rupture in the Seattle fault zone because modeling shows that such a rupture generates larger amplitude waves than from the Tacoma fault zone (Venturato et al., 2007). Earthquake-triggered (or other) landsliding in the Sound also could contribute to tsunami effects (Bourgeois and Johnson, 2001).

Because of the temporal and geographical correlation of vented-sediment deposits with mapped faults and the deposits' association in most cases with land-level change, we consider seismic loading to be the most likely initiator of liquefaction in the studied cases. However, because there were ruptures on multiple fault zones within the error of radiocarbon dates, and because it is difficult to assign vented sediments to specific faults, we draw no conclusions about the extent of strong shaking of any specific earthquake.

The vented sediments are most likely related to fault rupture in close proximity to each field site--the Seattle fault zone for the Snohomish delta and Issaquah Creek, the Saddle Mountain fault zone for the Skokomish delta, and either the Tacoma or Seattle fault zones for Lynch Cove. However, there is also a similar-aged record of rupture on the Cascadia subduction zone (Atwater et al., 2004), which may have caused local liquefaction in the Puget Lowland. Moreover, we also can't rule out a deep-seated earthquake trigger such as the 2001 Nisqually event.

2.8 CONCLUSIONS

The stratigraphy of the Puget Lowland records sandy deposits related to fault ruptures about 1,100 years ago. We conclude that the Skokomish delta, Lynch Cove and Issaquah Creek deposits are vented sediment based on the presence of injected dikes, intraclasts from

lower stratigraphy in close proximity to dikes, sedimentary structures that change with distance from dikes, and variable thickness and general stratigraphy over both outcrop and map scale. For the Lynch Cove case, our interpretation differs from prior published results attributing this deposit primarily to a tsunami (Hemphill-Haley, 1996; Jovanelly and Moore, 2009). At Gorst, we interpret the (lower) sandy unit to be a tsunami deposit given its generally uniform thickness and sedimentary texture as well as its fining-upward structure (also see Chapter 3). We agree with the earlier conclusion of Bourgeois and Johnson (2001) that the thin, widespread and consistent sandy deposit in the Snohomish delta is a tsunami deposit, with some vented-sediment bodies indicated by local areas of domed thickness and variable stratigraphy.

Above all, we urge paleoseismologists to consider both vented sediments and tsunami deposits when working in marine, estuarine, lacustrine, and shoreline settings. The interpretation of these deposits is important for hazard analysis and for the study of earthquake history and prehistory.

Table 2.1 AMS dates from plant material in sand deposit from Issaquah Creek.

Measured, 14C yr B.P.	Calibrated 2 sigma range	Limiting	Material	Latitude	Longitude	ID NOSAMS
1280±35	AD 660-860	limiting maximum for vented sediment	leaf	47.5577	-122.05843	78399
1340±30	AD 640-770	limiting maximum for vented sediment	leaf	47.5577	-122.05843	78398
1140±30	AD 780-980	limiting maximum for vented sediment	leaf	47.5577	-122.05843	78397

Dates were calibrated using IntCal 09 (Reimer et al., 2009). All analysis was performed by the National Ocean Sciences Accelerator Mass Spectrometry Facility (NOSAMS). Calendar age was calibrated using IntCal 09 (Reimer et al., 2009) using the online program OxCal (https://c14.arch.ox.ac.uk/oxcal/) All material was collected from the same outcrop.

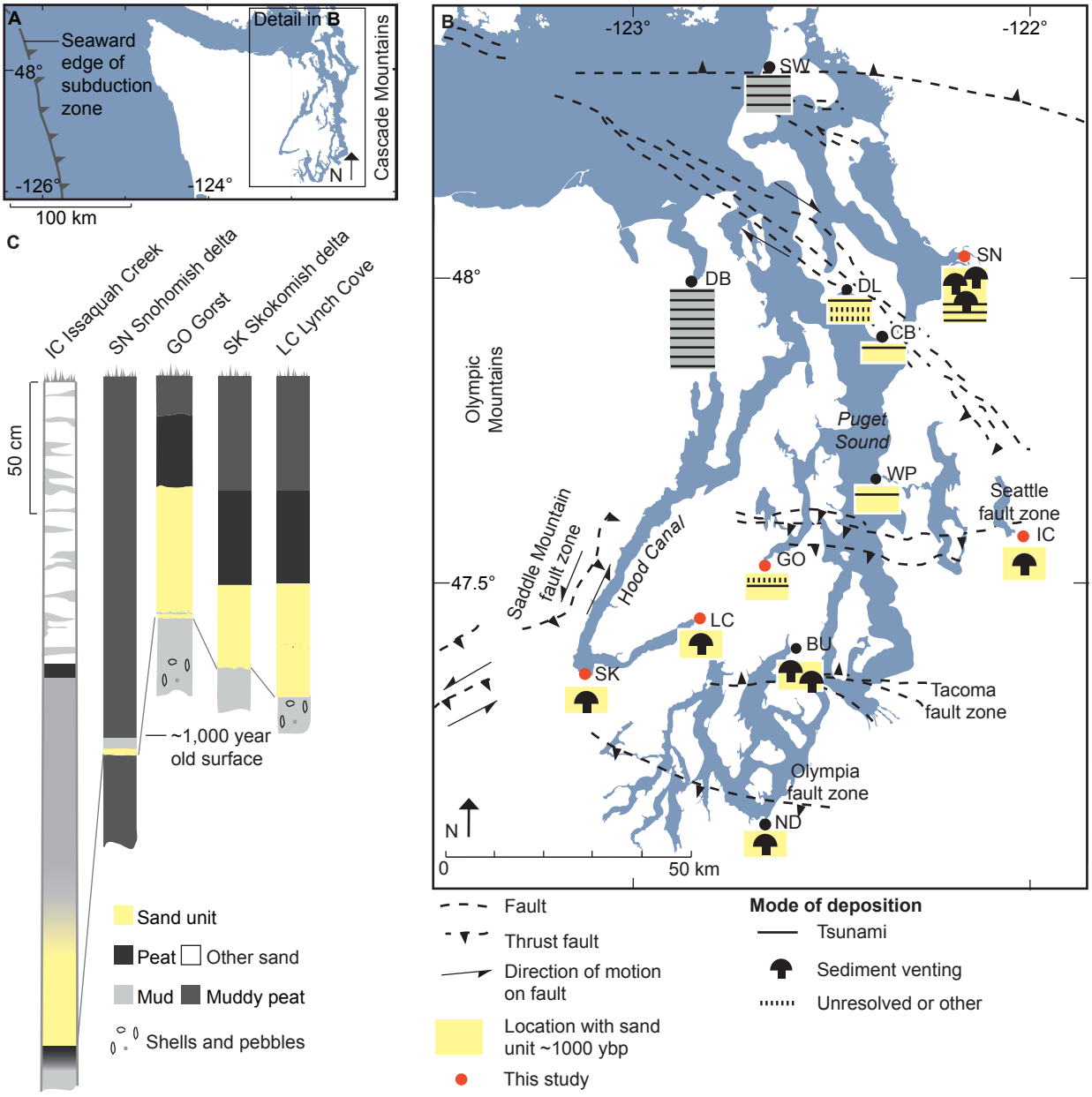

Figure 2.1 A. Map of Washington and Cascadia subduction zone. B. Location of sediment layers and major fault traces in the Puget Lowland and C. Generalized stratigraphy of the field sites in this study. B. Sediment layers taken from IC. Issaquah Creek, this study; SN. Snohomish delta, Bourgeois and Johnson, 2001; GO. Gorst, this study; SK. Skokomish delta, this study; LC. Lynch Cove, this study; DL. Deer Lagoon, Bourgeois, unpublished data; BU. Burley, Bucknam et al., 1992; DB. Discovery Bay, Williams and Hutchinson, 2000; SW. Swantown marsh, Williams et al., 2005; ND. Nisqually delta, Barnhart and Sherrod, 2001; CU., and WP. Cultus Bay and West Point, Atwater and Moore, 1992 Fault information is from Johnson, et al., 1996; Gonzalez et al., 2004; Kelsey et al., 2008; Sherrod et al., 2001; 2008; Witter et al., 2008; and Blakely, 2009. C. Generalized stratigraphy showing sediment units dating to ~1,000 ybp.

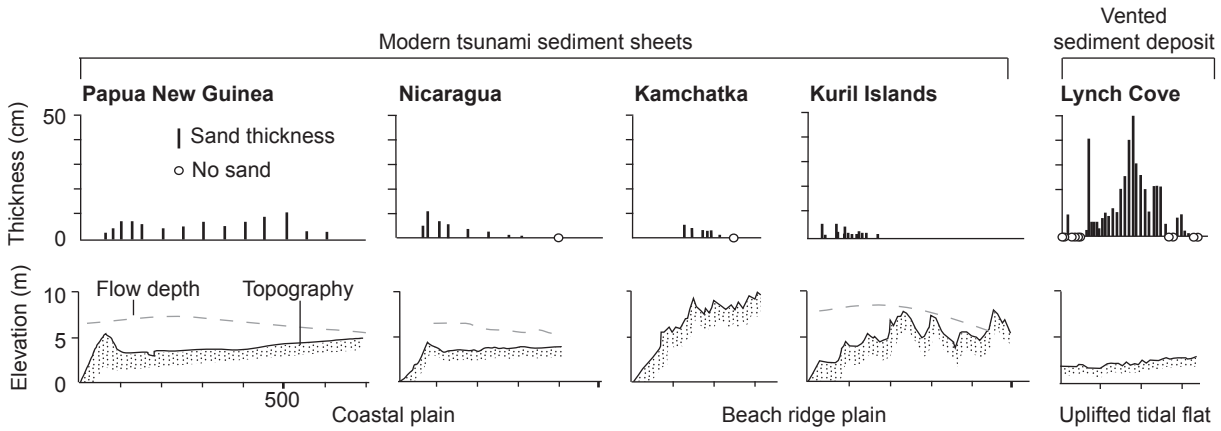

Figure 2.2 Sediment thickness over topographic profiles perpendicular to the shoreline showing landward trends in sediment thickness. Tsunamis were generated by earthquakes of magnitudes 7-8, a similar to slightly larger magnitude to those hypothesized for the Puget Lowland (ten Brink et al., 2006). All profiles trace the sediment unit to its inland extent except for Lynch Cove where the inland extent of the sediment unit is unknown. 1998 Papua New Guinea tsunami, earthquake Mw 7.7, (Gelfenbaum and Jaffe, 2003);1992 Nicaragua tsunami, earthquake Mw 7.7, (Higman and Bourgeois, 2008 and Bourgeois, raw data); 1997 Kamchatka tsunami, earthquake Mw 7.8 (Bourgeois et al., in prep); 2006 Kuril Island tsunami, earthquake Mw 8.3, (MacInnes et al., 2009); Sediment unit from Lynch Cove, Washington— topography is of the top of the mudflat deposits, the inferred surface at the time of the event (Jovanelly and Moore, 2009). No modern vented sediment studies were found using a comparable methodology to tsunami studies of measuring deposit thickness along a 100+ meter topographic transect.

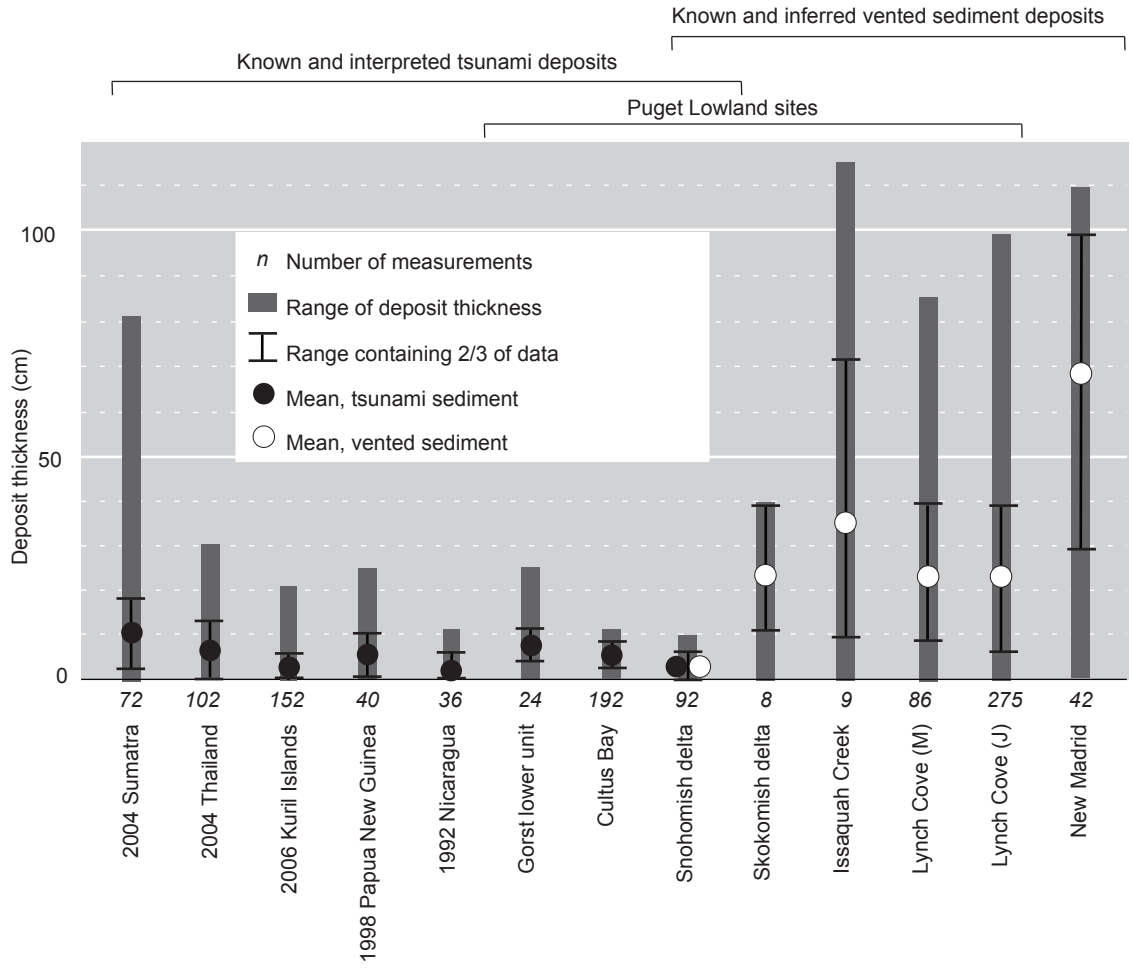

Figure 2.3 Mean sediment thickness averaged over sites where sediment layer is present. For publications, all nonzero data points in publication were used. Where reported as outcrops, thickness was measured each meter. 2004 Sumatra (Paris et al., 2007); 2004 Phra Thong Island, Thailand (Jankaew et al., 2008); 2006 Kuril Islands (MacInnes, 2009); 1998 Papua New Guinea (Gelfenbaum and Jaffe, 2003); 1992 Nicaragua (Higman and Bourgeois, 2008); Gorst, this study; Cultus Bay (Moore, 1994); Snohomish delta (Bourgeois and Johnson, 2001; Bourgeois raw data); Skokomish delta, this study; Issaquah Creek, this study; Lynch Cove 1, this study; Lynch Cove 2 (Jovanelly and Moore, 2009); New Madrid (Tuttle and Schweig, 1996).

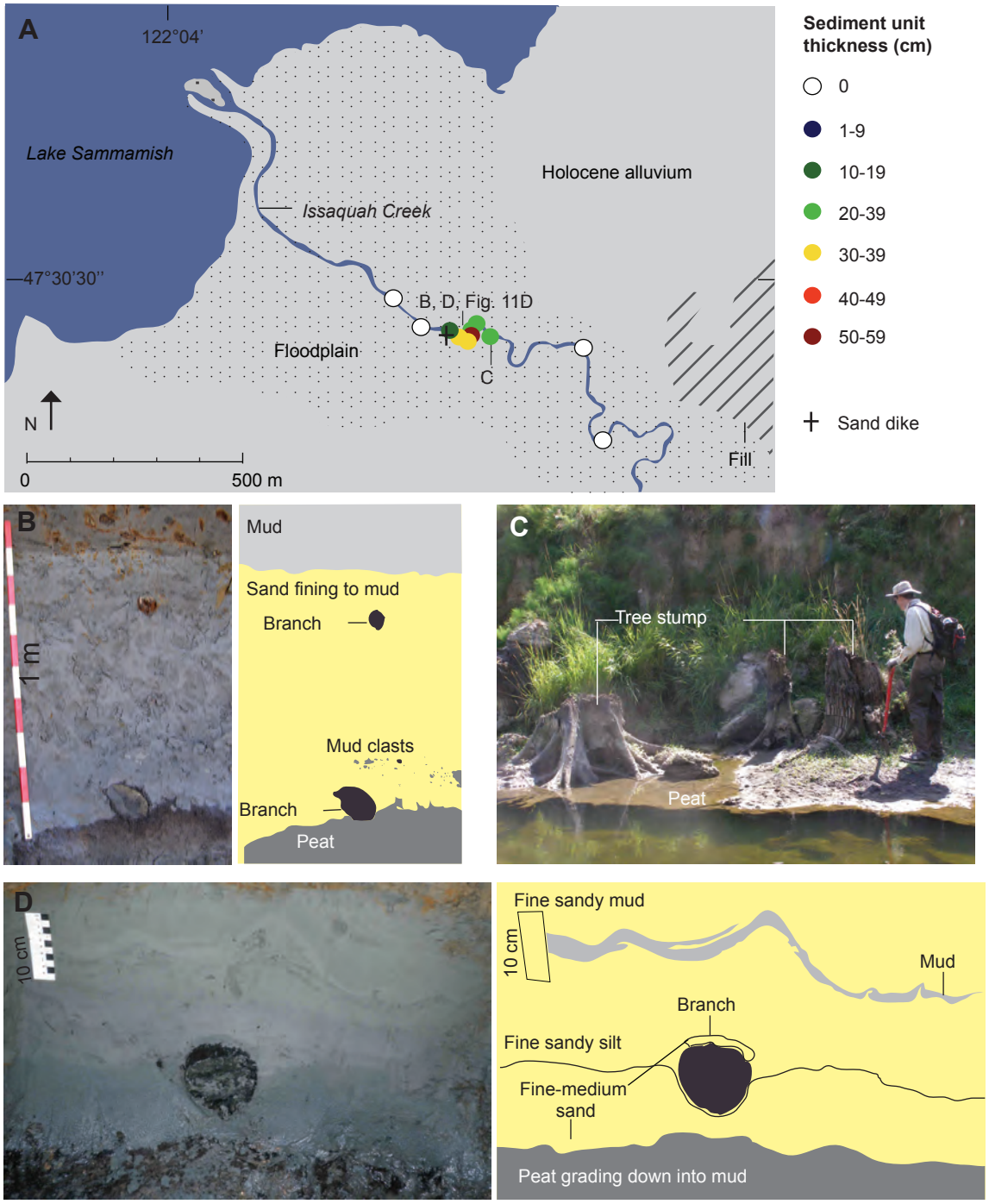

Figure 2.4 Map and details of the sediment unit along Issaquah Creek. A. Map of sediment unit thickness, including sand and mud layers. Geological information taken from Booth and Minard (1992). B and D. Photos and sketches of sediment unit with branches of buried trees and in D soft-sediment deformation. C. Trees buried by sediment unit eroding out into the stream channel. Person standing on ~1,000 year old swamp surface for scale.

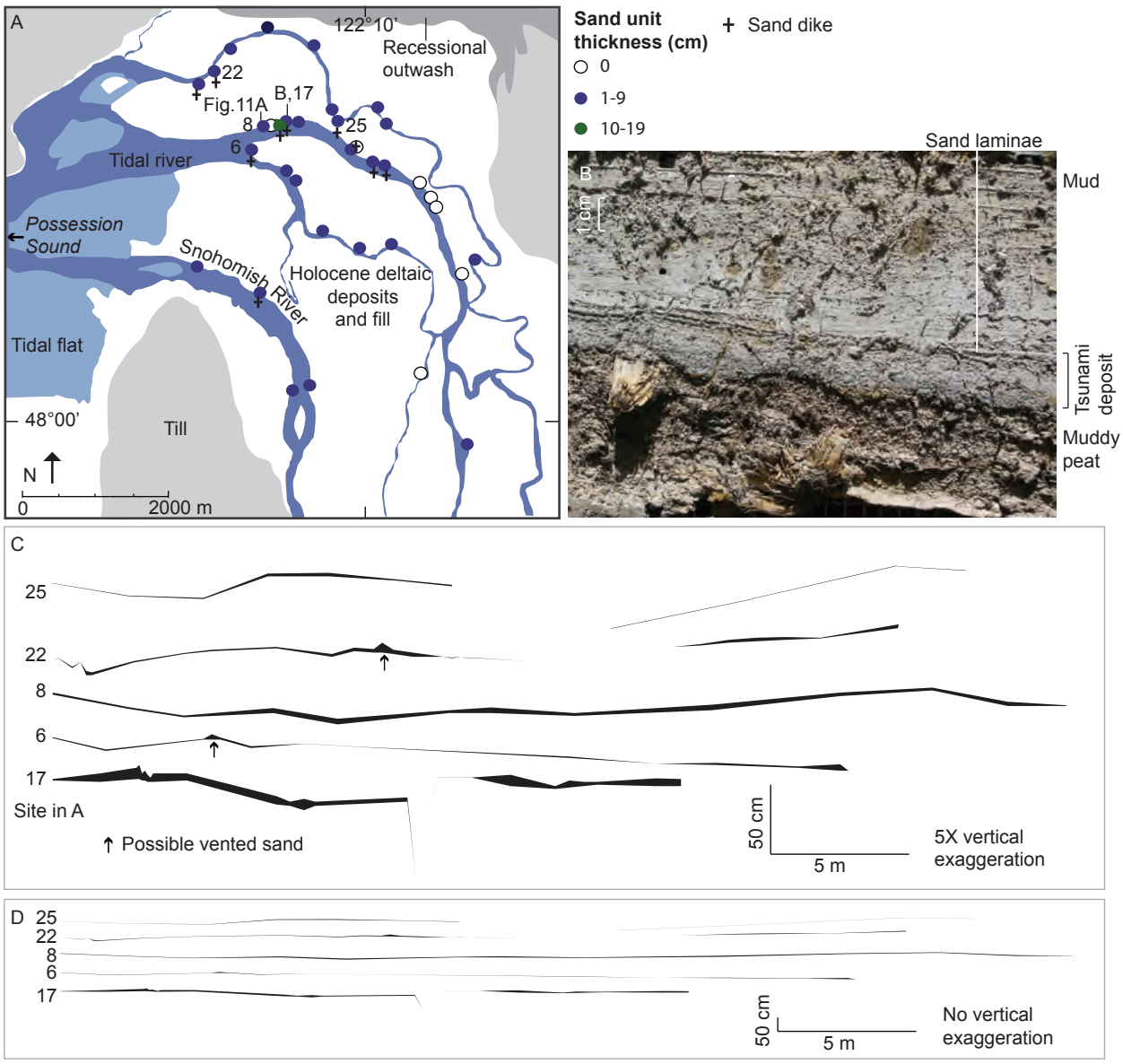

Figure 2.5 Map and details of the sediment unit at the Snohomish delta. A. Geological map of the Snohomish delta modified from Minard (1985) showing sand-layer thickness and locations of sediment dikes and lateral spreads. B. Sediment peel detailing the sandy tsunami deposit with overlying laminae. Light source is from the top of the peel. C. and D. Thickness of sand deposit along continously cleaned outcrops. MEasurements were taken every 5 m and where thickness and elevation varied. Outcrop numbers from Bourgeois and Johnson (2001). Arrows demark local depositional doming and thickening, potentially by sand venting. Location 17 is anomalous in thickness and structure and may have been thickened by sand injection during later liquefaction events.

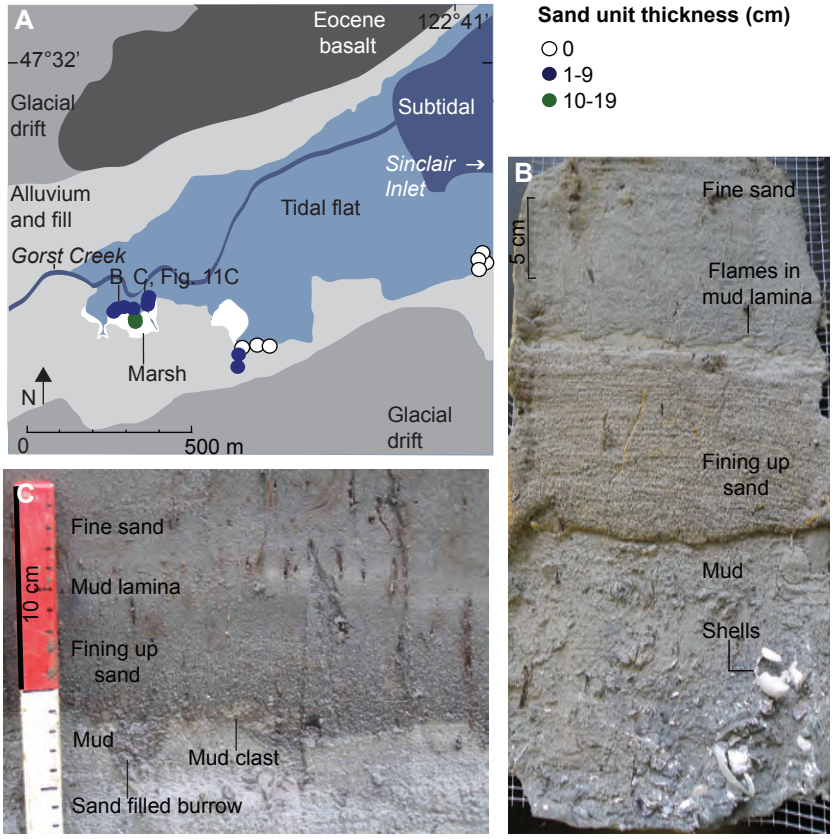

Figure 2.6 Map and details of the sediment unit at Gorst. A. Map of thickness of the (lower, fining-upward) sandy bed treated in this study. Geologic map from Haugerud, 2009. B. Sediment peel of fining-upward lower unit from the salt marsh capped by a mud lamina with flame structures, overlain by upper sandy unit. C. Sediment unit from Gorst marsh detailing sedimentary features.

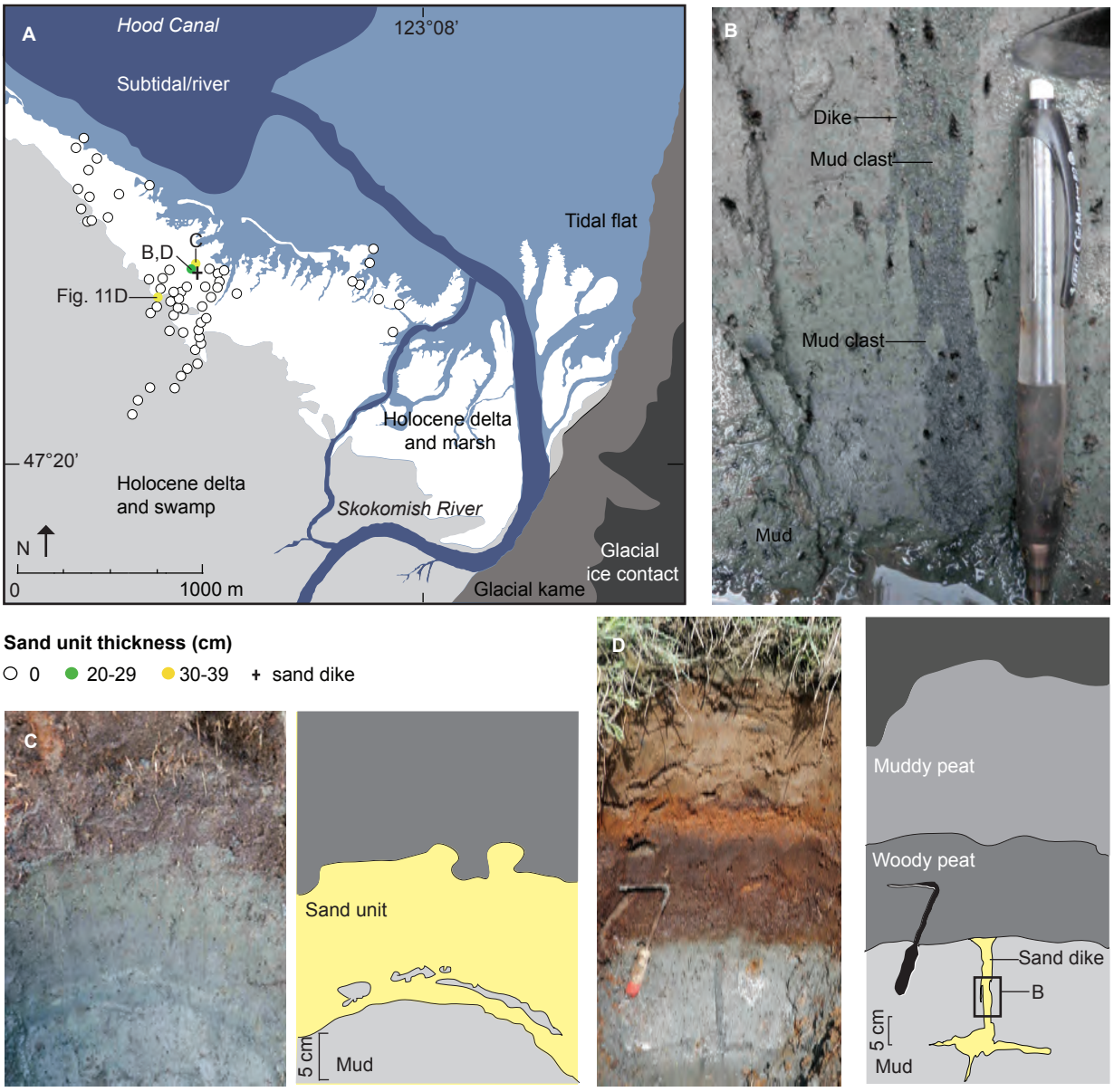

Figure 2.7 Map and details of the sandy sediment units at the Skokomish delta. A. Map of sand-body thickness and location of sediment dike in B and D. Geologic information from Polenz et al. (2010). B. Detail of injected sand dike in D. C. Sand unit containing mud clasts from the salt marsh. D. Branching sand dike.

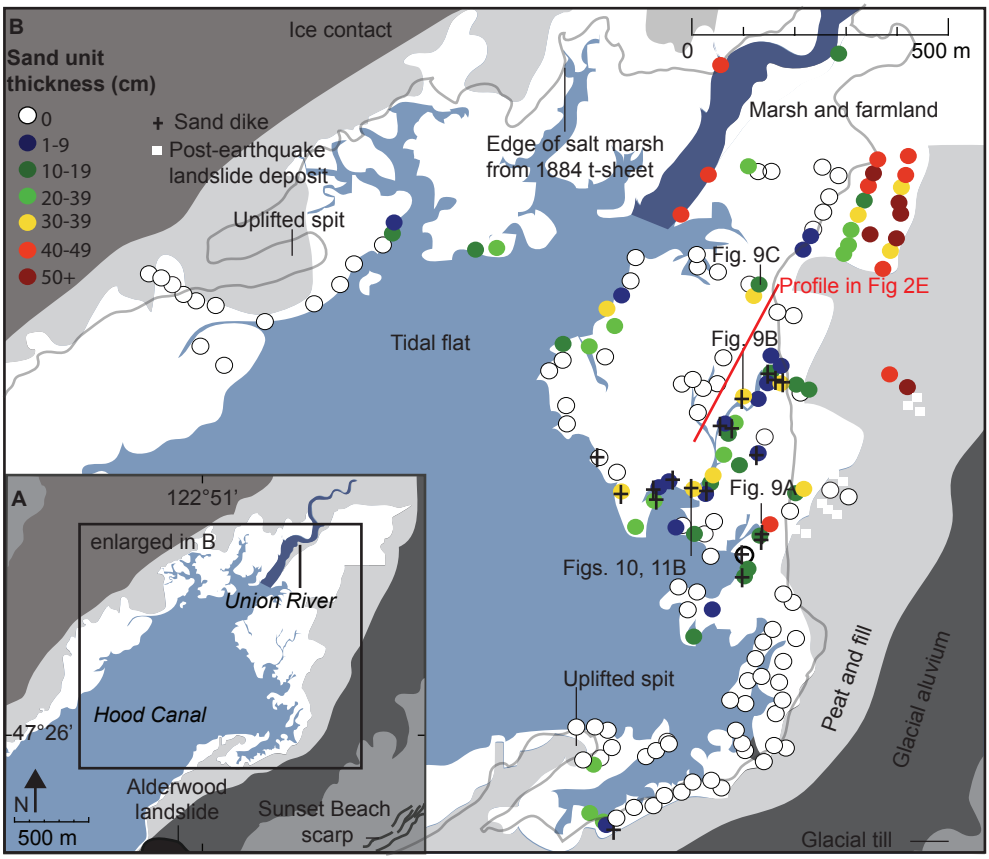

Figure 2.8 Geological map and details of the sediment unit at Lynch Cove. A. Geological map of the Lynch Cove area modified from Polenz et al. (2009)--modified due to our cores indicating the small peninsula to the SE is an uplifted spit and not landslide deposits. B. Map showing thickness of the sandy unit at Lynch Cove. In some locations the unit is covered by a younger, slopeward-thickening pebbly gravel through which we could not core. The pebbly gravel is inferred to be related to slope failure.

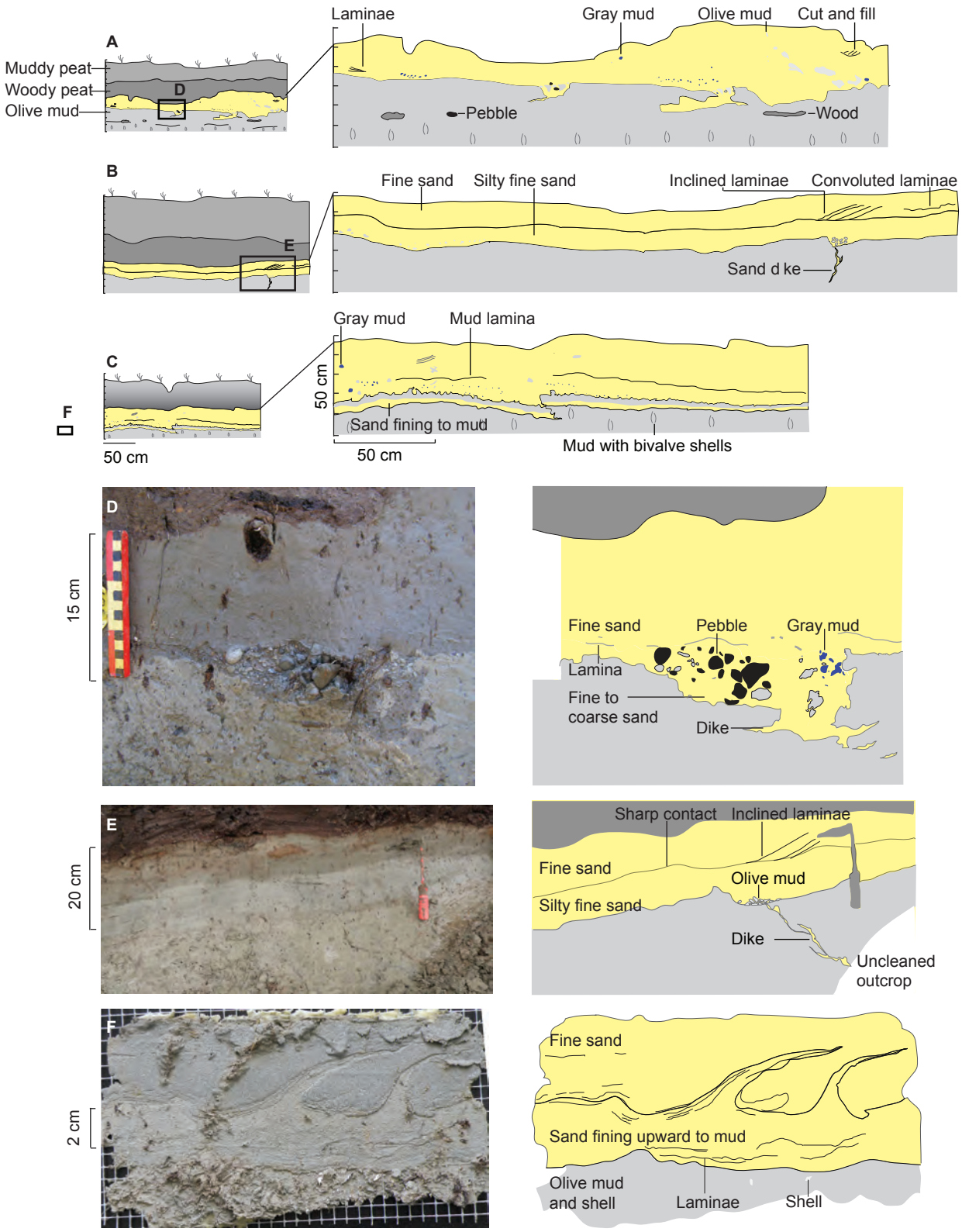

Figure 2.9 Examples of variability of sedimentary structure and thickness in the sediment unit at Lynch Cove; locations shown in Fig. 8B. Note how structures change over short distances and note high concentrations of mud clasts near the dikes. A-C are sections measured with line level and described in the field; same scale for all three. D. Detail from A of emergent dike associated with pebbles and mud clasts. E. Detail from B showing concentration of mud clasts near dike and inclined laminae F. Detail from a peel taken <1 m to the left of C showing flame structures and laminae; note mud clasts common in C are not present.

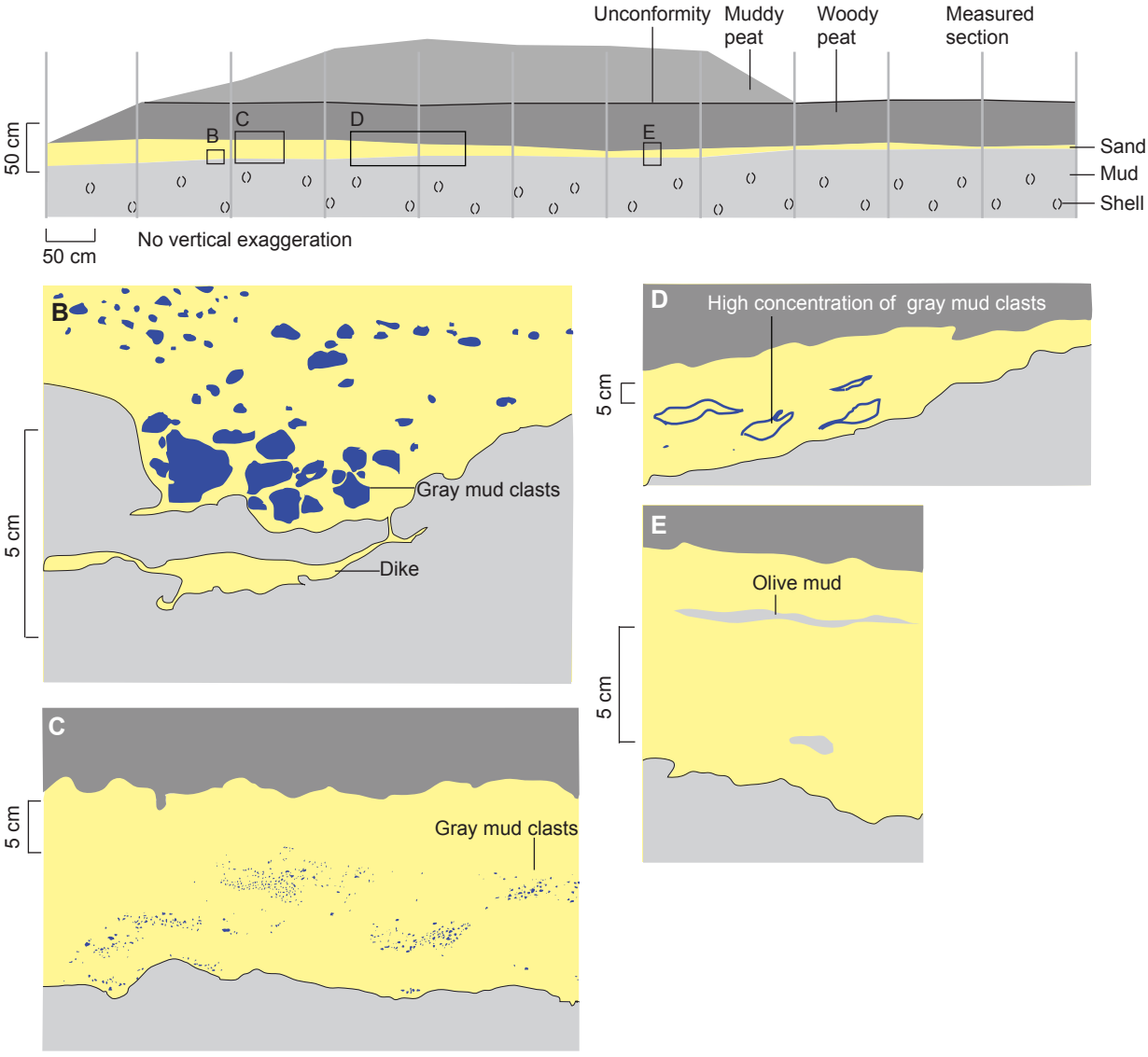

Figure 2.10 Example of variability of sedimentary structure and thickness in the sediment unit at Lynch Cove along a single outcrop (located on Fig. 8B). A. Thickness of sediment units along outcrop, surveyed in with a transit. B-E are drawings made from photographs of outcrop sections, located in A. B. Detail of mud clasts and sediment dike. C. Distribution of mud clasts in outcrop. D. Detail of outcrop showing a decrease in quantity of mud clasts farther from the dike. Photograph was taken slightly oblique to outcrop. E. Mud lamina in outcrop; note blue mud clasts are no longer present in outcrop.

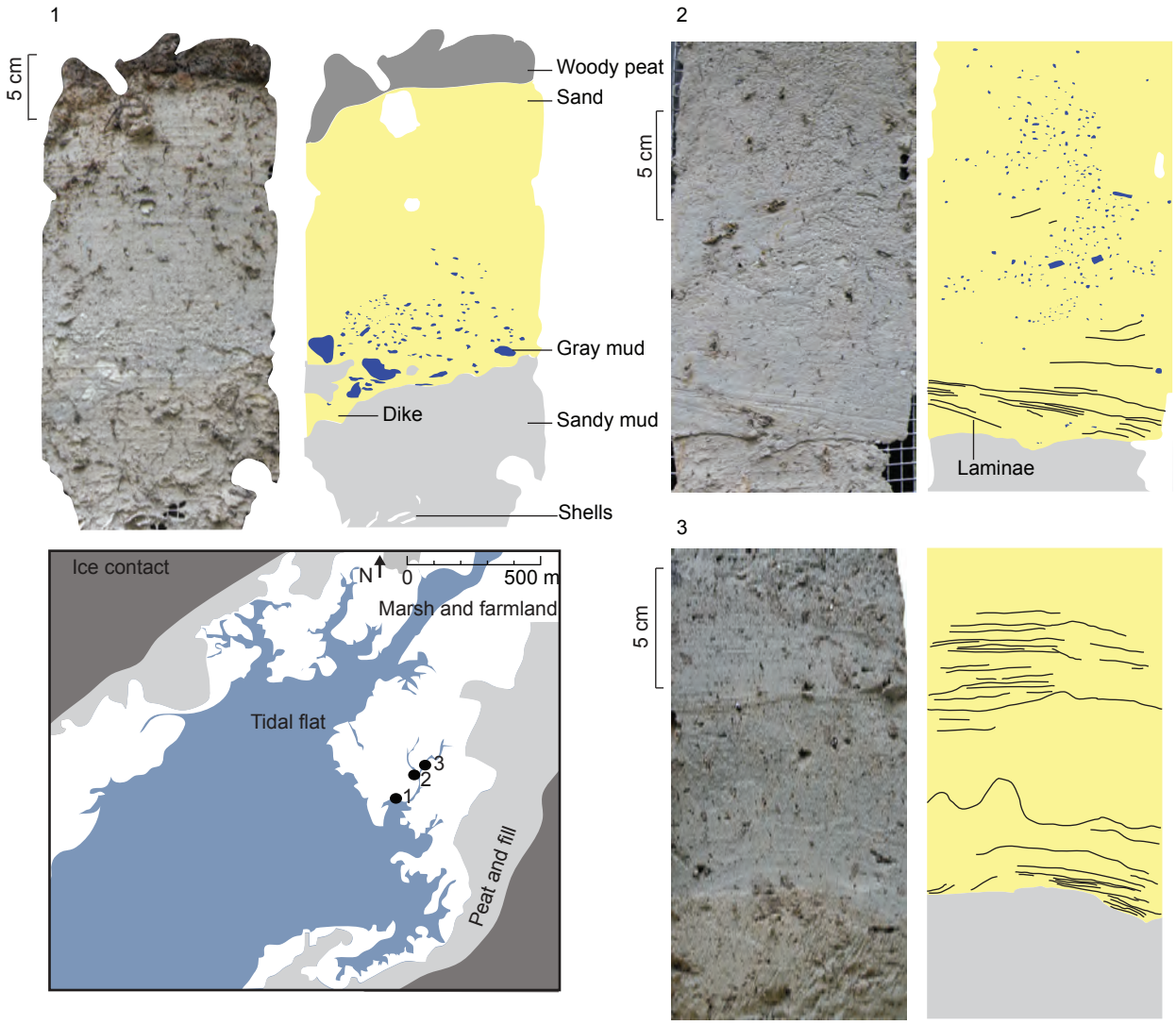

Figure 2.11 Peels of the vented sands at Lynch Cove

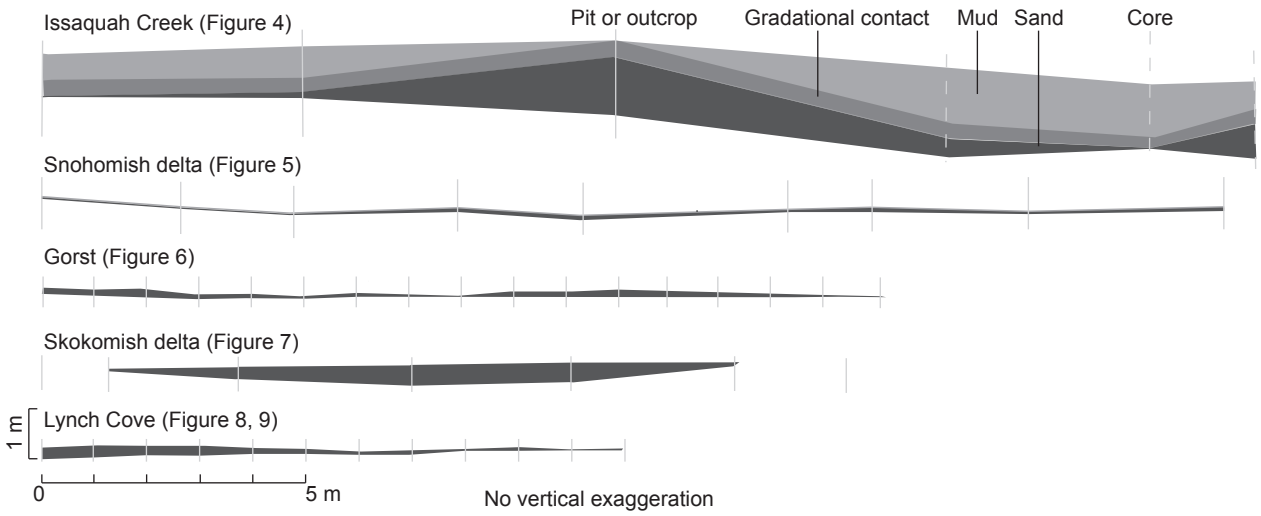

Figure 2.12 Measured vertical sections of thickness of studied sandy sediment units in outcrop plotted at the same scale (see also Figs. 5, 9 and 10).

CHAPTER 3

Superposed sedimentary evidence for uplift, a tsunami, and a sandy debris flow from an earthquake about 1,100 years ago near Bremerton, Washington

3.1 INTRODUCTION

The Seattle fault zone, a series of active east-west trending thrust faults, poses a seismic threat to the Puget Sound region, but the structure of the fault and the lateral and down-dip extent of a rupture AD 900-930 are not established (Figure 3.1). Though constrained by surface ruptures, uplifted bedrock and seismic imaging (Gower et al., 1985; Bucknam et al., 1992; Johnson et al., 1999), models for the underlying structure of the fault zone vary (Pratt et al., 1997; Johnson, 2004; Brocher et al., 2004; ten Brink et al., 2006; Kelsey et al., 2008; Liberty and Pratt, 2008). Many of these models use the distribution of marine terraces uplifted in an AD 900-930 earthquake to validate the subsurface geometry hypothesized from geological and geophysical studies of the fault zone.

This study identifies additional evidence for uplift in coastal marsh facies that may influence models of deformation. This study also documents two other kinds of stratigraphic evidence for a paleoearthquake in the Puget Lowland near Bremerton (Gorst locality, Figure 3.1) and thereby extends the geographic record of tsunami and debris flows for the AD 900-930 earthquake.

The field locality at Gorst (Figure 3.2) is situated to record paleoearthquakes and their geological effects. At the end of Sinclair Inlet (Figure 3.1), Gorst lies to the south and west of

uplifted bedrock terraces and has the potential to extend the zone of known deformation of the AD 900-930 Seattle fault earthquake. Also, the low-lying area makes it a potential recorder of tsunamis and slope failure triggered by this and other earthquakes. Expanding the mapped record of this earthquake is important for the entire Puget Lowland metropolitan area and especially because Gorst lies less than four kilometers from Bremerton and its Naval Base.

3.1.1 Stratigraphic evidence for a large earthquake

Cores and excavations in the wetlands fringing the terminus of Sinclair Inlet (Figure 3.2) reveal a sedimentary sequence of marine mud sharply overlain by sandy deposits and freshwater peat. Outcrops, pits and cores in the remnant wetlands reveal an abrupt upward change from sandy mud with articulated bivalves to freshwater forest peat, a change in the modern that requires at least a 3-m elevation rise (Figure 3.3 and 3.4). In lower lying areas, forest peat is in turn overlain by salt-marsh peat of the modern depositional environment, indicating (subsequent) submergence. In some areas, the mud-peat contact is separated by two sandy deposits (Figure 3.2); the lower sand unit (Unit A) is present only in the low-lying wetland, and the upper unit (Unit B) extends from the wetland up the valley of Gorst Creek for two kilometers. I interpret these sandy layers as rapidly accumulated event deposits of a tsunami (Unit A) and a debris flow (Unit B). This study examines the origin of the vertical facies changes in the wetland and of the sandy deposits in order to determine their age and source, as well as the relation of prehistoric events at Gorst to other events of the same age in the Puget Lowland.

3.2 GEOLOGICAL SETTING

Much of the geology and geomorphology of the Puget Lowland is explained by its position as the forearc basin of the Cascade Range and the glacial history of the region. Discussed below are the Pleistocene and Holocene geological history of the lowland and an examination of the impact of location and glaciation on the preservation of paleoseismological records.

3.2.1 Puget Lowland Quaternary history

Understanding the tectonic history of the Puget Lowland necessitates an understanding of its Pleistocene glacial history as well. The Puget Lowland is a glacially modified zone, bounded by the Olympic Mountains to the west and Cascade Mountains to the east (Figure 3.1). Several mostly east-west-trending faults run beneath the lowland, and though none has generated a large (Mw >7) historical (since ~1850) earthquake, they have generated large Holocene earthquakes (Ludwin et al., 1994; Bucknam et al., 1992; Sherrod et al., 2004; Sherrod et al., 2008; Blakely et al., 2009).

Pleistocene glacial ice sheets modified the Puget Lowland and obscured portions of the geological history of the region. The last glaciation, the Fraser glaciation, reached its peak in the Vashon stade ~15 ka (Booth, 1994). Associated with the Fraser glaciation are glacial till, advance, outwash, and lake deposits (Figure 3.2). Glacial overprint obscured the long-term seismic history of the area by beveling the landscape and blanketing much of the Lowland with Pleistocene deposits, masking offset along faults.

After retreat of the ice sheets, the regions sea level rise tapered off ~5,000 years ago (Clague and Boborowsky, 1990; Dragovich et al., 1994), but the Puget Lowland shows

evidence of relative sea level variations since this time. Due to the low viscosity of the mantle below the Puget Lowland the majority of isostatic rebound was completed by 9,000-10,000 years ago (James et al., 2000). Peat stratigraphy from northern Hood Canal shows a gradual relative sea level rise of about 6 m the last 6000 years with less than 1 m of the rise in the last 1,000 years (Eronen et al.1987). Beale (1990) worked at six marshes in the region and found a similar sea level rise in the last 1,000 years. Also in eastern Puget Sound, using almost 100 years of tide gauge records, Holdahl et al. (1989) found 1-2 mm submergence a year, yet Verdonck (2006) found no evidence for submergence using tide gauges. Compiling a variety of geologic records, Shipman (1989) predicted the area around Gorst to be submerging 1 mm/yr.

In some areas, ruptures on shallow faults have resulted in Holocene changes in relative sea level. Rupture on multiple faults about 1,100 years ago generated a wide variety of geological records in the Puget Lowland with many of these records linked to the Seattle fault zone (Figure 3.1). The Seattle, Tacoma, Saddle Mountain, and Olympia fault zones show evidence for rupture during this time period (Bucknam et al., 1992; Sherrod et al., 2004; Hughes, 2005; Sherrod, 2001).

3.2.2 Seattle fault zone

The Seattle fault zone location and structure are known from seismic reflection, uplifted bedrock, and evidence of an earthquake dated to AD 900-930 (Johnson et al., 1999, Haeussler and Clark, 2000; Atwater, 1999; Figure 3.1). The Seattle fault zone is a blind thrust fault with subsidiary faults. Near the main arm of Puget Sound, the Seattle fault zone is traced well based on seismic reflection surveys (Johnson et al., 1999) and on coseismic deformation from a large fault rupture AD 900-930 (Bucknam et al., 1992; Nelson et al.,

2003; ten Brink et al., 2006; Kelsey et al., 2008). This earthquake, estimated to have been Mw 7.0-7.5 (ten Brink et al., 2006) uplifted marine terraces along Puget Sound (Bucknam et al., 1992; Ota et al., 2006; Figure 1C). To the east the Seattle fault zone can be traced east of Lake Sammamish where it possibly interacts with the South Whidbey Island fault zone (Liberty and Pratt, 2008). To the west, uplifted bedrock near Gorst (Haeussler and Clark, 2000; Figure 3.2, Eocene basalt) indicates the Seattle fault zone extends into this region.

Several uncertainties remain about the extent of the Seattle fault zone (Figure 3.1) and about the specifics of a fault rupture dated to AD 900-930 (Kelsey et al., 2008; Liberty and Pratt, 2008; Atwater, 1999). 1) There is no consensus on the specific structure of the fault (Pratt et al., 1997; Johnson et al., 1999; Blakely et al., 2002; ten Brink et al., 2006; Kelsey et al., 2008; Liberty and Pratt, 2008). 2) The east-west extent of the Seattle fault is unknown, but recent studies have attempted to trace it across Hood Canal (Blakely et al., 2009; Karel et al., 2008). 3) Beyond the extent of the terraces, the zone of deformation associated with the AD 900-930 earthquake is not well mapped. To the east, no evidence of surface rupture has been found on faults near the western shores of Lake Sammamish (Sherrod, 2002) though movement on the blind thrust is possible in this area. To the west, no evidence of coseismic deformation has been published previous to this study, which traces influence of the AD 900-930 event several kilometers west and south of the mapped terraces (Figure 3.1C).

3.2.3 Gorst

The geology of the Gorst Creek drainage shows evidence of both long-term uplift and glacial overprinting. Uplifted Eocene basalts crop out to the north of the Gorst Creek drainage and Sinclair Inlet (Haugerud, 2009; Figure 3.2). The basalts are part of the uplifted bedrock of the Seattle uplift, which is part of a series of basins and uplifts in the Puget

Lowland (Figure 3.1). Blanketing the basalt are unconsolidated deposits of the last glacial maximum. Outwash sands and dead-ice deposits abound along the Gorst Creek drainage (Figure 3.2). In many areas surrounding Gorst, landslides and slope failures have reworked glacial deposits (Haugerud, 2009; Figure 3.2).

The Gorst locality consists of three main modern environments—the forest and alluvial plain along Gorst Creek, the urbanized zone between Otto Jarstad Park and Sinclair Inlet, and the alder swamp and salt marsh of the wetlands (Figure 3.2). The wetlands consist of fresh- and saltwater marsh and swamp. The end of Sinclair Inlet has an extensive muddy intertidal zone that accommodates a spring-tide range of 3.58 m as measured at the tide gauge at Bremerton (Mofjeld et al., 2002).

Settlement of the Gorst locality began before the first U.S. Coastal Survey maps were made of the area in 1881 (Ellicott, 1881). After the area was logged, the City of Bremerton protected the Gorst Creek drainage first as a municipal water supply and then as salmon habitat. Currently, people have built on much of the flat, low-lying areas, thereby impeding geological studies.

3.3 LAND-LEVEL CHANGES, TSUNAMIS, AND DEBRIS FLOWS

Sedimentological features are tools in the reconstruction of events associated with past earthquakes (McCalpin, 2009). For example, abrupt tectonic land-level change can both induce environmental changes and trigger tsunamis, leaving behind sharp facies changes and tsunami sand layers, respectively. Strong shaking can generate liquefaction and landslides, and these events can leave behind vented sands and deposits of gravity-driven flows. Differentiating between seismic and non-seismic initiation of these features can be difficult,

although multiple features appearing in conjunction strengthen the argument for seismic triggering.

The Seattle fault-zone rupture has been linked to land-level change (Bucknam et al., 1992; Ota et al., 2006; Figure 3.1), surface rupture (Nelson et al., 2002; Sherrod et al., 2004; 2005) and secondary features such as tsunami deposits, landslides and liquefaction features (e.g. Atwater and Moore, 1992; Karlin and Abella, 1992; Bourgeois and Johnson, 2001; Chapter 2). At the Gorst locality, there is evidence of abrupt land-level change, a tsunami and a debris-flow deposit. The following section outlines the processes relevant to the study at Gorst and their expected stratigraphic record.

3.3.1 Coseismic land-level change

During thrust and normal-faulting earthquakes, rapid environmental change can occur in areas sensitive to seismically triggered variation in land level. This land-level change can be cumulative and thus long term such as in flights of uplifted Quaternary and Holocene marine terraces (Lajoie, 1986) or can be transient (that is, subsequently reversed) such as in subduction cycles in some localities (e.g. Shennan et al., 1996). In deltas and marshes, the vegetation and microfossil assemblages most sensitive to land-level change are typically near shorelines, where decimeter changes in sea level can induce salinity changes, and in areas where fault motion changes the water table. These changes have been documented using micro- and macro-fossils as proxies for facies changes by comparing fossil assemblages to modern assemblages (e.g. Mathewes and Clague, 1994; Sawai et al., 2004). Other indicators of rapid, coseismic land-level change include sharp facies changes, especially those without an intermediate step; e.g., a high-salinity to low-salinity facies without intervening moderate-salinity facies indicates rapid uplift.

Previous studies of coseismic land-level change in the Puget Lowland have successfully used stratigraphy and macro- and microfossil changes to document Holocene fault movements. Bucknam et al. (1992) used both abrupt facies changes in marsh stratigraphy and uplifted marine terraces in several sites in the central Puget Lowland as evidence for earthquakes 1,100 years ago. Delta and marsh stratigraphy in the southern Puget Lowland also reveals evidence for facies changes linked to fault rupture (Sherrod, 2001; Barnhardt and Sherrod, 2006). On the Snohomish delta north of Seattle, abrupt facies changes indicating rising water were interpreted by Bourgeois and Johnson (2001) as evidence of local subsidence due to strong shaking, rather than to fault-induced subsidence.

3.3.2 Tsunamis

Tsunamis are impulse-initiated, long-period, surface-gravity waves that can both erode and deposit sediment on coastlines. Tsunamis are most commonly generated by coseismic deformation of the sea floor (or lake bottom) and by landslides under or into water, both of which rapidly disrupt the water column. A tsunami wave train can lead to multiple inundations of a coastal area, and as each wave comes onshore it erodes while accelerating and deposits while decelerating (e.g., Gelfenbaum and Jaffe, 2003). Different phases of tsunami flow can result in deposition, including slowing of flow, reversing of flow, and gravity-driven outflow (Paris et al., 2007).

While no single characteristic defines tsunami deposits, many tsunami deposits share certain characteristics (see Chapter 2). High-energy transport and grains falling out of suspension commonly dominate tsunami deposition on a coastal plain. Suspended-load sedimentation typically leads to massive, laminated, or fining-upward sandy deposits (Bourgeois, 2009). Tsunami deposits are also often described as thin (typically less than 25

cm thick), sheet-like, thickening into depressions, and fining landward (e.g., Dawson and Shi, 2000; Tuttle et al., 2004; Morton et al., 2007).

The Puget Lowland has several historical tsunamis and paleotsunamis. Historical tsunamis such as the 1-2-m 1949 tsunami near Tacoma (Chleborad, 1994) have all been landslide generated and are typically small, local, and unlikely to leave a geologic record. The best studied example of a paleotsunami deposit in the Puget Lowland is a sand layer, likely left by a tsunami from the AD 900-930 Seattle-fault earthquake, which has been well studied in several locations (Atwater and Moore, 1992; Bourgeois and Johnson, 2001; Figure 3.1).

3.3.3 Debris flow

Debris flows are mass flows that occur when a sediment-charged flow becomes concentrated to the point that fluid is no longer the transporting medium and grains cannot settle independently (Scott and Peterson, 1989). Debris flows commonly originate as saturated-slope failures that then transform into debris flows. Initial slope failure can occur with or without a generating impulse (e.g. earthquake or volcanic eruption), and other factors can play a role including slope steepness, sediment cohesion, and destabilization such as by undercutting of a slope. Saturation can occur before slope failure or after the sediment is in motion. As saturated sediment begins to flow down-slope it becomes a gravity-driven flow of a sediment-water mixture (Takahashi, 1981; Iverson, 1997; Major, 1997).

Typically, debris-flow deposits are characterized by massive bedding, but debris-flow characteristics and deposits even of a single flow can vary through space and time (Pierson and Scott, 1985; Scott, 1988). Debris flows are thought either to freeze or to evolve into more dilute flows. In more dilute flows the deposit becomes more stratified downstream and up

section. The deposits from this more dilute flow can exhibit more internal sedimentary structure and fewer fines than a less dilute flow (if the original material contained clay and fine silt) (Pierson and Scott, 1985). In experimental work, Major (1997) found saturated flows typically lack internal structure even when the deposit represented multiple debris-flow surges. In some cases, the base of a debris flow deposit is finer than the upper portion of the deposit (inverse grading), a characteristic observed in many ancient debris-flow deposits (Vallance and Scott, 1997; Zehfuss, 2005).

Prior work in the Puget Lowland has focused on historic and prehistoric slope failures and debris flows generated by weather and by tectonic and volcanic activity. Most historic cases are linked to unconsolidated glacial deposits and prolonged winter rainy seasons that along with steep slopes make the region prone to landslides (Thorson, 1989; Shipman, 2001). In the geological record, landslides and turbidity currents in lakes, and rockfalls in the Olympic Mountains have been linked to fault ruptures about 1,100 years ago (Karlin and Abella, 1992; Logan et al., 1992; Schuster et al., 1992). However, the largest and best-understood debris-flows deposits in the Puget Lowland are from Cascade-volcano lahars (e.g. Pierson and Scott, 1985; Scott et al., 1995; Zehfuss, 2005). There have been few detailed studies of other types of subaerial debris flows in the Puget Lowland.

3.4 METHODS

At Gorst, I quantified land-level change relative to sea level using a combination of field surveys and lab analysis, with results compared to modern analogs. In conjunction with the relative sea level work, I mapped two anomalous sand deposits at a stratigraphic contact indicating uplift (relative sea level drop). Finally, I conducted tsunami modeling to bracket

timing and magnitude of events. Each site was located using a hand-held GPS and was plotted onto a georeferenced map (Figure 3.5).

Radiocarbon dates helped to correlate the stratigraphic units to other events in the Puget Lowland. Material from outcrops was subsampled in the field and lab and sent to Beta Analytic and the National Ocean Sciences Accelerator Mass Spectrometry Facility (NOSAMS) for radiocarbon dating. A marine reservoir correction of 400 years was used for the date on the bivalve shell.

3.4.1 Relative sea level change

The record of land-level change in Gorst stratigraphy is quantified using a combination of field survey of modern vegetation, delineation of stratigraphy, and lab analysis of macrofossils. Key indicators of land elevation relative to sea level are sedentary organisms such as nestling clams and rooted vegetation. To quantify the relationship of paleo- to modern vegetation, this study measured a topographic profile using a transit and hand level and then mapping modern vegetation along the profile (Figure 3.3) to compare to macrofossils in peat samples. For this profile, I used species-cover abundance to characterize different vegetation zones, with the vegetation zones of Sherrod (1999) serving as a basis for grouping the data from Gorst. I compared time and sea level of the profile to sea level at the Bremerton tide gauge. The shells of mollusks and fragments of plants were collected from the stratigraphy and identified in the lab.

Macrofossils of plants and mollusks from different stratigraphic units characterize the ancient environments. For macrofossil faunal and floral analysis, I took bulk samples in the field, and then picked and identified macrofossils under a binocular microscope in the lab. For identification I used botanical reference collections from the University of Washington

Biology department and faunal reference collections from the University of Washington Burke Museum. Yuki Sawai examined the diatoms of some samples.

3.4.2 Sandy deposits

In order to interpret the mode of deposition of the sandy deposits that in places lie at the shelly-mud – woody-peat contact, I mapped the two sand bodies and described their internal characteristics, both in outcrop and in the subsurface (Figure 3.5). I used peat-, auger- and vibra-coring, as well as hand-dug excavations and backhoe trenches to examine the stratigraphy. This work resulted in over 100 stratigraphic sections (Figure 3.5; Appendix 2). Where possible I made excavations and cleaned cut banks to observe the sedimentary structures and variability within the deposit. Where the deposit displayed internal structures, I made sedimentary peels of excavation walls or sampled monoliths to examine these structures (e.g., Fig 3.4E and F).

I used grain-size analysis to compare sandy deposits to various sedimentary sources. Grain size was measured using a settling column and a Retsch CAMsizer. In the studied sections, I took samples at 1-cm intervals from outcrops in the field and monoliths in the lab. I also took bulk samples from various glacial outcrops and the creek bed to compare with the sandy deposits in question.

3.4.3 Tsunami modeling

In order to simulate the hypothesized paleotsunami from about 1,100 years ago, I used standard methods for establishing fault parameters and for modeling tsunamis. Sea-floor deformation was created from fault parameters using a model based on Okada (1985). Modeling of Seattle and Tacoma fault scenarios used GeoClaw (LeVeque and George, 2008; Berger et al., in press; LeVeque et al., in press). This forward model uses shallow-water-

wave equations and adaptive-grid refinement to simulate tsunami waves across bathymetry and onto topography. The input of bottom friction in the form of Manning's formula used a coefficient of 0.025.

Model simulations used the combined bathymetry and topography of the Puget Lowland by Finlayson (2005). The finest grid-cell size used was 0.0006875 degrees square (~76 m x 52 m). I used modern bathymetry and topography for modeling because the paleobathymetry is not well enough understood to use for this problem.

3.5 OBSERVATIONS AND INTERPRETATIONS

3.5.1 Field area

There are three main areas in the Gorst locality (Figure 3.2). The wetland fringes Sinclair Inlet and consists of modern salt marsh and freshwater swamp. Otto Jarstad Park is a former homestead site along Gorst Creek that is now a City of Bremerton park. I refer to the area upstream of Otto Jarstad Park as the Gorst Creek area. In each of these areas I documented many stratigraphic sections.

Multiple lines of evidence for a large earthquake about 1,100 years ago are present in stratigraphic sections below the wetlands and forest surrounding Sinclair Inlet. Sedimentologic and facies evidence for uplift, tsunami and debris flow indicates coseismic land-level change and strong shaking.

3.5.2 Evidence for relative sea level change

Observations

The difference in elevation between modern intertidal mudflat devoid of vegetation and the lowest trees and salt-intolerant vegetation is 0.9-1.1 m (Figure 3.3) a value in

agreement with other vegetation profiles in the Puget Lowland that found values of 1.2-1.5 m (Sherrod, 1999; Sherrod, 2001).

In stratigraphic sections, the basal sandy mud contains articulated bivalves and other shells (Table 3.1). Typically, the top 10-20 cm of the mud unit does not contain shells, possibly due to dissolution by acidic groundwater from the overlying peat. The shells indicate a lower intertidal environment (Kozloff, 1983; Megan Dethier, Friday Harbor Laboratories, personal communication, 2010).

The dark brown woody peat overlying the (sandy units and) shelly mud contains macrofossils of *Thuja plicata* (western red cedar), including trunks protruding from the marsh surface, and other swamp-forest species (Table 3.1). The lowest occurrence of this woody peat occurs 1.5 m below the lowest modern trees (Figure 3.3). A similar change from mud containing shells to freshwater peat also occurs at Ross Creek (Figure 3.1), 3 km down inlet from Gorst though no sand layer is present at this location

The woody peat has a sharp to gradational upper contact with a muddier peat containing salt-tolerant species including *Triglochin maritimum* (arrow grass) leaf bases and *Distichlis spicata* (salt grass) rhizomes.

A bivalve shell from the top 5 cm of the basal sandy mud unit dated to AD 790-1050 (Table 3.2). A *Tsuga heterophylla* cone from the basal 2 cm of the woody peat dated to AD 1240-1390 (Table 3.2; Figure 3.4).

Interpretation

Facies changes confirmed by macrofossils indicate the Gorst marsh site was uplifted at least 3 m 1,100 years ago and then later subsided. Macrofossil content in the sandy mud compared with the overlying woody peat indicates an environmental change from lower

intertidal to cedar swamp or forest (Table 3.1). In the modern environment, the minimum elevation difference between trees and the lower intertidal is approximately 3.5 m (Figure 3.3). I conservatively estimate a minimum uplift of 3 m because of fossil-free deposits about 0.5-m thick between the shelly mud and the forest peat. This value is a minimum because the mollusks' habitat extends for at least a meter below the upper elevation used in this calculation, and cedar forests extend many meters above their lowest limit used in this calculation.

Rapid uplift generated the change from intertidal to forest environment. This facies change is not due to sea level drop because there are no records of a rapid eustatic or Puget Sound basin sea level drop in the last 1,500 years; instead sea level has been rising in this time (Clague et al., 1982; Eronen et al., 1987; Beale, 1990; Dragovich et al., 1994). The interpretation of rapid uplift is based further on the sharp contact of the woody peat and mud unit (where sand is absent) and the stratigraphic skipping of salt-marsh facies expected in a normal prograding sequence. If the wetland's change from intertidal to freshwater was gradual, deposits from the lower and upper marsh environments would be expected in the stratigraphy as the area slowly emerged into progressively fresher-water environments. However, woody peat always overlies the shelly mud, and the only intervening deposits are tsunami and debris flow, not muddy marsh deposits.

Since the time of this uplift, the area has experienced submergence--in some locations, the cedar-forest peat is now eroding out into the intertidal zone. The difference in elevation between the lowest woody peat in cores and the modern equivalent environment is 1.5 m (Figure 3.3), indicating at least this much submergence since the abrupt uplift event. It is unclear if this submergence was rapid or gradual. Because the contact between the woody

peat and muddy peat is not always sharp and because the contact is between two adjacent facies in the modern environment, it is difficult to determine the rate of submergence.

3.5.3 Tsunami and debris-flow deposits

Observations

Two kinds of sand deposits intervene between the shelly-mud -- forest-peat contact in the wetlands along Sinclair Inlet (Figure 3.4) and one of these deposits can be traced in cut banks and cores along Gorst Creek. However, the sand units are not present on the northern shore of Sinclair Inlet and cannot be traced for more than a few meters laterally, away from and above Gorst Creek (Figure 3.5).

In wetlands sections, a silty sand deposit up to 1.6-m thick (Figure 3.4) lies at the abrupt facies change from sandy, shelly mud to peat (Figure 3.5; 3.6). It has a sharp basal contact and a sharp to gradational contact with overlying peat and soil. The deposit in the wetlands typically contains two units. The lower unit, Unit A, fines upward from medium and coarse sand and pebbles to fine sand and silt, in places capped by a thin, discontinuous mud lamina. Unit A is overlain by Unit B, dominated by silty, fine to medium sand. Of the 75 measured sections in the wetlands, in 23 I was able to differentiate a contact between the Unit A and Unit B, the contact marked by a mud lamina (Figure 3.4); that is, the mud lamina marks the boundary between the upper and lower sand where present. Where the lamina is not present, the similar grain sizes of Unit B and the upper portion of Unit A make the contact difficult to distinguish, especially in cores. Where the contact between the Unit A and B was not distinguishable, I could not measure the thickness of (or confirm the presence of) the lower sand.

Unit B extends upstream along Gorst Creek for at least 2 km (Figure 3.5). The deposit remains >50 cm thick except for where it has been cut into by people. Based on 14 cores and cut banks and three backhoe trenches, I divide Unit B into two Units--Unit B1, which is largely massive, and Unit B2, which contains cross laminae.

Unit C is found only in the wetlands. It differs from Unit A and B based on sedimentary structures and grain size.

Unit A

Unit A is characterized by normal grading, typically fining from coarse sand and pebbles upward to fine sand. It is found only in the wetlands. Pebbles consist of lithics or rounded mud clasts similar to clasts in the modern tidal channels. The mud lamina caps Unit A in some sites and is less than 0.5 cm thick. In one site, (Figure 3.4E) the mud lamina is deformed into flame structures 0.5-1.5 cm high. Where possible to measure, Unit A is typically 5-7 cm thick, and up to 24 cm thick. It is thickest in lower-elevation sites and is observed to thicken into depressions, for example, in the g3 excavation (Figure 3.4). Also, in some sites, the sand fills invertebrate burrows into the lower muddy unit. I found no datable material in Unit A.

Unit B

A typically massive basal deposit (Unit B1) overlain by laminae and cut-and-fill structures (Unit B2) characterize Unit B. In the wetlands, the sedimentary structure of the deposit is mostly massive (B1) though in some locations the unit contains one or more laminae in the upper portion. At Otto Jarstad Park, the basal 5-8 cm of the deposit (B1) is massive fine sand and silt with rare soft-sediment clasts. Unit B1 has a sharp upper contact with B2, a fine to medium sand with cross-laminae (Figure 3.5; 3.7). Along Gorst Creek,

Unit B1 is 30 cm thick and contains rip-up clasts and leaves near the base. Overlying Unit B2 is 70 cm thick and contains structures including inclined laminae and coarser and finer layers (Figure 3.5),

Unit B is over a meter thick in some locations but typically is 30-40 cm thick (Figure 3.5). In general, Unit B thins and becomes patchier perpendicular to Gorst Creek, up the side of the valley, and at higher elevations (Figure 3.3; Figure 3.7 trench 3; Figure 3.8). Of the three backhoe trenches at Otto Jarstad Park, in the one closest to the slope (trench 3) the deposit is thinner and patchier than in the other two trenches.

Charcoal from the paleosol below Unit B in Otto Jarstad Park gave a date of AD 570-690 (Table 3.2). Along Gorst Creek, the base of Unit B1 contains rip-up clasts of peat and leaves (Figure 3.5). Three different leaves from the lowest 5 cm of Unit B1, 2.3 km upstream from Sinclair Inlet, gave radiocarbon ages corresponding to AD 890-990, 720-940, and 690-880 (Figure 3.5; Table 3.2).

Unit C

In two, close-by sites in the wetlands, the shelly mud-peat contact is split by a local pebbly sand (Figure 3.9), Unit C. These locations are on the southwest end of the inlet near where a small drainage enters the wetlands. The deposits are faintly laminated and contain mud intraclasts. In no area in the wetland or along Gorst Creek do Units A and B contain such high concentrations of pebbles, so I call this deposit Unit C.

Interpretations

Age of coseismic uplift and sandy deposits

Radiocarbon dates from above and below the sand layers place the coseismic uplift in marsh and subsequent deposition of event beds at about 1,100 years ago (Table 3.2). This indicates

the events at Gorst correlate with the time period of ruptures on multiple faults in the Puget Lowland including the Seattle fault zone (Atwater, 1999; Sherrod et al., 2004; Barnhart and Sherrod, 2000; Blakely et al., 2009).

Unit A – Tsunami deposit

Unit A has many sedimentary characteristics typical of tsunami deposition (Chapter 2). Further, the deposit is temporally and geographically associated with an event known to have generated a tsunami (Atwater and Moore, 1992; Bourgeois and Johnson, 2001). Consistent with modern tsunami deposits, Unit A fines upward, in this case from coarse sand and pebbles to silt and fine sand. It has a sharp basal contact, a somewhat consistent thickness, and is stratigraphically associated with an apparently abrupt land-level change. The deposit disappears landward, indicating deposition from a Sinclair Inlet source, although the small geographic extent of the observed deposit limits conclusions that can be made about landward thinning and fining.

Intriguingly, Unit A is typically not found in areas where Unit B is not present, specifically on the northern edge of Sinclair Inlet (Figure 3.4). This may be because in areas where Unit B was deposited, it protected Unit A from erosion and bioturbation. In sites in the wetland where I was unable to distinguish the presence of Unit A, the Unit-B event may have eroded the underlying mud lamina and part or all of the Unit-A sand layer.

Unit B -- Debris-flow deposit

The mapped extent and internal sedimentary structure of Unit B indicate that it likely originated as a slope failure up Gorst Creek that then flowed down the creek as a sandy debris flow. The presence of the deposit along Gorst Creek but not along tributaries indicates the origin of the deposit from the watershed of Gorst Creek. The massive structure of the

deposit is consistent with deposition by debris flow rather than by a river. However, cut-and-fill structures and lamination in the upper portion of the deposit indicate the debris flow either became less concentrated through time or was later reworked by braided-stream processes. Channel processes are evident from the cross-laminae present in the upper portion of Unit B (Figure 3.7), and a braided stream is inferred from the sudden influx of sediment into the valley.

Thick, steep outcrops of recessional glacial outwash sands along Gorst Creek (Figure 3.2) provide likely source material for the slope failure and deposit. Also, it is possible that either a landslide or a landslide-dam failure generated the debris flow; prehistoric landslide-dammed lakes are known from the Puget Lowland (Logan et al., 1998). The exposures along Gorst Creek are commonly steep and comprise unconsolidated glacial-age materials including sand and laminated mud. If these moderately well-sorted outwash sands are the source material, it would explain why the deposit shows little variation in grain size (Figure 3.6).

Unit C—Reworked slope failure

The pebbly Unit C (Figure 3.9) in the wetlands likely represents local slope failure from another sediment source possibly from up the nearby drainage. The laminae indicate that deposition in this area may have been due to a lower-concentration flow than the Gorst Creek debris flow. The small spatial distribution of the pebbles indicates this sediment pulse was not as large as the one that blanketed the rest of the wetlands.

3.5.4 Tsunami simulations

Model parameters--fault slip and sea level

Tsunami simulations were used to replicate Seattle and Tacoma fault-zone tsunamis in Sinclair Inlet. Fault-slip parameters were based on previous regional tsunami simulation work for hazard analysis (Venturato et al., 2006) and on simulations validated using the tsunami deposit at Cultus Bay (Koshimura et al., 2002). Simulation runs included Seattle and Tacoma fault scenarios as well as a model with higher slip on the western end of the Seattle fault, the latter in order to represent the uplift I measured in the field (Table 3.3). Both the Seattle and Tacoma fault scenarios of Venturato et al. (2006) are based on reconstructing co-seismic uplift(s) that I correlate temporally with deposition of the tsunami sand sheet at Gorst. Using the parameters from Venturato et al. (2006), I also ran simulations of the Seattle and Tacoma fault zones rupturing at the same time to represent the hypothesized case of the Seattle and Tacoma fault zones rupturing simultaneously (Johnson et al., 2004; Sherrod et al., 2004).

I ran simulations at several different sea levels. Most simulations were run with the water at zero elevation though I ran various Seattle fault scenarios at approximately, modern MHHW (Mean Higher High Water, +3.5 m) and at MLW (Mean Low Water, -1 m). Previous modeling of the AD 900-930 Seattle fault zone tsunami (Koshimura et al., 2002) set the sea level to -1 m due to approximately 1 m of submergence of the Puget Lowland in the last thousand years (Eronen et al., 1987; this study). They concluded with a sea level 1 m lower than modern, that the tsunami would have needed to occur at high tide to explain the deposits at Cultus Bay (Atwater and Moore, 1992). Unlike Cultus Bay, Gorst is in the zone of coseismic deformation for the Seattle fault zone. Before the Seattle-fault earthquake, sea

level was relatively higher at Gorst. This higher sea level is demonstrated by marine shelly mud above modern tide range at the landward end of the modern vegetation profile (Figure 3.3). Therefore, because the tide level at the time of the tsunami is unknown, simulations at various tide ranges allowed me to examine the error in tsunami wave height from variability in paleo-sea level (Figure 3.10B)

Interpretation

All tsunami models based on the Seattle fault zone produced wave heights of 4.0-5.5 m at Gorst, and models based on the Tacoma fault produced significantly lower wave heights (0.2-0.5 m; Figure 3.10). For all Seattle fault-zone models the first wave is the largest of the tsunami wave train, with the wave reaching Gorst almost immediately after the earthquake and the peak amplitude arriving in less than 20 minutes. For Tacoma fault-zone models the second wave is the largest, and the first wave arrives after about 30 minutes, with the peak of the first wave at approximately 40 minutes. Simulating the Seattle and Tacoma faults rupturing at the same time did not increase the maximum wave height in Gorst but did increase the height of later waves in the tsunami wave train.

It is more likely that the Seattle fault zone generated tsunami deposited the sand layer at Gorst. The Tacoma-fault-zone scenario produced no more than a 0.5-m wave height at Gorst. It is unlikely a half-meter wave could produce the up to 20-cm thick deposit that is found in the wetlands, so I attribute the Unit A deposit to a Seattle fault zone tsunami. Because both faults rupturing at the same time did not change the wave pattern, the Seattle and Tacoma faults rupturing at the same time could also have generated the deposit at Gorst.

I ran simulations at various grid resolutions (Figure 3.10A) in order to test the ability of my grid resolution to simulate the tsunami waves. Other studies have shown that better

grid resolution typically increases wave height, although the waveform begins to converge at increasingly higher resolutions (Titov and Synolakis, 1997; Pan et al., 2010). Simulations at three resolutions show convergence of the waveform of the first, highest wave but divergence on later waves. Due to my interest in only the maximum wave height, I conclude my bathymetric grid accurately simulated the tsunami waves resulting from fault deformation.

3.5.5 Timing of tsunami and debris flow

Stratigraphic relationships between the deposits and thus the associated events indicate uplift, shortly followed by a tsunami, followed by a debris flow from up Gorst Creek (Figure 3.11). The close stratigraphic association of the uplifted paleo-surface with an overlying tsunami deposit is best explained if the uplift was co-seismic and the tsunami produced by the same regional co-seismic deformation. Modeling of the tsunami indicates it originated along the Seattle fault zone rather than the Tacoma fault zone.

How much time passed between the tsunami and the debris flow is not as well constrained. Flame structures within the capping mud of the tsunami deposit indicate this mud was still saturated when the debris flow covered the mud lamina, but the fine grains that form the lamina had time to settle out of suspension. Persistent saturation is more likely for a winter, rainy-season event, which is consistent with analysis of tree rings indicating the Seattle fault earthquake occurred between growing seasons of trees (Jacoby et al., 1992). Further constraints on timing include a lack of evidence of vegetation or soil formation on top of the lamina before burial by the debris flow. Given co-seismic uplift into a forest zone, this lack of weathering or vegetation indicates a growing season did not pass before the debris-flow sands were deposited.

If, as is likely, the debris flow was initiated by shaking, the tsunami and debris flow may have interacted, but the preservation of two distinct deposits in the wetlands do not support this interaction. Unit A likely was deposited by the 1st tsunami wave because it was the largest wave based on simulations. The mud lamina that separates the two deposits indicates at least a short time interval between the two events in the wetlands as mud needs time and deceleration to settle from suspension. The mud may represent the lull that occurred after the first wave, approximately one hour after the earthquake (Figure 3.10). Therefore, it is unlikely that the debris flow was initiated during the earthquake but rather occurred some time in the hours to weeks after the earthquake. Also, if a local slope failed during the earthquake and immediately formed a debris flow, that flow would have reached the wetlands about the same time as the modeled tsunami.

Estimations of debris flow speed indicate that the debris flow initiated some time after the earthquake or that the debris flow had a low velocity. Debris flow speed is dependent on slope, concentration and grain size of the flow (Iverson, 1997), and peak flow speeds for debris flows are over 36 m/s (Iverson, 1997), at which rate the Gorst debris flow would have traveled the 2 km from farthest mapped deposit in approximately a minute. However, the slope of Gorst Creek makes it unlikely the debris flow achieved that velocity. A velocity at the low end recorded for debris flows maybe more realistic. With a velocity of 1.8-2.0 m/s (Davies et al., 1992; Genevois et al., 2001) the debris flow would have entered the wetlands 15-20 minutes after traveling 2 km. However, it is likely that the debris flow initiated at some point farther upstream. The headwaters of Gorst Creek are approximately 4 km from the wetlands, and if the debris flow initiated there the slow debris flow would take

30-40 minutes to reach the wetlands. It is possible that an old-growth forest that formerly filled the Gorst Creek valley may have slowed the flow further.

Given the evidence and arguments that the debris flow was delayed long enough to allow a mud lamina to be preserved on top of the deposit of the tsunami's first wave, but short enough that there is no evidence of a passing season between the tsunami and debris flow, there remain several explanations for the stratigraphic order. 1) The debris flow was slowed by the low slope of Gorst Creek and the old-growth forest. 2) The debris flow was triggered by an earthquake on another fault or by an aftershock. 3) The slope failure occurred hours to days after the earthquake--although seismically generated landslides typically fail during the earthquake, in some cases, such as the 1949 Tacoma Narrows slide (Chleborad, 1994), slides occur days after the earthquake. 4) A landslide-dammed lake formed and later failed catastrophically (as in McCaffrey et al., 2009).

3.6 DISCUSSION AND CONCLUSIONS

3.6.1 AD 900-930 Seattle fault earthquake deformation

This study indicates a wider and higher band of coseismic deformation during the AD 900-930 Seattle-fault-zone rupture than previous fault interpretations (ten Brink et al., 2006; Kelsey et al., 2008), and this uplift may have implications for the fault structure. A minimum of 3 m of uplift at Gorst, as found in this study, is double the uplift estimated by previous fault models (Koshimura et al., 2002; ten Brink et al., 2006). This work indicates that the zone of deformation of the Seattle fault may not be as narrow as estimated by the presence of marine terraces. This study also shows evidence of uplift 3 km west and 1.5 km south of the farthest extent of mapped terraces. South of West Seattle, 3-m-high marine terraces are

traced approximately the same distance south of the Seattle fault as Gorst (ten Brink et al., 2006), indicating a broader zone of deformation along the length of the AD 900-930 rupture. A broader zone of deformation indicates either a wider slip on the fault, a shallower dip, or splay faults farther to the south. An anticline in the bedrock north of Gorst (Figure 3.1C) might also have been the origin of higher than expected uplift in Gorst. It is unclear if the anticline is an active or relict structure.

If Gorst's 1.5 m of submergence in the last thousand years cannot be explained as local compaction of sediments (which is unlikely), more uplift occurred along the Seattle fault in AD 900-930 than has been estimated previously. Widespread submergence would indicate that marine terraces formed in that event were originally 1.5 m higher above sea level than they are at present. This would increase the terrace height by 14-90% (Figure 3.10). If so, refined values of terrace heights including the additional 1.5 m may have an impact on reconstructions of fault geometry and slip. Moreover, the 1.5 m of submergence in the 1,100 years since the earthquake may have obscured the uplift record in areas with only a meter or two of coseismic uplift as these lower terraces would now be within the tidal range. Higher uplifts support my conclusion that the band of deformation from the AD 900-930 earthquake was broader than previously modeled.

3.6.2 Timing and causes of post-seismic submergence

Return of co-seismically uplifted, forested area to intertidal conditions occurred some time between AD 1520 and AD 1880 in portions of the wetlands. I base these constraints on an *in-situ Thuja plicata* snag in what is now the salt marsh and on the earliest maps of the region. Based on radiocarbon dating this snag died between AD 1520 and 1660. The tree had 218 rings indicating that the area remained habitable for trees for several hundred years after

the co-seismic uplift event about AD 900-930 (Carolyn Garrison-Laney, unpublished data). The earliest U.S. Coastal Survey map of the Gorst area shows the salt marsh at approximately its current extent (Ellicot, 1881). Therefore, the return to intertidal conditions occurred sometime between when the tree was alive (AD 1520 and 1660) and when the area was first mapped (AD 1880). These dates do not indicate if there was a rapid submergence event after AD 1520 or if slow submergence returned the forest to the intertidal zone after this time.

The source of the post-earthquake submergence is not well understood but is likely due to a combination of sediment compaction and processes related to the subduction zone. The minimum value of submergence I found at Gorst is 1.5 m in 1,100 years. A portion of the submergence is likely due to compaction of the marine mud and other deposit underlying the wetlands. In the northeastern portion of the wetlands, there is less than 3 m of sediment above bedrock. Thin Holocene sediments indicate at least some areas of the wetlands have little submergence due to compaction. Therefore, compaction is likely not the only factor in submergence.

Peat records from other areas indicate little sea level variation in the time period of interest and a regional signal of submergence. Clague et al. (1982) and Williams and Roberts (1989) found little to no sea level variation in the last 1500 years in southern British Columbia indicating that the submergence in Gorst is not due to eustatic or regional sea level rise. Peat records from north of Gorst in the Puget Lowland indicate <1 m of relative sea level rise in the last thousand years calculated (Eronen et al., 1987; Beale, 1990). The submergence values for peat were calculated in marshes north of the study area. This rate is 50% lower than the rate seen at Gorst.

Gradual or punctuated submergence in the Puget Lowland has been linked to the forearc setting. Many authors ascribe gradual land-level change in the Puget Lowland to stress from the subduction zone (Reilinger and Adams, 1982; Holdahl, et al. 1989; Shipman, 1989; Mitchell et al. 1994; Hyndman and Wang, 1995; Long and Shennan, 1998). However, Garrison-Laney (2003) hypothesized submergence at Gorst and other sites in the Puget Lowland may be linked to the AD 1700 Cascadia subduction zone earthquake. Though the clustering of tree deaths before AD 1700 (Garrison-Laney, 2003) is intriguing, the submergence at Gorst falls within the gradual background rates related to Gorst's location in the forearc basin. Better stratigraphic control on sea level change through paleoenvironmental methods and dating would help to clarify the rate and timing of submergence.

3.6.3 Implications for hazard planning

This study reiterates the threat of multiple hazards associated with earthquakes in the Puget Lowland, of which tsunamis are prominent in the case of Sinclair Inlet. Tsunami deposits at Gorst and tsunami modeling reiterate the tsunami threat in this inlet. Evidence for a tsunami in Sinclair Inlet is not unexpected based on the proximity to the Seattle fault zone and on previous tsunami models (Koshimura et al., 2002). Simulated wave heights of 4-5 m indicate tsunamis are not only a threat to the infrastructure in Gorst but also to the Naval base at Bremerton. Even an order-of-magnitude smaller Tacoma fault-generated tsunami would generate strong currents in the narrow straits and harbors near Gorst. Further tsunami simulations in the Puget Lowland including different fault scenarios would help determine the degree of hazard posed by locally generated tsunamis.

The presence of debris-flow deposits at the Gorst site underlines the dangers of slope failures in glacial sediments during earthquakes. Events such as the reconstructed debris flow could pose a large threat to buildings and infrastructure such as fish hatcheries along streams, during and after future large earthquakes.

Understanding background submergence rates is important for planning for future sea level rise. A rate of submergence of 1.5 m per 1,100 years is higher than predicted for the Gorst region (Shipman, 1989). Currently, the long-term rate of submergence and the variability in this rate across the Puget Lowland are constrained by only a few data points. Studies and detailed dating would help to bracket the rate of submergence and produce better input for models of sea level rise.

3.6.4 Conclusions

Stratigraphic evidence for co-seismic uplift, a tsunami and a sandy debris flow 1,100 years ago is present at the terminus of Sinclair Inlet. This study indicates that at least 3 m of uplift likely preceded a tsunami followed by a sandy debris flow. Modeling indicates tsunami flow depth from a Seattle-fault-zone-generated wave train was between 4 and 5 m, and stratigraphy shows the tsunami left a sandy deposit. Though the Seattle and Tacoma fault zones ruptured within the error of dating at Gorst, modeling indicates the Seattle fault generates an order of magnitude larger tsunami in the vicinity of Gorst than the Tacoma fault (Figure 3.10). Slope failure in unconsolidated glacial sands likely initiated a debris flow that surged at least 2 km down Gorst Creek valley and left a more-than-40-cm-thick deposit along the creek and in the wetlands. Finally, if the 1.5 m post-seismic subsidence is tectonic then the both the earthquake and subsequent tsunami of the AD 900-930 earthquake were larger than previously known.

Table 3.1: Marine shells and plant macrofossils

Unit	Species	Common name
Sandy mud*	*Euspira lewisii*	moon snail
	Lottia pelta	limpet
	Nassarius mendicus	lean basket-whelk
	Nucella lamellosa	frilled dogwinkle
	Macoma nasuta	bent nosed clam
	Mytilus trossulus	mussel
	Ostreola conchaphilia	Olympia oyster
	Clinocardium nuttallii	heart cockle
	Saxidomus gigantea	butter clam
Woody peat	*Thuja plicata*	western red cedar
	Tsuga heterophylla	western hemlock
	Apiaceae seeds	
Muddy Peat	*Triglochin maritimum*	common arrowgrass
	Disticlus spicata	saltgrass

Shells present in basal marine mud indicating lower intertidal environment and plant macrofossils from woody peat indicating swamp environment. Shells are from the base of the g2 outcrop (Figure 3.4).
*Dr. Elizabeth Nesbitt of the Burke Museum aided in identifying the shells.

Table 3.2: Radiocarbon dates from Gorst

Measured, 14C yr BP	Calibrated 2 sigma range, AD	Limiting age	Material	Location	Laboratory and sample number
1540+/-70	790-1050	Limiting maximum for Unit A and B	Shell in mud 5 cm below sand units	Wetland 47.526528, -122.692889	BETA 263044
700 +/-40	1240-1390	Limiting minimum for Unit A and B	Abies cone in cm above sand units	Wetland 47.52655, -122.69600	BETA 263042
1390 +/-40	570-690	Limiting maximum for Unit B	Charcoal in 5 cm below Unit B	Otto Jarstad park 47.530485 -122.708573	BETA 263043
1100 ± 25	890-990	Limiting maximum for Unit B	Leaf in basal 5 cm of Unit B	Along Gorst Creek 47.52988, -122.71923	NOSAMS 78396
1240 ±30	690-880	Limiting maximum for Unit B	Leaf in basal 5 cm of Unit B	Along Gorst Creek 47.52988, -122.71924	NOSAMS 78395
1190 ±30	720-940	Limiting maximum for Unit B	Leaf in basal 5 cm of Unit B	Along Gorst Creek 47.52988, -122.71925	NOSAMS 78394

Calendar age was calibrated using IntCal 09 (Reimer et al., 2009) using the online program OxCal (https://c14.arch.ox.ac.uk/oxcal/). BETA samples were processed by Beta Analytic and NOSAMS samples were processed by the National Ocean Sciences Accelerator Mass Spectrometry Facility. The shell date has a marine reservoir correction of 400 years (Deo et al., 2004).

Table 3.3: Fault parameters from tsunami models

	Fault segment	Length (km)	Width (km)	Dip	Rake	Strike	Depth (km)	Slip (m)
Seattle NOAA[1]								
	S1	15.2	35	60	90	87.9	0.5	1
	S2	6.3	35	60	90	86.6	0.5	1
	S3	8.9	35	60	90	96	0.5	12
	S4	3.2	35	60	90	99.3	0.5	11
	S5	11.5	35	60	90	99.3	0.5	4
	S6	14.9	35	60	90	81	0.5	1
Seattle Koshimura[2]								
	K1	15.2	6	60	90	87.9	0.5	4
	K2	6.3	6	60	90	86.6	0.5	6
	K3	8.9	6	60	90	96	0.5	8
	K4	3.2	6	60	90	128.8	0.5	8
	K5	11.5	6	60	90	99.3	0.5	6
	K6	14.9	6	60	90	81	0.5	4
	K7	15.2	38	25	90	87.9	5.5	2
	K8	6.3	38	25	90	86.6	5.5	4
	K9	8.9	38	25	90	96	5.5	6
	K10	3.2	38	25	90	128.8	5.5	6
	K11	11.5	38	25	90	99.3	5.5	4
	K12	14.9	38	25	90	81	5.5	2
Tacoma NOAA[1]								
	T1	10	14.1	45	90	268.9	0.5	5.6
	T2	10	14.1	45	90	260.812	0.5	3.4
	T3	10	14.1	45	90	274.046	0.5	3.8
	T4	8	14.1	45	90	276.274	0.5	1.4
	T5	8	14.1	45	90	279.473	0.5	1.4
Seattle up slip[3]								
	U1	15.2	35	60	90	87.9	0.5	4
	U2	6.3	35	60	90	86.6	0.5	3
	U3	8.9	35	60	90	96	0.5	12
	U4	3.2	35	60	90	99.3	0.5	11
	U5	11.5	35	60	90	99.3	0.5	4
	U6	14.9	35	60	90	81	0.5	1

Depth is to the top of the fault segment.
[1]Venturato et al., 2006; [2]Koshimura et al., 2002; [3]Modified from Venturato et al., 2006

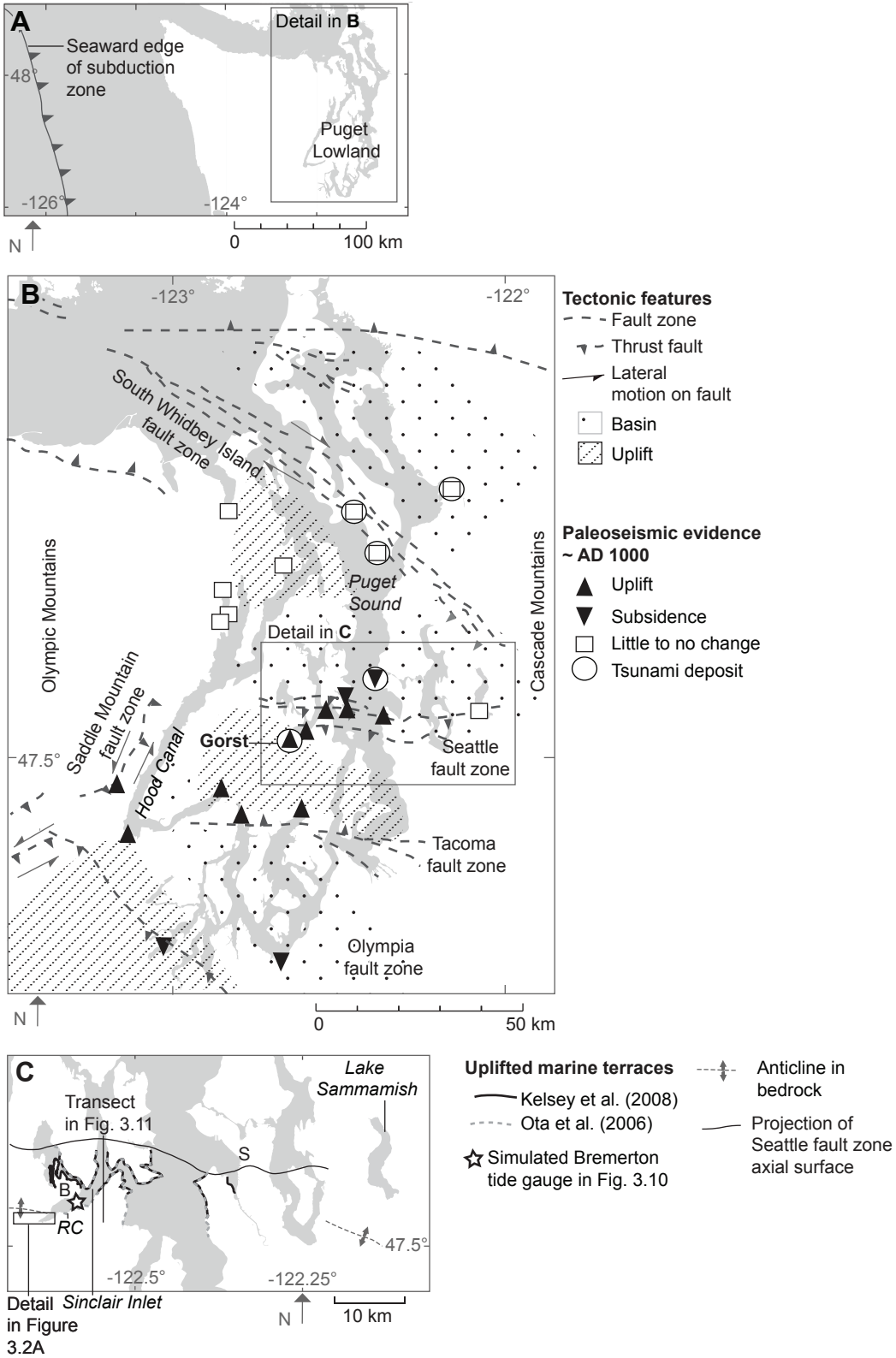

Figure 3.1 Maps of the tectonic setting of the Puget Lowland. A. Map of Cascadia subduction zone and coastline. B. Map of the Puget Lowland showing active faults and locations of paleo-seismic studies modified from Blakely et al. (2009). C. Location of mapped marine terraces associated with the AD 900-930 Seattle fault zone earthquake (Ota et al., 2006; Kelsey et al., 2008), *RC*=Ross Creek, B=Bremerton, S=Seattle. Projection of axial surface of Seattle fault zone from Kelsey et al. (2008)

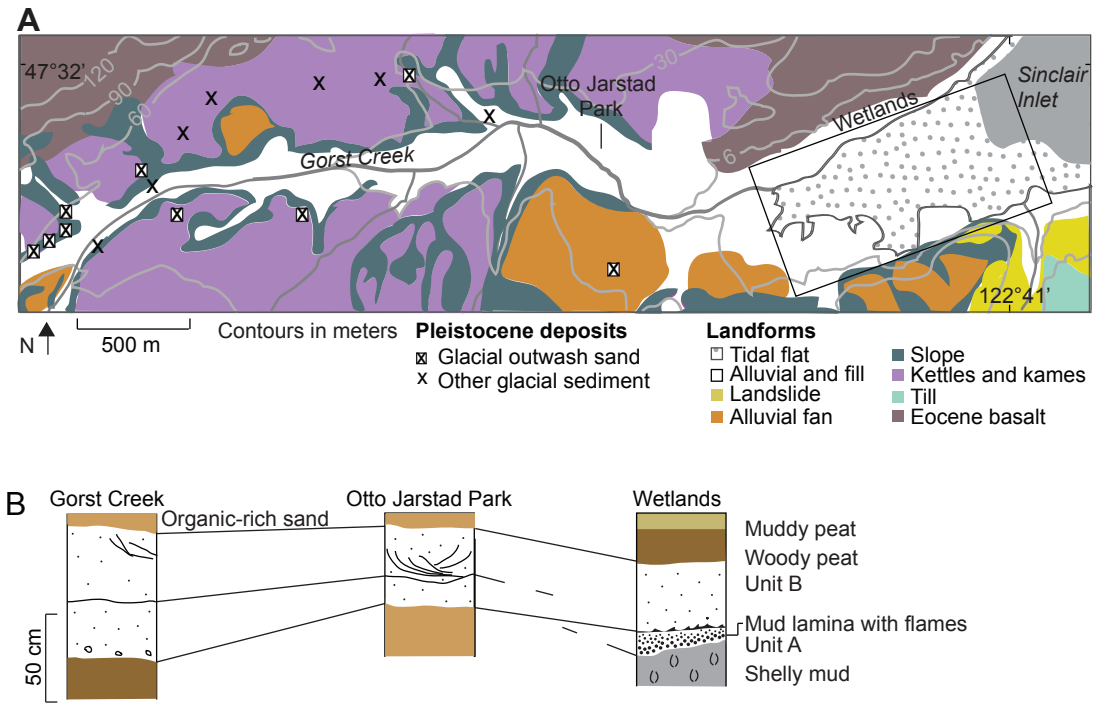

Figure 3.2 Map and generalized stratigraphic sections from Gorst. A. Geomorphic map of the Gorst Creek drainage and wetlands showing Pleistocene glacial outcrops and main areas of the field study showing widespread glacial outcrops. Map modified from Haugerud, 2009. "Wetlands" refers to swamps and marshes beside tidal flat B. Generalized sections from the field areas.

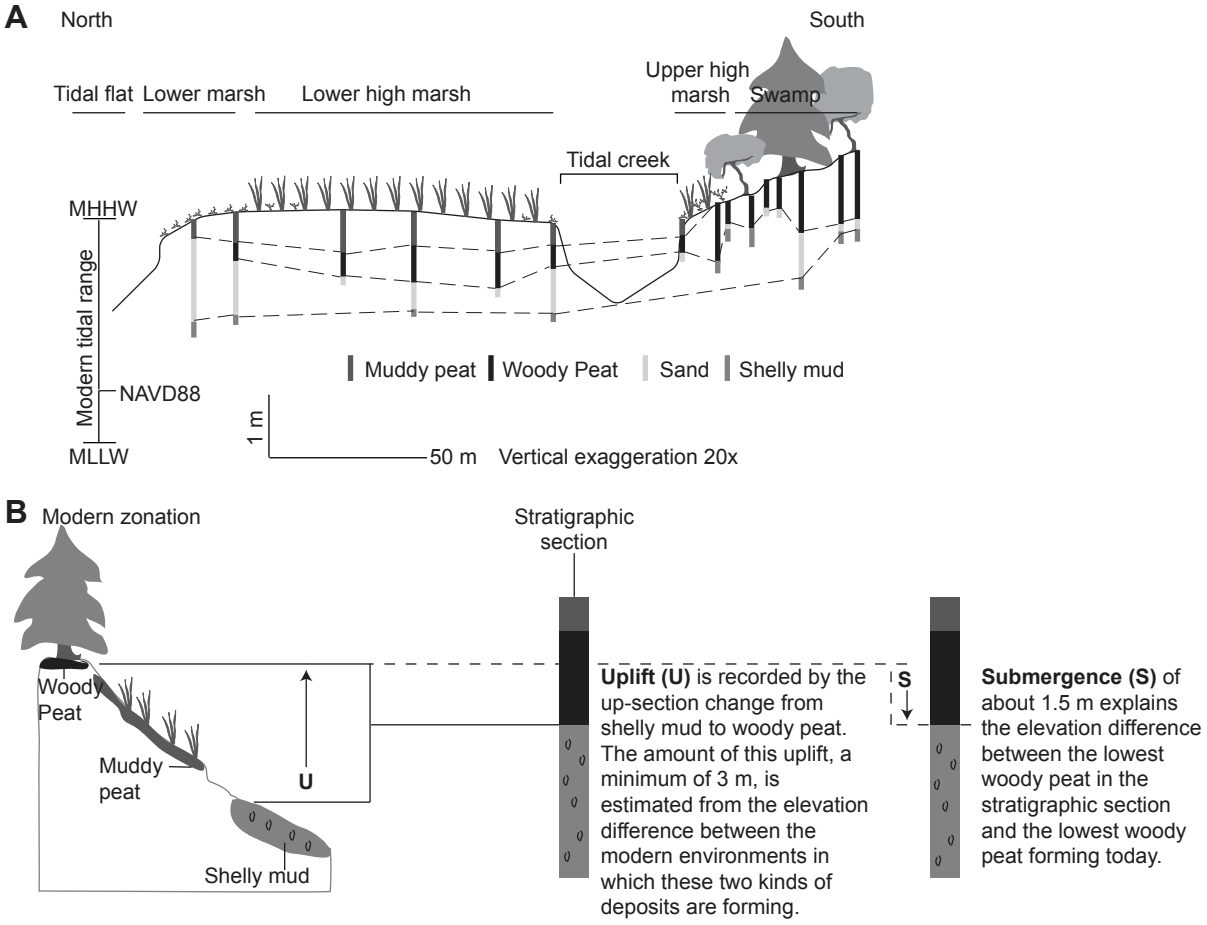

Figure 3.3 Modern environments and quantification of relative land level change. A. Topographic profile across Gorst marsh (location in Figure 2) detailing modern vegetation zones taken from Sherrod (1999) and stratigraphy. Bar to the left shows intertidal range between mean higher high water (MHHW) and mean lower low water (MLLW). B. Cartoons of stratigraphic and environmental elevations used in the quantification of land level change.

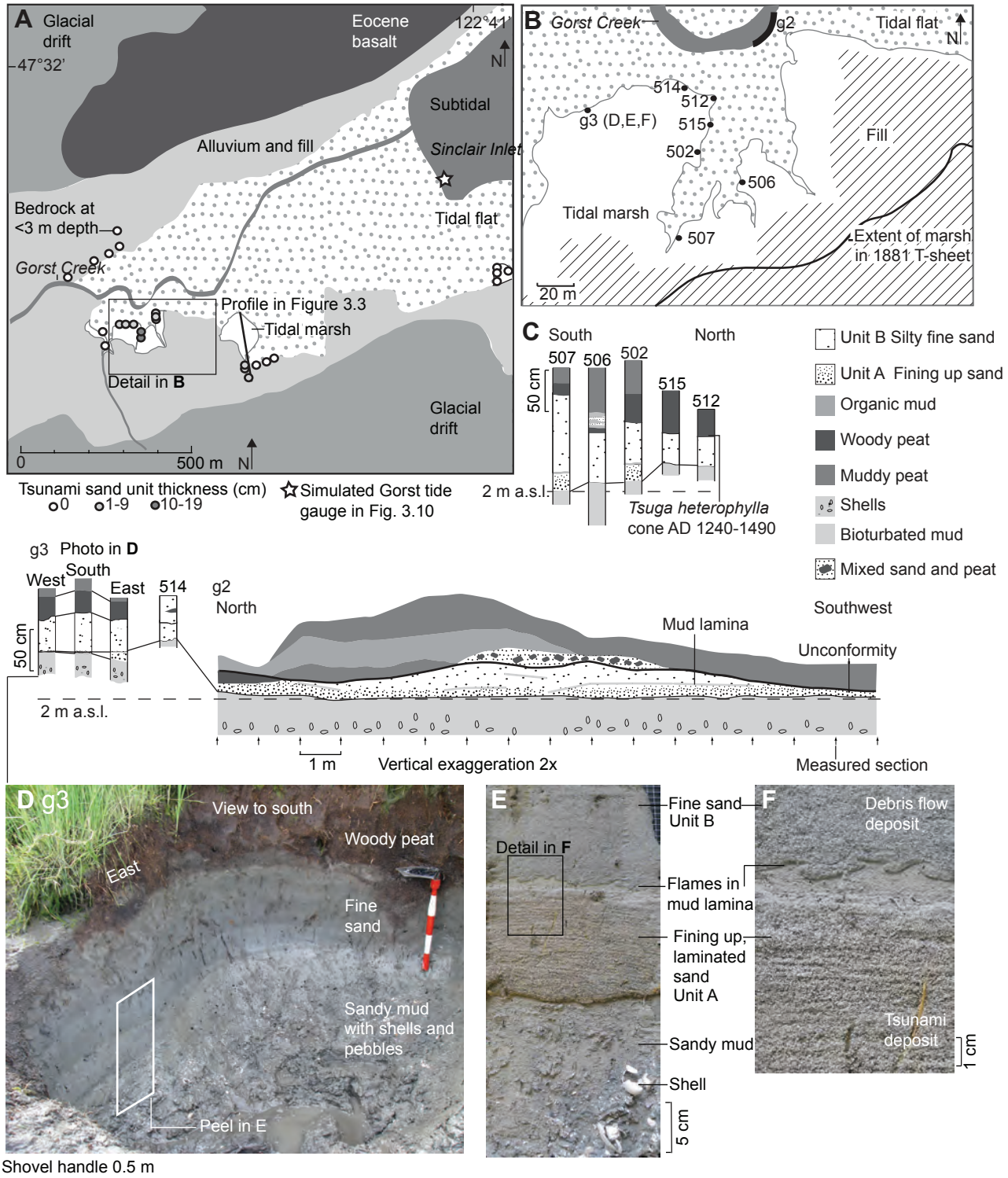

Figure 3.4 Maps, stratigraphic sections and photographs of the Gorst wetlands area detailing the relatively consistent thickness of Unit A relative to Unit B. A. Map of wetlands including thickness of unit A. B. Unit A thickness and outcrop locations in Gorst wetlands C. Stratigraphic detail of outcrops. D. Details of sedimentary structure from outcrop. Painted sections on shovel are in 10-cm increments. E. Sediment peel from outcrop in D. F. Detail of sedimentary peel in E.

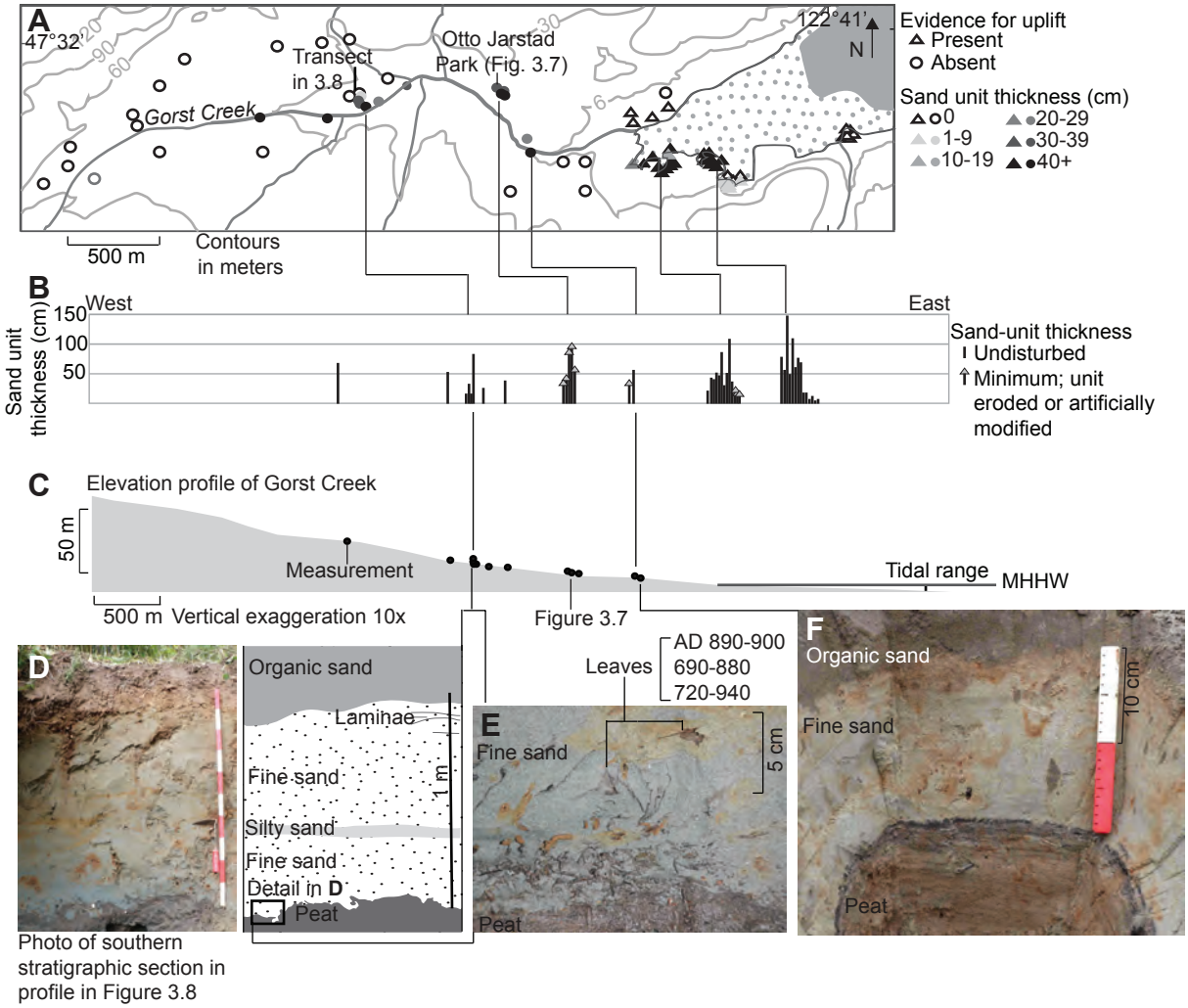

Figure 3.5 Sand thickness along Gorst Creek showing deposit is only present along Gorst Creek. A. Map of thickness variation. B. Total thickness of sand unit (A and B where both are present) along Gorst Creek and in wetlands. C. Profile along Gorst Creek showing measurement locations. D. Photograph of deposit from an outcrop along Gorst Creek. E. Detail of well preserved leaves entrained in sand deposit. E. Detail of sand deposit near Gorst Creek. In this location the top of the deposit was removed.

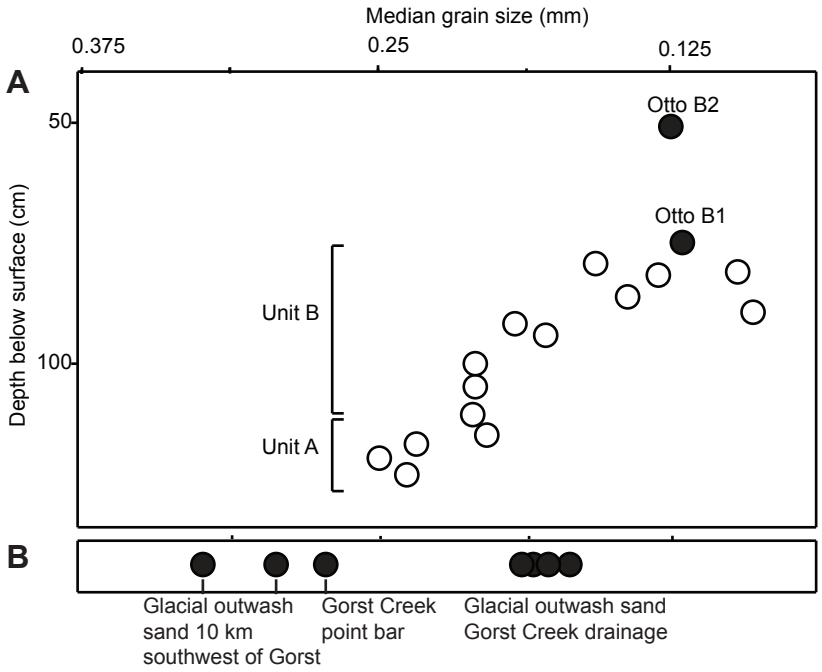

Figure 3.6 Median grain size of sedimentary units at Gorst showing fining upward nature of both unit A and Unit B. Also note Unit B and Glacial outwash sand are similar. A. Median grain size of Units A and B from the g2 outcrop in the wetlands. Otto samples are from Otto Jarstad park. B. Median grain size of glacial outwash sand from the area surrounding Gorst.

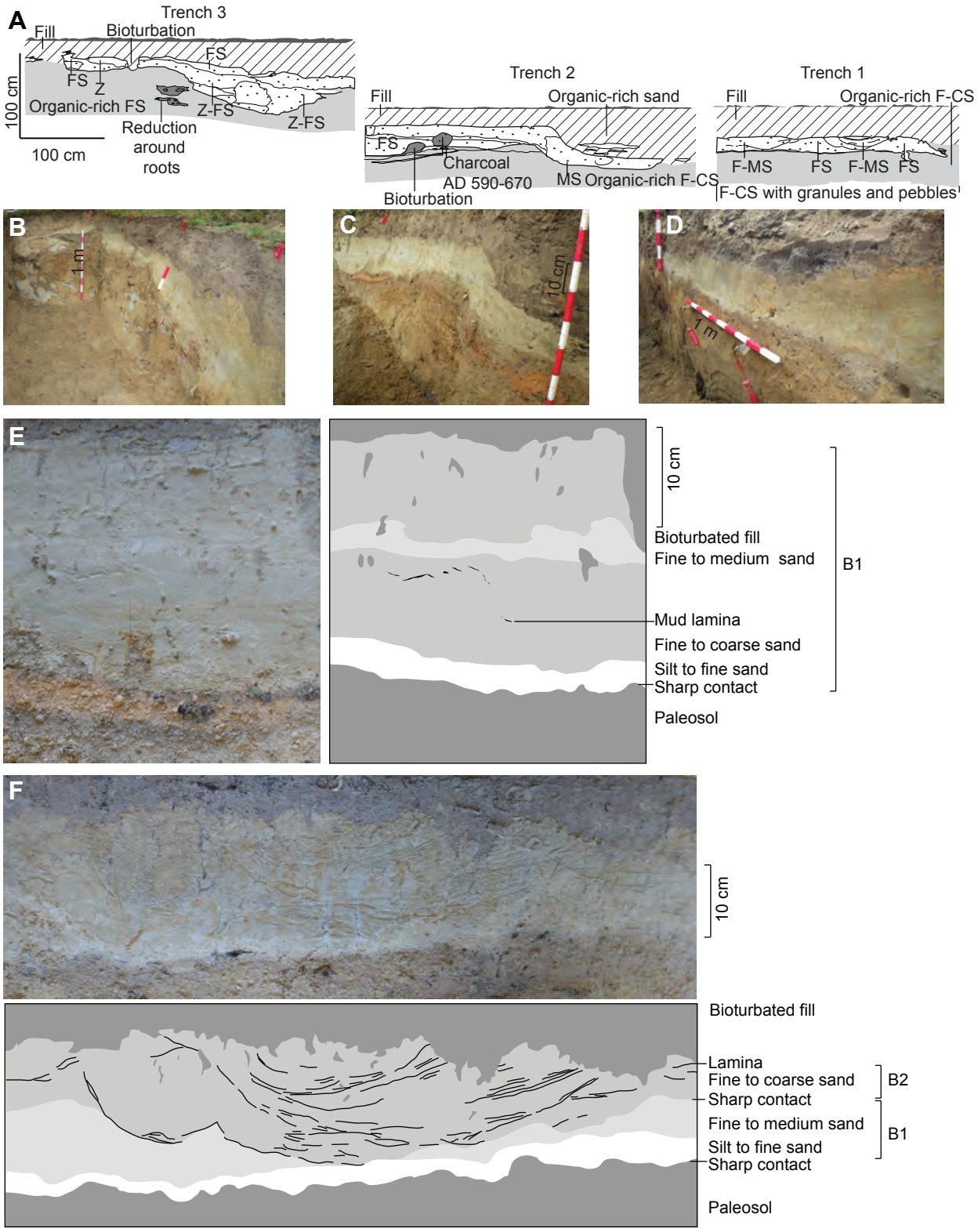

Figure 3.7 Unit B in Otto Jarstad Park showing massive structure of unit B1 and cut and fill structures in unit B2. A. Sedimentary structures of sand unit from backhoe trenches in Otto Jarstad Park. FS=fine sand, MS=medium sand, CS=coarse sand, Z=silt. B. Photo from of trench 3 C. Photo of trench 2. D. Photo of trench 1. E and F. Paired photos and interpretation of sediment peels made from trench walls. E. Trench 2, F. Trench 1.

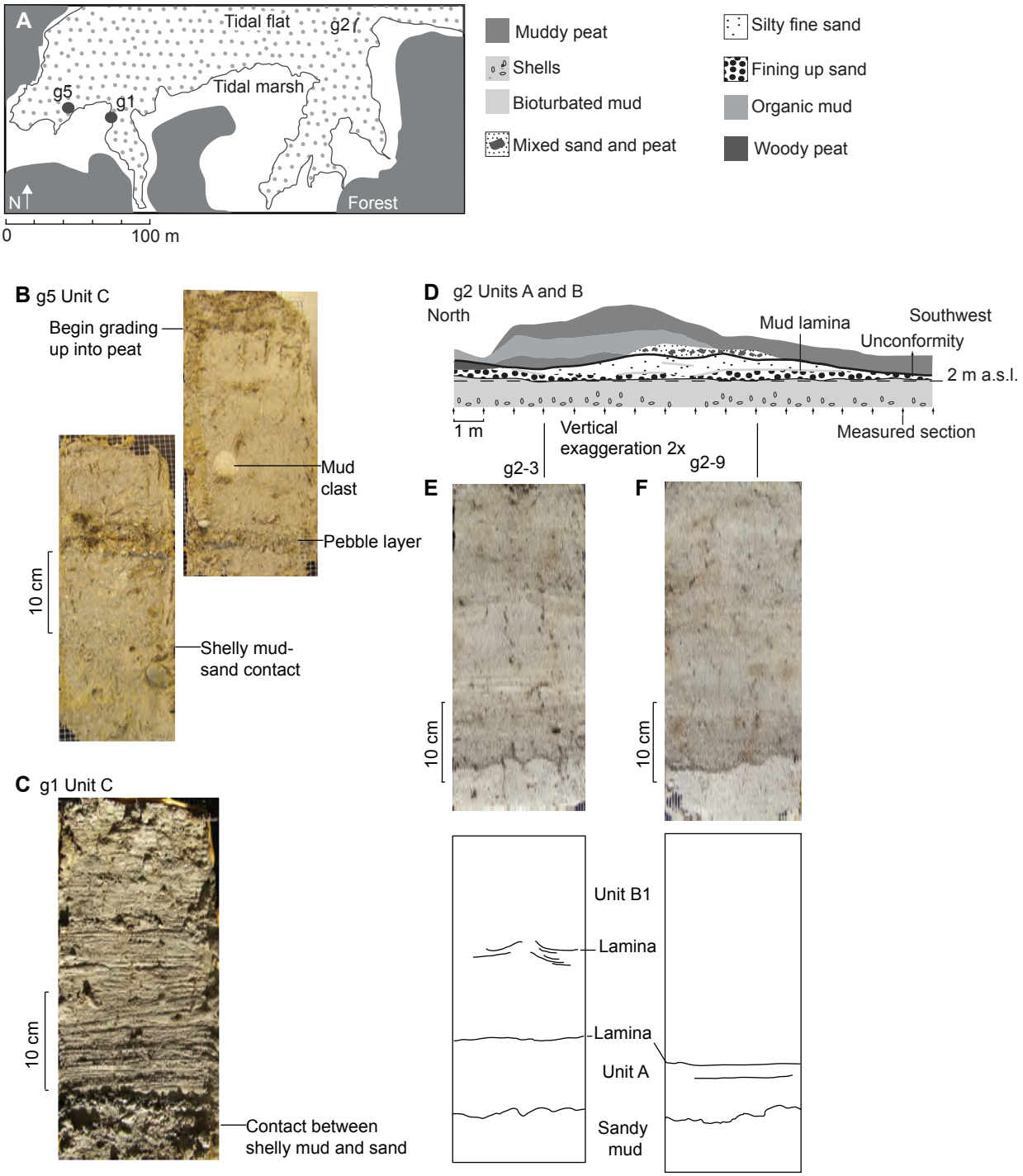

Figure 3.9 Peels of deposits from Gorst wetland. Unit C differs from units A and B in sedimentary structures and grain size. A. Index map. B and C at site g5. Peels of Unit C. B is two peels taken side by side to represent the entire deposit thickness. The pebbles in B and the distinct laminae in C are absent in E and F. D. Outcrop g2. E and F. Peels from outcrop.

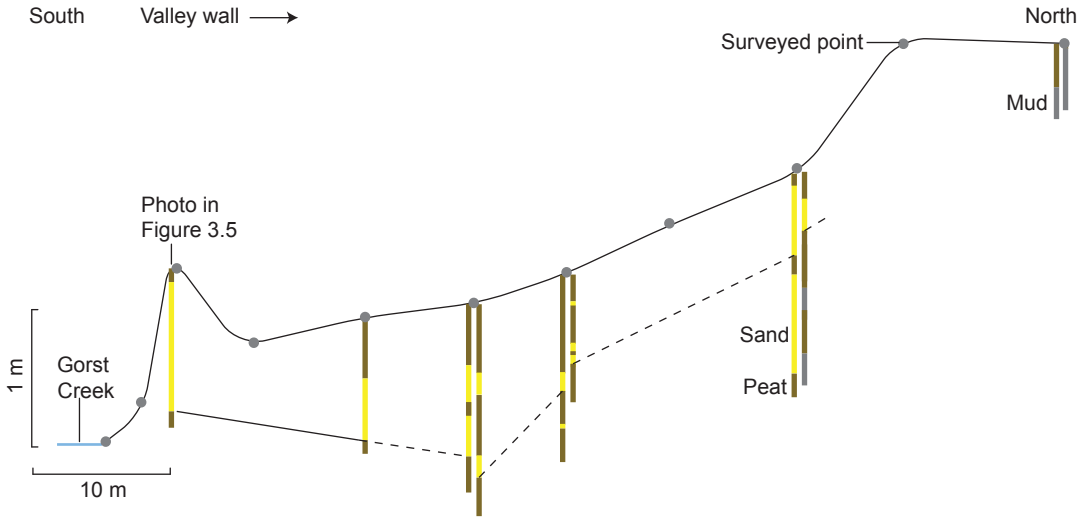

Figure 3.8 Topographic transect perpendicular to Gorst Creek showing the deposit thinning and becoming patchier toward the valley wall. Transect was measured using a hand level. The two southernmost stratigraphic columns were observed in outcrop, while remaining sites were observed in cores. At each site two cores were taken within 2 m of each other. Peat within the sand unit was introduced by bioturbation.

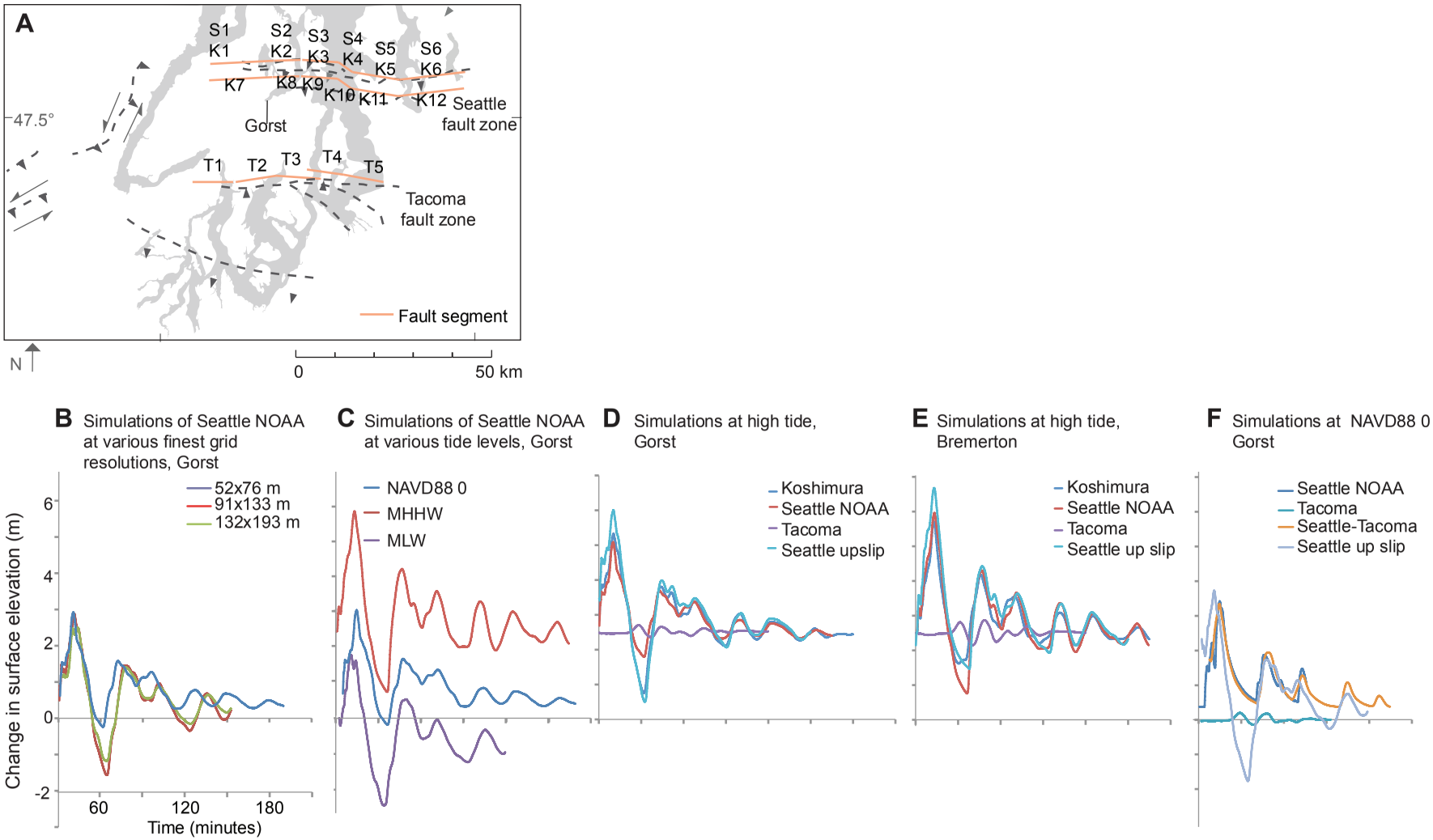

Figure 3.10 Simulated tide gauges from the Gorst locality for various tsunami model runs. Seattle fault simulations behave similarly and the Tacoma fault simulations are an order of magnitude smaller. Parameters for model runs are in Table 3. A. Gorst tide gauge for all figures but E. located at N47.531°, -122.685° (Figure 3.4A). Bremerton tide gauge for E at N47.5416, -122.6685 (Fig. 3.1). "High tide" is 2.5 m higher water level than NAVD88 0. Fault input parameters in Table 3.1.

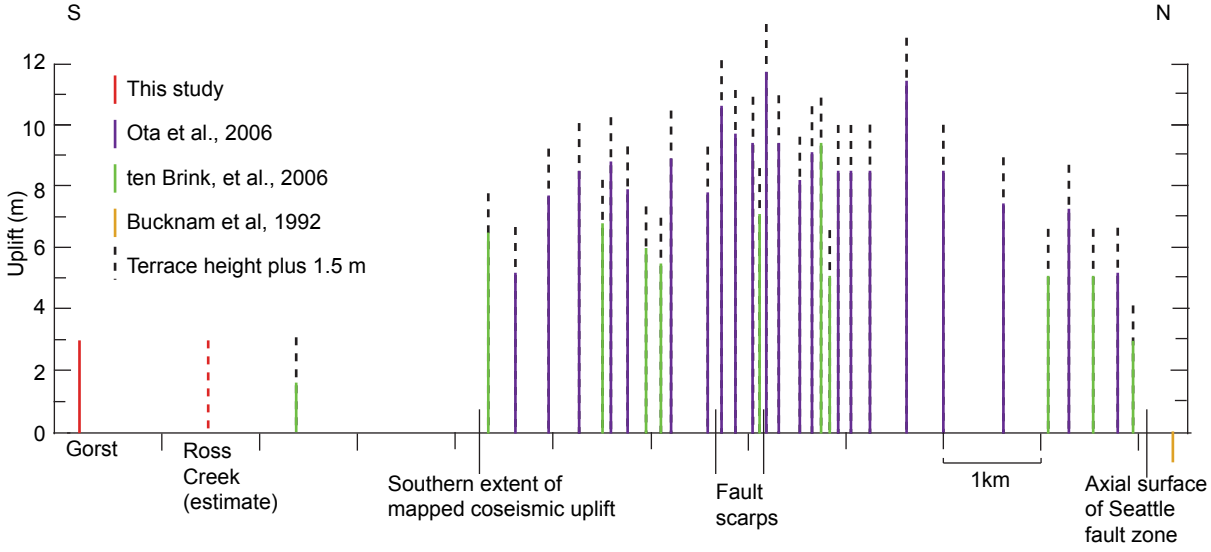

Figure 3.11 Terrace heights projected onto a north-south transect across the Seattle fault zone showing a reconstruction of initial terrace height factoring in 1.5 m of submergence. Transect location in figure 3.1. Uplift values from the AD 900-930 from marine terrace heights and marsh stratigraphy are projected onto the transect. ten Brink et al. (2006) estimate error in their terrace data to be +/- 1 m. Ota et al. (2006) estimate the error on terrace heights to be at least the +/-30 cm error of the LiDAR data used to measure terrace heights. Dashed lines represent terrace heights accounting for 1.5 m of submergence.

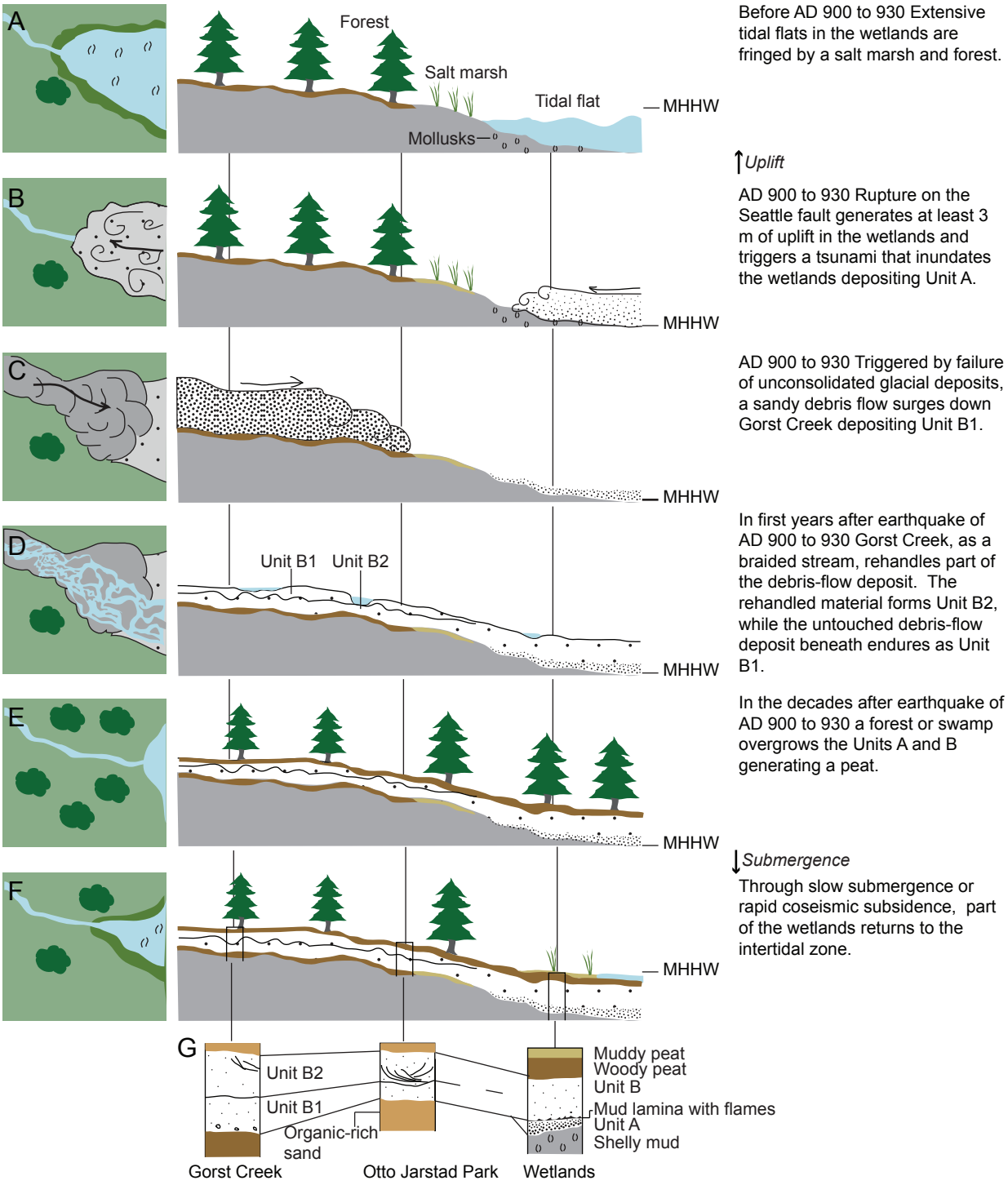

Figure 3.12 Cartoon of main geological events recorded at Gorst including relative changes in mean higher high water (MHHW). Map view in the left column schematic cross-section in the right column. A. Pre-earthquake conditions. B. Tsunami and deposition of unit A. C. Debris flow and deposition of unit B. D. Reworking of unit B by braided stream flow. E. Establishment of forest and swamp after the earthquake. F. Modern conditions. G. Generalized stratigraphic sections from Gorst placed below the location in the cross-section the stratigraphy represents.

CHAPTER 4

Shaking, uplift, and tilting about 1,100 years ago, and subsequent submergence, at the Skokomish River delta, Washington

4.1 INTRODUCTION

The Skokomish delta lies in a complicated tectonic setting at the edge of the Puget Lowland (Figure 4.1). The delta sits near the boundary of the currently uplifting Olympic Mountains and the subsiding Puget Lowland (Brandon et al., 1998; Holdahl et al., 1989), and tectonic stress at play in each area may generate relative sea level changes at the delta. Complicating the relative sea level story, two to three thrust-fault zones in the Puget Lowland trend toward the delta, but their nature in proximity to the delta is understood poorly (Blakely et al., 2009; Figure 4.1).

The Skokomish delta holds clues to several larger geological issues in the Puget Lowland. The delta is situated near both the Olympia and Saddle Mountain fault zones, two of the four fault zones that ruptured about 1,100 years ago (within the error of radiometric dating) (Figure 4.1). Signals of these ruptures may be left in the delta stratigraphy and help indicate the extent of these ruptures. Furthermore, a strange bathymetric depression off the western delta front has been interpreted as the scarp of a potentially tsunamigenic submarine landslide (Polenz et al., 2010) possibly linked to tsunami deposits at the end of Hood Canal (Jovanelly and Moore, 2009). However, I have interpreted the deposits at the end of Hood Canal as liquefaction features (Chapter 2) and the scarp as a pre-existing feature (this chapter). Skokomish delta stratigraphy may also aid in interpreting background rates of

relative sea level change as it relates to the impact of 21st-century sea level rise in Puget Sound.

The Skokomish delta is a valuable location to study recent tectonics of the region because delta stratigraphy and morphology can be highly sensitive to tectonic changes. For example, subsidence and uplift can induce changes in facies, geomorphology, and behavior of river systems on deltas, and the record of such changes can illuminate past seismic events (e.g. Holbrook and Schumm, 1999; Barnhardt and Sherrod, 2006). This study uses stratigraphy, geomorphology, and paleontology to examine the last 1,100 plus years of tectonic and depositional history at the Skokomish delta.

4.2 SETTING

4.2.1 Tectonic provinces

The Skokomish delta lies at the nexus of the Cascadia accretionary wedge and forearc basin--the Olympic Peninsula and Puget Lowland--and may hold clues to their interactions. Progressive accretion and exhumation of mostly marine sedimentary and volcanic rocks along the subduction zone formed the Olympic Mountains along north-south-trending thrust faults (Cady, 1975; Tabor and Cady, 1978b; Brandon et al., 1998). In contrast, faults in the Puget Lowland are east-west trending to accommodate shortening provoked by oblique subduction and by a rotating and northward-moving Oregon forearc (Wells et al., 1998; Mazzotti et al., 2002; McCaffrey et al., 2007). The difference in these regimes generates long-term emergence in the Olympic Mountains and subsidence in the Puget Lowland, with the boundary between this uplift and subsidence falling near the Skokomish delta. Due to different placements of the hinge zone, estimated rates of land-level change for the delta

range from -1 to 1 mm/yr (Reilinger and Adams, 1982; Holdahl, et al. 1989; Mitchell et al. 1994; Hyndman and Wang, 1995; Long and Shennan, 1998).

4.2.2 Active faults

Strain in the Puget Lowland and differential movement between the lowland and the Olympic Mountains generate shallow crustal faulting. Multiple fault zones in the vicinity of the Skokomish delta have experienced Holocene thrust and strike-slip ruptures. Several kilometers to the northwest of the Skokomish delta, the Saddle Mountain fault zone trends along the southeastern edge of the Olympic Mountains (Figure 4.1B). The Saddle Mountain fault zone accommodates the north-south contraction of the Puget Lowland as it moves along the Olympic Mountains, and also includes westside-up thrust (Blakely et al., 2009). Holocene activity on the Saddle Mountain fault zone includes rupture AD 650-1050 (Hughes, 2005), which created an east-side-up scarp and dammed streams (Carson, 1973; Wilson, 1975). Also in the region of the Skokomish delta, the lesser-understood, east-west-trending Olympia fault zone (Sherrod, 2001; Figure 4.1B) bends northward toward the Skokomish delta. The location and active status of the fault are based on geophysical anomalies and on marshes with uplift dated AD 800-940 (Sherrod, 2001). Additionally, two other faults zones in the Puget Lowland, the Seattle and Tacoma fault zones, show evidence of earthquakes about 1,100 years ago (Bucknam et al., 1992; Sherrod et al., 2004).

4.2.3 Pleistocene ice sheets

Pleistocene glaciation shaped much of the Puget Lowland. The last glaciation, the Fraser glaciation, reached its peak in the Vashon stade ~15,000 years ago in the Puget Lowland (Booth, 1994). Associated with the Fraser glaciation are till, advance and outwash deposits, and lake deposits. These unconsolidated deposits and those of prior glaciations blanket much

of the Puget Lowland including the plains flanking the Skokomish delta. The walls of the Skokomish Valley consist of Vashon and older glacial deposits capped with Fraser deposits (Carson, 1976; Polenz et al., 2010). Since the retreat of the glaciers, the general region of the Skokomish Valley is estimated to have had ~50 m post-glacial isostatic rebound that ended about 8,000 years ago (Thorson, 1989).

4.2.4 Holocene sea levels

Prior studies indicate rapid sea level rise in the early Holocene followed by slow rise in most examined localities. With the retreat of the continental ice sheets, sea level rose quickly, and about ~5,000 years ago the rate of sea level rise slowed in the Puget Lowland (Clague and Boborowsky, 1990; Dragovich et al., 1994), with evidence of varying rates of change in relative sea level since this time. In the western Puget Lowland, a peat record from northern Hood Canal showed a gradual sea level rise from about 6 m lower than present sea level 6,000 years ago, with less than 1 m of sea level rise in the last 1,100 years (Eronen et al., 1987). Other peat records from six marshes show <1 m sea level rise in the last thousand years (Beale, 1990).

More work on the last 100 years of relative sea level history has been done in the highly urbanized eastern Puget Lowland. Using differential InSAR Finnegan et al. (2008) found subsidence of more than 3 mm/yr for major river valleys in the eastern Puget Lowland. Using tide gauge records from eastern Puget Sound, Holdahl et al. (1989) found 1-2 mm of submergence a year whereas Verdonck (2006) found little to no evidence for submergence.

4.2.5 Puget Sound deltas

In tectonically active settings, local land level changes create changes in delta and river behavior. Uplift of a delta has the effect of lowering base level, therefore steepening the

grade of the river, resulting in downcutting in the channel and increasing rates of channel migration to maintain river gradient. Delta subsidence has the effect of raising base level, lowering the river gradient, leading to decreased channel migration (Adams, 1980). Faults crossing rivers can change river-flow patterns (Johnson and Schweig, 1996, Goodbred and Kuehl, 2000) and reduce or steer river-channel migration (Nanson, 1980; Kim et al., 2010).

Tectonic land-level change and the glacial history of drainages influence the morphology of Puget Lowland rivers and their valleys. For example, uplift during the AD 900-930 Seattle fault zone earthquake affected the morphology and behavior of the Duwamish River for 5 km upstream of the uplift (Collins and Montgomery, in press). In eastern Puget Lowland rivers, Collins and Montgomery (in press) conclude, however, that the impact of faults on Puget Lowland rivers and their valleys is local and that the larger geomorphic influence is the glacial history of the valley.

4.2.6 Skokomish River

The Skokomish River forms a delta at the elbow of Hood Canal where the fjord bends 145° from a north-south direction to a northeast–southwest direction (Figure 4.1). To reach Hood Canal, the Skokomish River flows through a 16-km-long, glacially carved, alluvium-blanketed valley. A lack of Holocene river terraces indicates the valley has been mostly aggradational since the stabilization of sea level (Bountry et al., 2009). Channel sediment consists of well-rounded pebbles downstream of the highway 101 bridge and coarsens to pebbles and cobbles upriver (Bountry et al., 2009). The modern delta (Figure 4.2) consists of salt- and freshwater marshes and swamps that are pristine in some areas, while in other portions of the delta people diked and drained the land for farming. Currently, the modern inter- to sub-tidal delta is growing seaward on the eastern end of the valley (Figure 4.2).

Evidence for lateral migration of the Skokomish River diminishes downstream. Upstream of the Highway 101 bridge (Figure 4.2), the river channel has migrated as much as 170 meters since 1938 (Bountry et al., 2009; comparison with airphotos posted at http://riverhistory.ess.washington.edu), and the entire valley bottom is crossed by abandoned meander channels (Figure 4.2). Downstream of the Highway 101 bridge, by contrast, no more than 20 m of natural channel migration has taken place in historical time, during which people straightened the river (Bountry et al., 2009; Figure 4.2); abandoned meanders here are limited to the eastern side of the delta. Furthermore, upstream of the Highway 101 bridge, the Skokomish River has a high avulsion potential, while downstream of the bridge the river has low avulsion potential, based on river slope relative to delta slope (GeoEngineers, 2006). The river mouth has been in approximately the same position since people made the first maps of the delta in the late 1880's (Figure 4.2)

4.2.7 Topographic and bathymetric anomalies

An enigmatic ridge crosses most of the Skokomish delta about 2.5 km up valley from the modern delta's shore (Figures 4.2, 4.3). The ridge trends approximately parallel to that shore and, much like the modern beach berm, consists of pebbly gravel. It descends southeastward from a maximum height of 6 m above the adjoining delta. Polenz et al. (2010) named it Lucky Dog Ridge and interpreted it as the geomorphic expression of a south-dipping thrust fault. I refer to it simply as the Ridge, and I propose that it was constructed by deposition along an ancient shoreline (section 4.4.4). The designation of the Ridge as a tectonic structure by Polenz et al. (2010) is based on the morphology, presence of inclined glacial strata to the west of the valley, and an aeromagnetic boundary near the Ridge. A date on detrital charcoal from 21-m depth (~13 m below modern sea level) in the Ridge gave a

radiocarbon date of BC 6650-6470. This date indicates the Ridge is not a relict glacial feature, as it formed well after retreat of the glaciers (Polenz et al., 2010).

Also enigmatic is an area of deep water that seemingly cuts into the western part of the delta front (Figure 2C). Polenz et al. (2010) ascribed this area to submarine landslide scars. Below, in section 4.4.3, I instead infer that this part of the delta has been unable to prograde in the millennia since the Ridge, and also eastward tilt of the delta, forced the river to remain on the east side of the valley.

4.3 METHODS

4.3.1 Fieldwork

Most fieldwork took place in the summers of 2008-2010. All outcrop sites required a mid to low tide. A hand-held GPS located each site.

I studied modern vegetation, landforms, and stratigraphy along four transects perpendicular to the shoreline (Figures. 4.2, 4.3). On transects 1 and 2 I used species cover abundance to identify vegetation zones. Based on species abundance, transects were grouped into the vegetation zones of Sherrod (1999). On other transects, I noted vegetation types and species for each core location, but did not estimate percent cover. For transects 1 and 2 on the Marsh (Figure 4.2), distance and elevation were surveyed using a transit level (error +/- 2 cm), and the tide level surveyed at the delta was compared to the tide gauge at Union (Figure 4.2) for tidal stage at the time of the survey. For transects 3 and 4 tall vegetation and wet, unstable ground made leveling impractical, so I used elevations from Light Ranging and Distance (LiDAR) data from the Puget Sound LiDAR Consortium (LiDAR; error +/- 30 cm).

Transect 3 does not follow a linear path, so in Figure 4.3 I projected elevation and stratigraphy onto a straight path between the start and endpoint.

I used outcrops, gouge cores, and soil-auger holes to examine stratigraphy at over 100 sites (Figure 4.2). Wherever possible I cleaned banks of tidal creeks and streams. Most of the cleaned sections were ~ 0.5 m in width. In each outcrop and core, I measured stratigraphy and sampled some sites for diatom and macrofossil analysis as well as for radiocarbon dating. I collected monoliths for further detailed sampling of several outcrops. I pushed gouge cores down to refusal in gravel, sand, or stiff mud, or to the 5-m depth extent of the extensions I carried.

4.3.2 Laboratory work

I used plant macrofossils and diatoms to help infer environments of deposition. Plant macrofossils were identified with a binocular microscope and the reference collection of the University of Washington herbarium. For diatom analysis, I cleaned sediment samples of 2 cm^3 in 30% hydrogen peroxide and then rinsed several times in distilled water. Slide preparation used samples settled out onto cover slips where the water evaporated, yielding a random distribution of diatoms on the cover slip. The cover slips were then mounted on microscope slides using Naphrax (refractive index D=1.7). Published taxonomic monographs aided in the identification of diatoms. Counts of between 400 and 1,200 diatom valves allowed for the diversity of the fossil assemblage. I counted more diatoms on slides that had high concentrations of one species. For samples 4a and 8a and all samples from the DNR core (Figure 4.2), low diatom density in samples prevented the counting of 400 valves. Percentages of diatom species are based on the total count per sample.

I made canonical correspondence analyses of diatom assemblages using the software package CANOCO (Ter Braak, 1987-1992) and the modern assemblage catalog of over 100 samples of Puget Lowland coastal environments expanded from Sherrod (1999). I plotted modern diatom data against salinity and a Standardized Water Level Index (SWLI; Horton et al., 1999), which is an elevation relative to mean water level that factors in variations in tidal range. On the same diagram I plotted the samples counted in this study against the modern diatom data using the similarity in abundance of species, and I used this plot to infer depositional environments.

4.4 DELTA ENVIRONMENT, GEOMORPHOLOGY AND STRATIGRAPHY

I divided the delta downstream of the highway 101 bridge into four areas based on the modern landforms, vegetation and environment, as well as the stratigraphy. From north to south they are the delta Marsh, Swamp, Ridge and Bog (Figure 4.2). These areas make up the study area. Modern environment, stratigraphy, and geomorphologic features for each region will be discussed in this section. First, I discuss the large-scale delta morphology.

4.4.1 Delta morphology

Slope

Profiles perpendicular to the river in the study area slope down to the river, whereas a profile upstream slopes up to the river (Figure 4.3). The Marsh, Swamp, and Bog all have a cross-delta slope of 30-40 cm per km (slope of 0.0003 to 0.0004) and the Ridge slopes at over 200 cm per km (slope of 0.0021; Figure 4.3). All of the study area slopes to the southeast. A profile from farther upstream where the river has migrated across the valley more recently shows the river levees as the highest part of the profile (Figure 4.3).

Ridges

At the landward end of transect 1 and 2 (Figure 4.4), a small berm with a slight elevation increase over the salt marsh permits the growth of trees and woody vegetation. In the underlying stratigraphy, a woody peat unit thins to 20 cm or less over a pebbly gravel at the berm. The gravel unit below the peat has a similar morphology to the modern gravel berm at the front of the delta. I refer to this ridge as the "ancient gravelly berm".

As noted previously, an enigmatic ridge ("the Ridge," discussed in detail below) trending approximately parallel to shore crosses most of the Skokomish delta about 2.5 km up valley from the current shoreline (Figures 4.2, 4.3). It descends southeastward from a maximum height of 6 m above the adjoining delta; the height difference is due in part to an alluvial fan on the western edge of the Ridge. Some of the original morphology is obscured by human activities, as a large portion of tribal housing and facilities are located on the Ridge.

Paleo-channels

In the Swamp and cutting across the Ridge are several seaward branching channels (the "paleochannels" in Figure 4.2). The eastern channel currently drains the Bog across the Ridge. The western channels drain very slowly, as they are blocked by vegetation and peat. The western channels are of similar width to the modern Skokomish channel and its distributaries, but are at up to 2.5 m higher elevation.

Two sets of cores taken in the western channels show evidence of modern and ancient freshwater deposition. Site 8 (Figure 4.6), at the more landward end of the channel, reveals an open-water swamp with a mix of *Thuja plicata* (western red cedar), *Salix* spp. (willow) and smaller vegetation. At site 8, cores reveal 20-30 cm of peat over a sandy gravel. Low

abundance prevented the counting of 400 frustules in the sandy gravel, but diatoms indicate fresh to brackish deposition (Figure 4.7, stratigraphic column 8). A radiocarbon date of a *Picea sitchensis* (Sitka spruce) seed from the bottom 5 cm of the peat had an age of AD 1680-1960.

Seaward of site 8 at sites 4 and 5, the vegetation is a mix of *Typha latifolia* (cattail), *Salix* spp. and *Lysichiton americanum* (western skunk cabbage). Vegetation covers most of the surface, but patches of open water exist. Large portions of the channel are floating marsh with pockets of water a meter or more deep. Cores reveal sand or gravel overlain in some cases by 1-10 cm of mud in turn overlain by a meter or more of peat and water. *Pseudotsuga menziesii* (Douglas fir) needles from the basal 3 cm of peat gave a radiocarbon age of AD 1400-1460. The channel banks consist of a pebbly gravel with freshwater diatoms (Figure 4.6, stratigraphic column 4).

4.4.2 Marsh

Modern environment

Along transects 1 and 2, the vegetation grades from more salt-tolerant species at the delta front to less salt-tolerant species farther inland (Figure 4.4). Most of these profiles are inundated during the highest tides. The species found at the lowest elevations are *Salicornia virginica* (pickleweed) and *Jaumea carnosa* (marsh jaumea). Also at low elevations were *Distichlis spicata* (saltgrass) and *Triglochin maritimum* (common arrowgrass). The majority of vegetation on the transects consists of *Juncus effusus* (common rush), and other *Juncus* spp. (rushes) and *Carex lyngbyei* (Lyngbye's sedge). The lowest-elevation woody vegetation is *Rosa* spp. (rose). The only conifer along these transects is *Picea sitchensis* at the highest elevations and farthest distance inland. The difference in elevation between intertidal mudflat

devoid of vegetation and the lowest trees (from transit surveys) is 1.5 m, and the separation between abundant salt-tolerant vegetation and non-tolerant trees is 1.1 m (Figure 4.4) a value in agreement with other vegetation transects in the Puget Lowland that found values of about 1.5 m separating mudflat and trees (Sherrod, 1999; Sherrod, 2001).

Stratigraphy

Transects 1 and 2 in the Marsh show a similar stratigraphy of pebbly gravel and mud overlain by woody peat (Figure 4.4). The basal marine deposit varies in grain size, but in general is pebblier toward the eastern end of the delta. The woody peat becomes muddier upward and the muddy peat thins landward. Between the seaward ends of transects 1 and 2, five seeds from the base of the woody peat gave a radiocarbon date of AD 780-1000 (Table 4.1).

In transect 2 an *in situ Pseudotsuga menziesii* stump rooted into mud has been eroding out of the woody peat (Figure 4.5) Though wood is common in the peat, this stump was the only one where enough was visible to determine the stump was *in situ.* Thin roots <2 cm in diameter at the distal end extend from the trunk more than 5 m and are horizontally rooted in the mud, indicating the stump is in growth position The death of the tree was assigned an age of AD 868-1198 (recalibrated from Polenz et al., 2010); the dated root had 82 growth rings with the outermost rings near the bark closely spaced, indicating stress or age. The date was measured from the 34th to 43rd rings counted inward from the bark. The stump is currently eroding out into the intertidal zone 1.6 m below the lowest living conifer (*Picea sitchensis*). No *Pseudotsuga menziesii* currently grows on this part of the delta.

Diatom analysis of the mud and woody peat at the location of the *Pseudotsuga menziesii* stump indicates brackish to marine conditions for both units (Figure 4.8), a

seeming anomaly to be discussed below. The mud that surrounds the tree roots abounds in the brackish and marine diatoms *Diploneis interrupta* and *Nitzschia granulata.* *Diploneis interrupta*, a salt-marsh species, dominates the diatom assemblage 1 cm above the mud contact in the woody peat. Also, foraminifera tests in this unit indicate an intertidal marsh setting for the woody peat in this location. Higher in the section, the peat becomes more muddy and dominated by salt-tolerant species including *Triglochin maritimum* leaf bases and *Distichlis spicata* rhizomes.

In two locations, a sand body more than 30-cm thick splits the peat-mud contact. In both locations, the sand body thins to zero centimeters in less than 10 horizontal meters from the sand's thickest point. In one location, the sand body is associated with an injected sand dike (Figure 4.5). These sand bodies are interpreted to be sand blows related to earthquake-induced liquefaction (Ch. 2).

4.4.3 Swamp

Modern environment

Most of transect 3 (Figure 4.4) is standing water, and a mix of *Salix* spp. and *Typha latifolia* dominate the vegetation taxa. The standing water varies in depth from a few centimeters to over a meter. The only areas without standing water are small islands of slightly higher elevation supported by living, old growth *Thuja plicata*. These islands have a higher diversity of plant taxa. Closer to the river, at site 6 (Figure 4.8), the vegetation is a mix of *Rosa* spp. and *Typha latifolia*.

Stratigraphy

Cores along transect 3 (Figure 4.4) reveal a similar stratigraphy to the Marsh, that is, peat overlying muddy deposits and sand. The transect starts on the berm at the end of

transects 1 and 2. The peat thickens to the south off the berm, and the underlying gravel of the berm is replaced by mud. In the middle of the Swamp, cores revealed sand overlain by up to 150 cm of mud and 30-120 cm of peat. In some cases, the lower 20-40 cm of the mud was silty to sandy. The mud contains *Navicula digitoradiata, Diploneis interrupta* and *Nitzschia granulata* all brackish low-marsh species (Yuki Sawai, personal communication).

In three cores taken closer to the river (Figure 4.9, site 6), sand was overlain by more than a meter of mud that in turn was overlain by a muddy peat with remains of *Typha latifolia* and foraminifera. Both the mud and muddy peat contain a variety of *Aulacoseira* spp., and *Navicula peregrina* frustules. The mud also contains high percentages of *Diploneis smithii* and *Sellaphora pupula,* whereas the mud contains *Pinnularia biceps*, *Luticola mutica* and *Diploneis interrupta*. The mud contains freshwater and brackish diatoms and the muddy peat contains brackish diatoms (Figure 4.9).

4.4.4 Ridge

Vegetation

The Ridge is forested with conifers, deciduous trees, and undergrowth. Much of the vegetation has been modified by human activity such as logging, and building of roads and structures.

Stratigraphy

Because the ridge is very gravelly, I collected no cores on the Ridge, but I examined samples from a geotechnical core obtained by Washington State Department of Natural Resources (Polenz et al., 2010, Figure 4.2, DNR core). Most of the 25-m core consisted of pebbly gravel and yielded no diatoms or macrofossils with which to determine depositional environment. A muddy sand at 21-22 m yielded a few fragments of *Fragilaria* spp*., Diatoma*

hiemale, other, unidentified diatoms, and charcoal. Charcoal in this muddy sand yielded a radiocarbon age corresponding to 6650-6470 BC (Polenz et al., 2010).

4.4.5 Bog

Vegetation

Along transect 4 (Figure 4.4) the vegetation varies from conifer and deciduous trees at the northern end, where the transect ramps up onto the Ridge, to a mix of *Typha latifolia*, *Salix* spp., and open water at the southern end. To the west at the location of core 9, the vegetation transitions to a dryer *Vaccinium oxycoccos* (small cranberry) –sphagnum-moss bog with scattered *Salix* spp. The drainage of this zone into the eastern channel is hampered by beaver fortification.

The environment in the Bog is currently in transition as is evident from dead trees around the fringe. These dead trees are not apparent on 1938 aerial photographs (Puget Sound River History Project).

Stratigraphy

Cores along transect 4 (Figure 4.4) revealed sand overlain by up to 2 m mud and up to 2 m wet, loose peat. At the southern end of the transect, the 5-m extent of the core barrels we had did not reach the base of the mud unit. Both the sand and mud layers thin toward the north onto the Ridge. Diatoms from transect 4 (Figure 4.7, stratigraphic section 10) indicate freshwater deposition, including high percentages of *Aulacoseira* spp., *Fragilaria capucina* and *Cocconeis placentula* in the sand and *Gomphonema ovilaceoides*, *Fragilaria capucina* and *F. brevistrata*. Both units contained large numbers of broken *Fragilaria* spp. fragments.

To the west of transect 4 the vegetation transitions to a *Vaccinium oxycoccos* - sphagnum bog with scattered *Salix spp*. It is in this zone that Polenz et al. (2010) collected a

core and dated plant material from the mud to AD 1200-1280. Diatom analysis from samples of this core show all units are from a freshwater environment, with a slight saltwater influence in the mud (Figure 4.7). Freshwater species *Aulacoseira* spp., including *A. italica* and *A. granulata* along with *Fragilaria construens* and *F. capucina* dominate the diatom counts from the upper mud and sand. The lower mud contains high percentages of *Cocconeis placentula*, *Fragilaria virescens*, *F. vulgaris*, and *Diploneis elliptica*. The diatom assemblage in the lower mud indicates a marine influence (Figure 4.7).

The mud unit in the Bog is different than the mud unit in the Swamp and Marsh. The Bog mud is younger and is freshwater in contrast to the brackish mud to the north of the Ridge.

4.4.6 Chronology

The Ridge is the oldest feature mapped in this study. The single date from the Ridge in conjunction with an absence beneath the Ridge of units present below the Swamp and Bog indicate the Ridge is older than 1,100 years. The ages of sediments below the Marsh, Swamp and Bog overlap and indicate the units mapped in this study represent the last few thousand years.

Dates from units underlying the Ridge and Swamp indicate facies changes in the Bog may have occurred at the same time as those in the Marsh and Swamp. Dates from seeds and the tree stump in the bog indicate the transition from brackish mud to peat occurred before AD 780-1000 (Table 4.1). Dates from channels that cut the Ridge and Swamp indicate the channels were abandoned before AD 1290-1410. The transition from sand to mud in the Bog occurred before AD 1180-1290, and the transition to peat occurred after this time.

The presence of the *Pseudotsuga menziesii* stump in the Marsh indicates at least 100 years of freshwater conditions before a return to brackish conditions. Colonization of an unvegetated area by forests after a large disturbance takes decades and depends on site factors including soil type and distance to seed source (del Moral and Wood, 1993; Titus et al., 1998). For that reason, colonization and 82 years of growth rings would require at least at least 100 years. Therefore, freshwater conditions persisted for at least 100 years.

4.5 TECTONIC INTERPRETATIONS

4.5.1 Earthquake about 1,100 years ago

Shaking and uplift

Paleoecology and stratigraphic features in the Marsh and Swamp area indicate a fault rupture on or near the Skokomish delta from before AD 780-1000 (Table 4.1). There are several indicators of this earthquake. 1) In the Marsh and Swamp, brackish-marine deposits abruptly change to freshwater deposits (Figure 4.4). An AMS date on seeds from the bottom centimeter of peat yielded an age of AD 780-1000 indicating the transition occurred slightly before. The uplift was likely rapid because the contact between the mud and peat is sharp or grading over 1 cm or less. 2) The stratigraphy skips the marsh facies. If the facies change was due to elevation gain resulting from build up of sediments through time, the expected transition would be marine mud to salt-marsh peat and then to high marsh and trees. In the modern environment the elevation change from intertidal mud to an environment supporting conifers is 1.0-1.5 m. 3) This rapid facies change occurred at a time when sea level in the Puget Lowland was relatively stable or slowly rising, and therefore signals of relative sea

level fall are unexpected. 4) In the Marsh the facies change is coupled with vented sands, an indicator of strong shaking.

Together these data indicate coseismic uplift of a minimum of 1 m. Uplift may have been greater than 1 m as indicated by the mud-peat contact occurring >1 m above the modern intertidal zone on transect 3. If the mud was from an intertidal environment, and if the submergence rate does not vary across the delta, marine mud above modern tides would indicate >2.5 m of uplift. However, samples for paleoenvironmental analysis were not collected at this site and local compaction effects are difficult to determine.

The apparent co-occurrence in the woody peat of salt-tolerant diatoms (Figure 4.8, sample 3a) and a rooted, salt-intolerant tree stump likely represents the mixing of two stages in the delta history. If waves deposited the stump in brackish mud as driftwood, it is unlikely that the preserved long, thin roots would have survived transport or survived at the surface long enough to be encompassed by both the marine mud and overlying brackish woody peat. Therefore, it is likely that the tree stump and brackish peat represent two separate stages in the delta history. First, the stump represents the time when this site was uplifted out of the zone of tidal influence, where the tree could take root and grow. Second, submergence occurred that possibly killed the tree and washed away surface organic soil. An alternative interpretation is that brackish diatoms in the peat are a local occurrence representing pooling and concentration of brackish water in one location.

The gravel berm that marks the boundary between the delta front and the Swamp (Figure 4.4) is interpreted to be the approximate paleoshoreline at the time of uplift. The berm has a similar morphology and grain size to the modern gravel berm fringing the seaward edge of the salt marsh (Figure 4.2; Figure 4.3). The presence of marine to brackish

mud in the stratigraphy of the Swamp, landward of the ancient berm, indicates that the berm acted as a protective barrier, as does the modern berm, which, protects large mudflats along the middle shoreline of the delta (Figure 4.2).

Stratigraphic evidence for the earthquake (about 1,100 years ago) on other portions of the delta is not as clear as in the Marsh and Swamp stratigraphy. The abandonment of the channels that cut across the Ridge occurred some time before AD 1290-1410, the time when deposition changed from sand to peat. It is possible that channel abandonment could have occurred in the same event as uplift on the delta front or at another time. Also ambiguously, the facies change in the Bog from sand to mud occurs at approximately the same time as uplift in the Marsh and Swamp (before AD 1200-1280). These changes are from one freshwater environment to another, however, and could represent a gradual progression from higher to lower energy environment.

Tilting

Tectonic uplift most likely generated tilting of the Skokomish delta. The Skokomish River is generally aggradational and thus because the river has been in a similar location for 1,100 years, the eastern side should be higher than the western side of the delta, yet the reverse is true (Figure 4.3). The fault that generated the uplift/tilting was most likely the Saddle Mountain fault zone and is consistent with motion on that fault zone around the same time as uplift on the Skokomish delta, within the error of dating. If the Ridge is the geomorphic expression of a fault, as suggested by Polenz et al. (2010), this fault did not cause the tilting because the slope is the same on both sides of the Ridge.

Shoreline-parallel profiles across the Skokomish delta do not have the typical morphology of deltas in non-tectonic areas (Figure 4.3). In most deltaic settings the natural

river levees are higher than the surrounding delta, and, through time, the side of the delta with the river channel builds up through aggradation. Inactive parts of the delta subside due to sediment compaction, until the channel avulses to the lower surface. In contrast, on the lower part of the Skokomish delta, profiles perpendicular to the river through the Marsh, Swamp, Ridge, and Bog all descend toward the river (Figure 4.3). The Marsh, Swamp, and Bog all have a very slight slope of 30-40 cm per km, and the Ridge slopes at ~200 cm per km. A slope down to the river is unexpected because the eastern side of the delta is actively receiving fluvial sedimentation and has for the last 1,000 years or more. Other studies on the Skokomish have shown that the river channel is aggrading, and has been doing so through most of the late Holocene (Jay and Simenstad, 1996; Stover and Montgomery, 2001; Bountry et al., 2009). Because the eastern delta receives sedimentation and the western delta does not, the eastern side should be building higher than the western side.

The uninterrupted stratigraphy across the Marsh, Swamp and Bog and the morphology of the delta indicate that the river has not migrated across the field area for the last 1,100 years. Since the time of uplift, the 1,100-year-old contact has not been eroded or been overlain by fluvial gravel. In all of these areas, fine-grained sedimentary units and peat are traceable from the east to west (Figure 4.3), and no abandoned meander channels cut the landscape as they do farther up stream (Figure 4.2). Furthermore, the morphology of the intertidal and subtidal delta, with deep water off of the western delta and wide shallow flats off of the eastern delta (Figure 4.2), indicate the river mouth has remained on the eastern side of the delta for at least 1,000 years, feeding sediment to the shoreline.

The event that uplifted the Marsh and Swamp is also the most likely cause of the delta tilting. With the assumption that the tidal-flat deposits that underlie the peat in the Marsh and

Swamp were originally approximately flat, then the tilting of the delta either coincides with or postdates the cessation of marine deposition in these areas, i.e. during the uplift event. The origin of the tilt may be due to differential uplift during the earthquake, which generated land level change on the delta. Although differential subsidence in the delta could also generate a slope across the delta, it is less likely because the eastern side of the delta hosts the active channel and flood plains and has been receiving sediments over the last thousand years.

If the muddy-peat-to-mud contact at site 6 (Figure 4.8) from the eastern part of the Swamp represents the same time horizon as the mud-peat contact in the middle of the swamp (Figure 4.4, transect 3; Figure 4.8, site 5), then the slope (tilt) was likely generated at the time of uplift. At site 5, there is a transition between brackish mud and freshwater peat, whereas at site 6, the transition is between two brackish facies. This difference could indicate that site 6 was uplifted less than site 5, as site 6 shows no evidence of purely freshwater deposition, which would be expected if site 6 was uplifted out of the intertidal zone. However, the continued brackish deposition at site 6 may also be due to the proximity of this low-lying site to the Skokomish River and its floodwaters.

The abandoned channels cutting perpendicular the Ridge and Swamp may have become relict during the event that tilted the delta. The abandoned channels cutting across the Ridge indicate the Skokomish River may have been on the west side of the valley at an earlier time, or the abandoned channels may represent an older drain for the Bog similar to the modern eastern channel. In either case, the channels are no longer active and are higher in elevation than their modern equivalents. Uplift on the Ridge may have caused abandonment of the channels by making the preferred flow gradient toward the east.

No evidence of delta failure or a tsunami

The narrow, western intertidal zone is not due to a landslide as hypothesized by Polenz et al. (2010) but instead due to little or no sediment supply. In contrast, the 2-km wide unvegetated intertidal zone on the eastern half of the delta front is an effect of the river mouth being restricted to this side of the delta at least since the earthquake 1,100 years ago. Thus the eastern delta has prograded while the sediment-starved western delta has been in stasis or eroding.

The absence of evidence of a large landslide coupled with the absence of sedimentary evidence for a tsunami on the delta (Chapter 2), leaves the Skokomish delta with no evidence of tsunamis or tsunamigenic landslide events. Therefore, there is no source or sedimentary evidence for hypothesized tsunami deposits near or at the end of Hood Canal. The reinterpretation of the western bight of the Skokomish delta, and the lack of tsunami deposits on said delta, support the conclusion in Chapter 2 that the sand deposit at Lynch Cove is not a tsunami deposit.

4.5.2 Locus of faults related to uplift and tilting about 1,100 years ago

Origin of the Ridge

The Ridge (Figure 4.2) may be the expression of a blind fault or may have formed due to a combination of tectonic and beach processes, the latter favored by results of this study. The Ridge has existed for at least 800 years and overlies deposits 7700 years old. It may have formed above a blind thrust fault (Polenz et al., 2010) or as a beach berm that was later uplifted. The lack of expression of the Ridge in the glacially fluted uplands indicates the underlying fault, if present, is not a long fault. Moreover, uplift in the Marsh and Swamp areas indicates that the northern side of the Ridge went up, not down, the latter postulated by

Polenz et al. (2010). However, it is also possible that the Ridge represents an older gravelly berm, which grew wider than the modern berm due to a stable shoreline through a long period of submergence.

The geographic extent and geometry of the pre- and post-earthquake units indicate that the Ridge existed throughout the more than 800 years represented by the units on either side of it. In pre-earthquake stratigraphy the presence of marine deposits seaward of the Ridge and predominantly freshwater deposits landward of the Ridge indicates that during pre-earthquake time the Ridge was approximately the shoreline. However, the cores collected in this study do not indicate how high the Ridge may have been before uplift of the delta. The thinning of mud and peat units of transect 4 from the Bog onto the Ridge (Fig. 4.4) indicates the Ridge was present during the deposition of those units, that is, for at least 800 years. A date from the middle of the mud unit indicates deposition of the unit began before AD 1180-1290 (Polenz et al., 2010).

Two lines of evidence support the Ridge being the surface expression of a fault. First, a geomagnetic boundary crosses the delta (Blakely et al., 2009). Second, the Ridge is an anomalously high, linear feature in an alluvial plain. Several factors, however, complicate the hypothesis that the Ridge is the surface expression of a fault, elaborated below. Thus if the Ridge is the surface expression of a fault, multiple faults are responsible for the stratigraphic and geomorphic features on the delta.

The origin of the Ridge as a south-dipping thrust fault (Polenz et al., 2010; Figure 4.10) is not supported by facies evidence for uplift of the Marsh and Swamp areas, unless a separate fault generated uplift on the delta front or the Ridge is part of a series of thrust faults. A north-dipping fault underlying the Ridge remains a possibility though it does not fit

geomagnetic lineaments in the area (Blakely et al., 2009; Polenz et al., 2010). Very similar southeastern dips on the north and south side of the Ridge do not support uplift induced by faulting under the Ridge. All portions of the field area are highest on the western side of the delta. If a thrust fault underlies the Ridge, one side of the fault would be uplifted more than the other in an earthquake. This would almost surely generate a different tilt on each side of the fault, and the Swamp and Bog would not be expected to have the same tilt. If the Ridge is cored by an active structure, the tilt of the delta must be induced by a separate mechanism.

Another argument against the Ridge being a tectonic structure is the lack of obvious geomorphic continuation of the Ridge into the glacially fluted uplands above the Skokomish Valley. The Ridge post-dates glacial beveling, and therefore movement on a structure should offset the prominent glacial fluting on the uplands surrounding the Skokomish delta (Figure 4.2A).

An alternative interpretation of the Ridge is that it formed as a shoreline ridge (Figure 4.10), just as a narrow gravel berm flanks the modern marsh (Figure 4.2). Former stability of the shoreline location and slow submergence could have made the ridge wider and taller than the modern berm, as observed in the development of beach ridges in general (Taylor and Stone, 1996). Ridge formation and morphology are dependent on sediment supply, climatic conditions and offshore gradients (Taylor and Stone, 1996). Submergence can initiate or accelerate ridge formation by remobilizing sediment in the beach (Meyers et al., 1996), and as long as sediment supply is high, the ridge will continue to grow rather than to erode (Anthony, 1995). This submergence could have been tectonic or related to eustatic sea level rise. The limiting maximum age of Ridge formation is 6650-6470 BC indicating that it potentially formed before sea level began to stabilize ~5000 years ago. After the formation of

the Ridge, subsequent coseismic uplift could have lifted the Ridge out of the intertidal zone. Multiple earthquake events (uplift and tilting) could account for the greater height of the western part of the Ridge relative to the modern berm and also its greater tilt relative to other areas.

Fault-generated uplift and tilting

Faults other than one under the delta are more likely responsible for uplift and tilting on the delta, of which the most likely is an east-dipping thrust fault related to the Saddle Mountain fault zone. This fault zone is the closest known to the Skokomish delta, which is on its hanging wall (Figure 4.1). Furthermore, rupture on the Saddle Mountain fault zone occurred within the error of dating for the event on the Skokomish delta, with ruptures on both the Saddle Mountain East and West faults in the time range AD 1050-650 and uplift on the delta before AD 780-990 (Hughes, 2008; Witter et al., 2008).

Nearby and also with known ruptures within dating error of uplift on the Skokomish delta are the Olympia and Tacoma fault zones (Figure 4.1). However, their trend toward the west is not well understood. The trace of the Olympia fault in the area (Blakely, et al., 2009) is to the south of the delta, and is south side up, making the Olympia fault zone an unlikely candidate for the uplift on the delta. The trace of the Tacoma fault zone is not known in the vicinity of the delta. It is a north-side-up thrust, so in order for the Tacoma fault zone to induce uplift on the delta, it would need to be located south of the delta. There is currently no evidence of the Tacoma fault bending south of the Skokomish delta.

4.5.3 Origin of post-earthquake submergence

Since the time of abrupt uplift, the front of the delta submerged at least 1.6 m. This number is based on the elevation difference between the current elevation of the about 1,000

year old *Pseudotsuga menziesii* stump on transect 2 and the lowest elevation that conifers currently are growing on the delta (Figure 4.4). No *Pseudotsuga menziesii* are currently growing on this part of the delta, so the lowest surveyed conifer elevation is to *Picea sitchensis.* The presence of salt-tolerant diatoms in the lower part of the peat above and near the dated *Pseudotsuga menziesii* indicates this area returned to the intertidal zone soon after, possibly causing the tree to die. Submergence of the delta may be part of the reason for currently dying trees and expanding wetlands noted by Bountry et al. (2009).

Stratigraphic changes in the Bog may be due to natural progression or be associated with the submergence seen in the Marsh. The mud unit has no modern analog on the delta and could represent ponding due to tectonic changes in drainage of the area or increasing fine grained sedimentation due to an input of muddy sediment from Pleistocene lake deposits up stream (Smith et al., 2007). Less than 800 years ago, either through natural progression or due to a tectonic event, the Bog transitioned from depositing mud to depositing peat. This could be due to natural progression. As the Bog filled it may have transitioned to a peat-forming environment. However, the contact between the mud and peat is sharp, possibly indicating an event spurred on this transition.

Though subsiding more recently, aforesaid local faulting has left the Skokomish delta with little net land level change. The presence of the Ridge potentially indicates net uplift, but the lack of paleoenvironmental indicators in Ridge stratigraphy makes this inference difficult, as the original elevation of deposition is unknown. The brackish sediments that were uplifted 1,100 years ago in the Marsh and Swamp are mostly now at an elevation where similar brackish sediments form (Figure 4.4). If shallow faults were not generating uplift events at the delta, there would be net subsidence.

Submergence of the Skokomish delta most likely is due to a combination of factors including sediment compaction, sea level rise, and slow, regional tectonic subsidence. In the last thousand years, relative sea level in northern Hood Canal rose a meter or less (Eronen et al., 1987; Beale, 1990). Based on peat cores, this value should include both eustatic sea level rise and tectonic submergence. Similarly, historic rates from the eastern Puget Lowland of 1 mm/yr (Holdahl, 1989) would indicate relative sea level rise of about a meter in the last thousand years. However, the submergence rate at the Skokomish delta (1.6 m in 1,000 yr) is higher than the projected rates, indicating other factors at play besides sea level rise and background rates of tectonic subsidence. Several other salt marshes at approximately the same latitude as the Skokomish delta also show evidence for uplift and later submergence of approximately the same amount (Garrison-Laney, 2003; Chapter 3), indicating that long-term rates of subsidence may be higher than extrapolated modern rates. Compaction of sediments contributes to this submergence, as may possible changes in stress during subduction-zone earthquakes.

4.6 INFERRED DELTA HISTORY

The Ridge is the oldest delta feature in the study area. The sediments below the Ridge are at least 7,000 years old and the Ridge as a geomorphic feature is older than 800 years and likely older than the earthquake 1,100 years ago.

The inferred late Holocene history of the Skokomish River delta begins before the 1,100-year-ago earthquake (Figure 4.11). The active gravel beach berm at this time was the ancient gravelly berm of Figure 4.2. In front (seaward) of this ancient berm the surface varied

between muddy and pebbly sediment, and behind the berm and in front of the Ridge was a large muddy tidal flat. At this time, behind the Ridge was a freshwater environment.

Then about 1,100 years ago an earthquake uplifted the Marsh and Swamp area of the delta and possibly a greater area and generated shaking that caused liquefaction. The fault rupture possibly raised the western side of the delta more than the eastern side. This differential uplift (tilting) most likely trapped the lower Skokomish River on the eastern side of the valley and may account for the abandonment of channels that cut the Ridge.

Since the earthquake, facies changes in the delta stratigraphy indicate additional environmental changes, though the timing of these changes has fewer constraints. Either through a somewhat constant rate of submergence or via coseismic subsidence, the delta front has submerged at least 1.5 m. The woody peat in the Marsh has a sharp to gradational upper contact with muddier salt-marsh peat. This change indicates either submergence or a receding shoreline. Since AD 1100 the Bog transitioned from a freshwater mud to a freshwater peat environment.

The delta is currently undergoing additional changes. Trees in the Bog are dying. Also, the western delta front is eroding, as is evident from the tree stump eroding out into the intertidal zone. Both of these processes may be signals of ongoing submergence.

4.7 CONCLUSIONS AND IMPLICATIONS

Landforms, stratigraphy, and paleoecology in the Skokomish delta provide evidence for an earthquake about 1,100 years ago. This earthquake, tentatively linked to the Saddle Mountain fault zone, resulted in at least 1 m of uplift on the delta front and in the triggering of sand blows. Differential uplift during the earthquake may have resulted in the eastward tilt

of the delta. This earthquake also may have caused the abandonment of channels on the western side of the delta and trapped the mouth of the Skokomish River on the eastern side of the delta. The river remaining on the eastern side of the delta for at least 1,100 years has resulted in a 2-km-wider unvegetated intertidal zone in the eastern than in the western bay.

The sequence of co-seismic uplift and later submergence is present in other Puget Lowland salt marshes such as Lynch Cove, Burley, and Gorst (Blakely et al., 1992; Sherrod et al., 2004; Chapter 3), though the cause of the submergence is still unclear. This co-incidence indicates the Skokomish is linked to lowland-wide tectonics and is more influenced by compressional tectonics of the lowland than by uplift of the Olympic Mountains. Though the study herein demonstrates that the delta has lately undergone submergence, the cause of submergence is unknown. Several causes have been proposed including slow subsidence related to several causes, or rapid subsidence related to changes in stress during subduction zone earthquakes (Holdahl, 1989; Garrison-Laney, 1996).

Understanding Holocene rates of uplift and subsidence in the Puget Lowland may aid in understanding the behavior of the Cascadia subduction zone, although lowland-wide records are difficult to distinguish from local effects. For example, between local, fault-generated uplift and possibly regional subsidence, the Skokomish delta has experienced little net land level change in the last 1,100 years. Patterns of uplift and submergence in forearc basins such as the Puget Lowland vary from basin to basin, and the underlying cause of land-level change may vary too (Xie and Heller, 2009).

Understanding slow or rapid submergence in the Puget Lowland aids in hazard planning, and better constraints on submergence rates are important in planning for sea level rise. The Skokomish delta is situated in an area where predicted submergence rates are

variable, and the longer-term rate of 1.6 m/ka deduced from my study may be important in refining sea-level predictions for the future. The rate of tectonic subsidence currently used to predict the economic impact of climate change on Washington in the region of the Skokomish delta is between 0 and 1 m/ka (WESC, 1996). If the long-term submergence rate of 1.6 m/ka at the Skokomish delta is not due largely to compaction, then rates of relative sea level rise for the region may be underestimated.

Table 4.1: Radiocarbon dates from the Skokomish delta.

Location	Measured 14C yr BP	Calibrated 2 sigma range	Material	Layer	Limiting	Author	Sample ID
3 (531)	1130±40 BP	AD 780-990	Seeds	Basal 2 cm peat	Minima for uplift	This study	Beta 263045
DNR core	7,740 ±50 BP	BC 6650-6470	Charcoal	School drill, 71 feet depth	Maxima for Ridge formation	Polenz et al., 2010	Beta 272798
9 (DNR Bog core)	780 ±40 BP	AD 1180-1290	plant material	bog, 9'6"-9'8" depth (in mud)	Maxima for peat formation	Polenz et al., 2010	Beta 273145
3 (209)	1050 ±60 BP	AD 830-1160	Submerged tree	Rooted into peat-mud contact	Minima for uplift	Polenz et al., 2010	Beta 273144
8 (2005)	90 +/- 40 BP	AD 1680-1940	*Pseudotsuga menziesii* needles	Basal 5 cm peat	Minima for channel abandonment	This study	Beta 282145
5 (1900)	600 +/- 40 BP	AD 1290-1410	*Picea sitchensis* seed	Basal 5 cm peat	Minima for channel abandonment	This study	Beta 282144

All dates in this study were AMS dates Calendar age was calibrated using IntCal 09 (Reimer et al., 2009) using the online program OxCal (https://c14.arch.ox.ac.uk/oxcal/). Location number in parenthesis is GPS location from Appendix 3, figures 4.6-4.9 plot stratigraphic locations of samples.

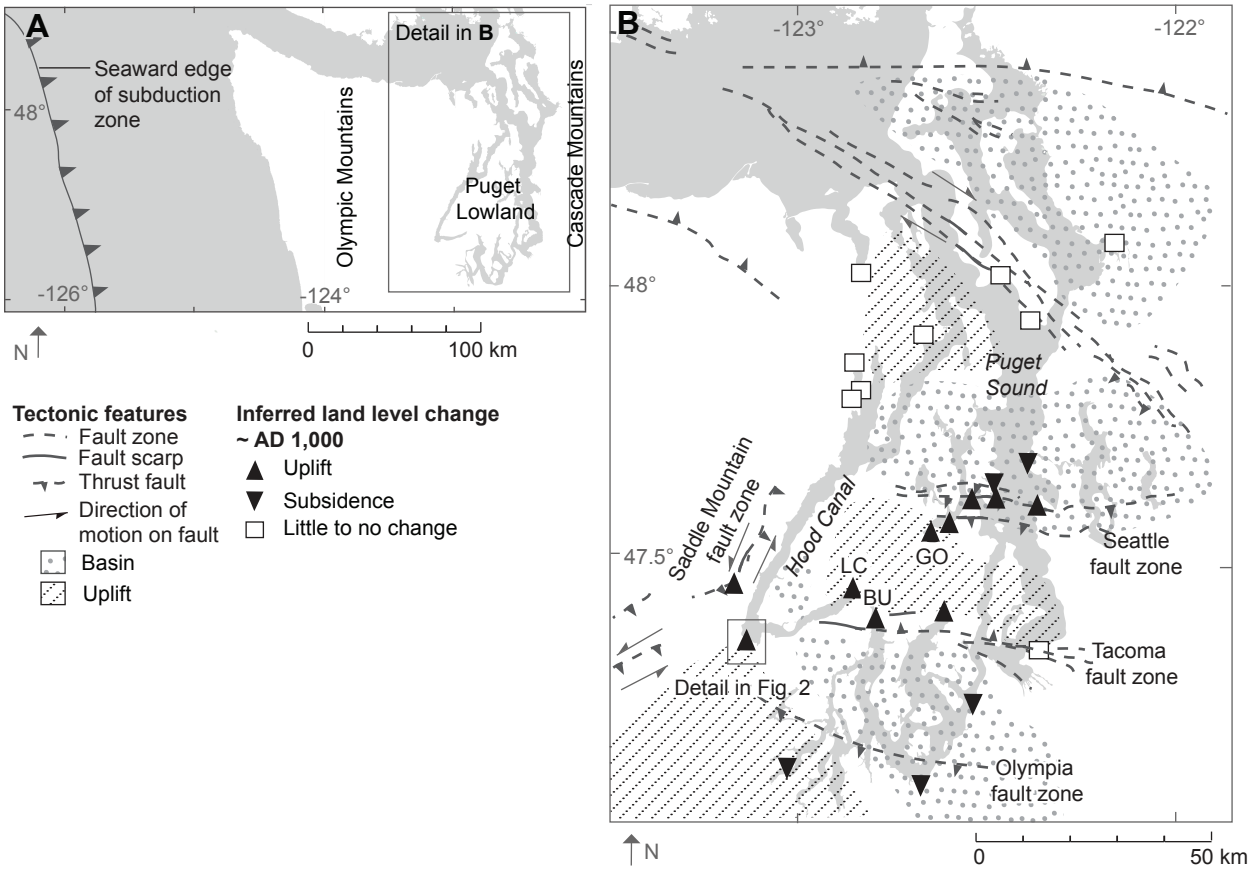

Figure 4.1 The tectonic setting of the Puget Lowland and crustal fault locations. A. Map of Cascadia subduction zone and coastline. B. Map of the Puget Lowland showing active faults and locations of paleoseismic studies. LC=Lynch Cove, BU=Burley, GO=Gorst. Modified from Blakely et al., 2009. Paleoseismic studies: Eronen et al., 1987; Beale, 1990; Bucknam et al., 1992; Sherrod, 2001; Bourgeois and Johnson, 2002; Blakely et al., 2009; Brian Sherrod, personal communication; Chapter 2.

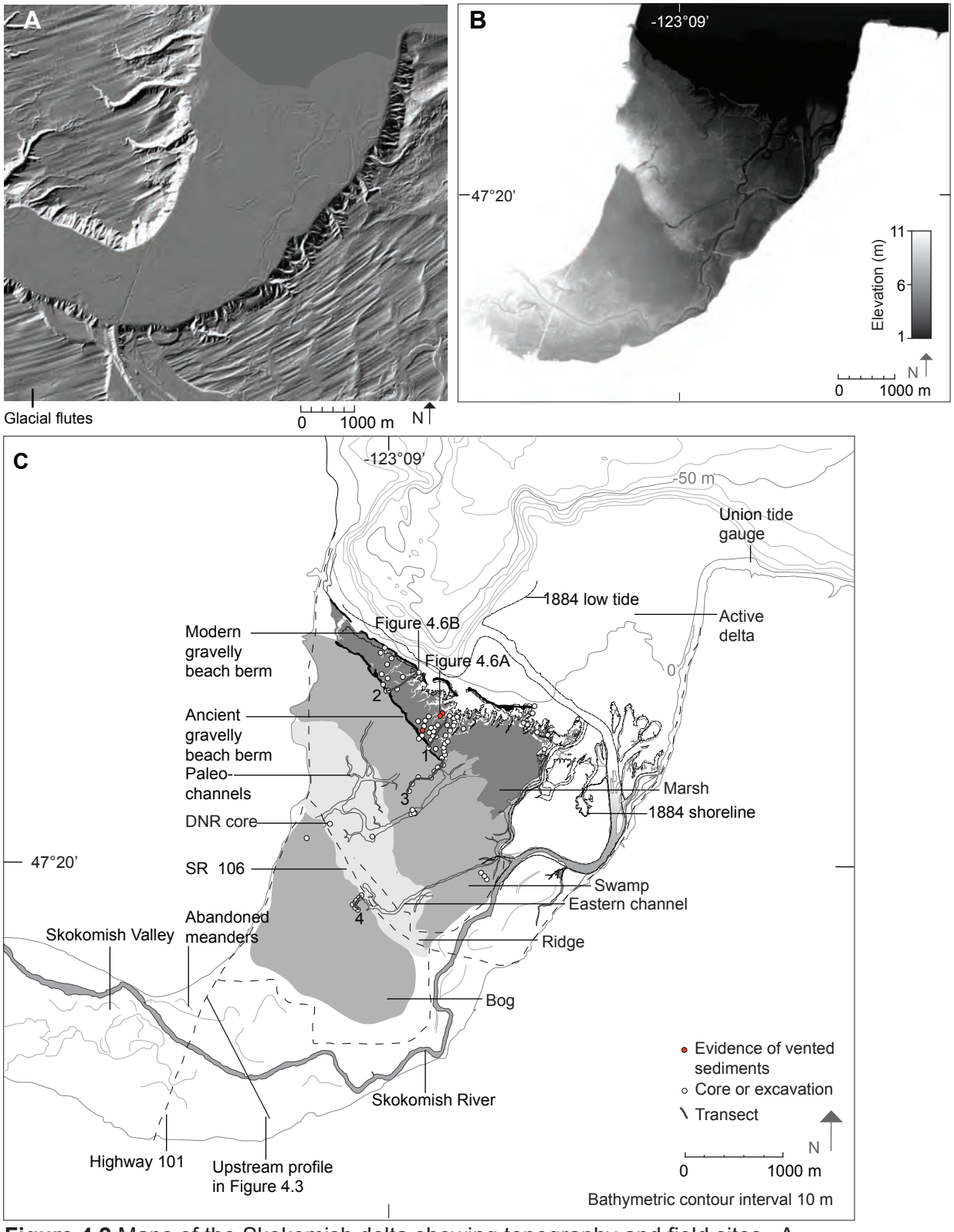

Figure 4.2 Maps of the Skokomish delta showing topography and field sites. A. Hillshade LiDAR image of the Skokomish delta and surrounding uplands. Light source is from the southeast. B. LiDAR image shaded from 1-11 m elevation detailing the geomorphology of the Skokomish delta and valley. C. Interpreted map of the Skokomish delta including locations of stratigraphic sections and transects. Historic shoreline taken from Gilbert (1884). Delta zones drawn based on a combination of stratigraphy, geomorphology and modern vegetation.

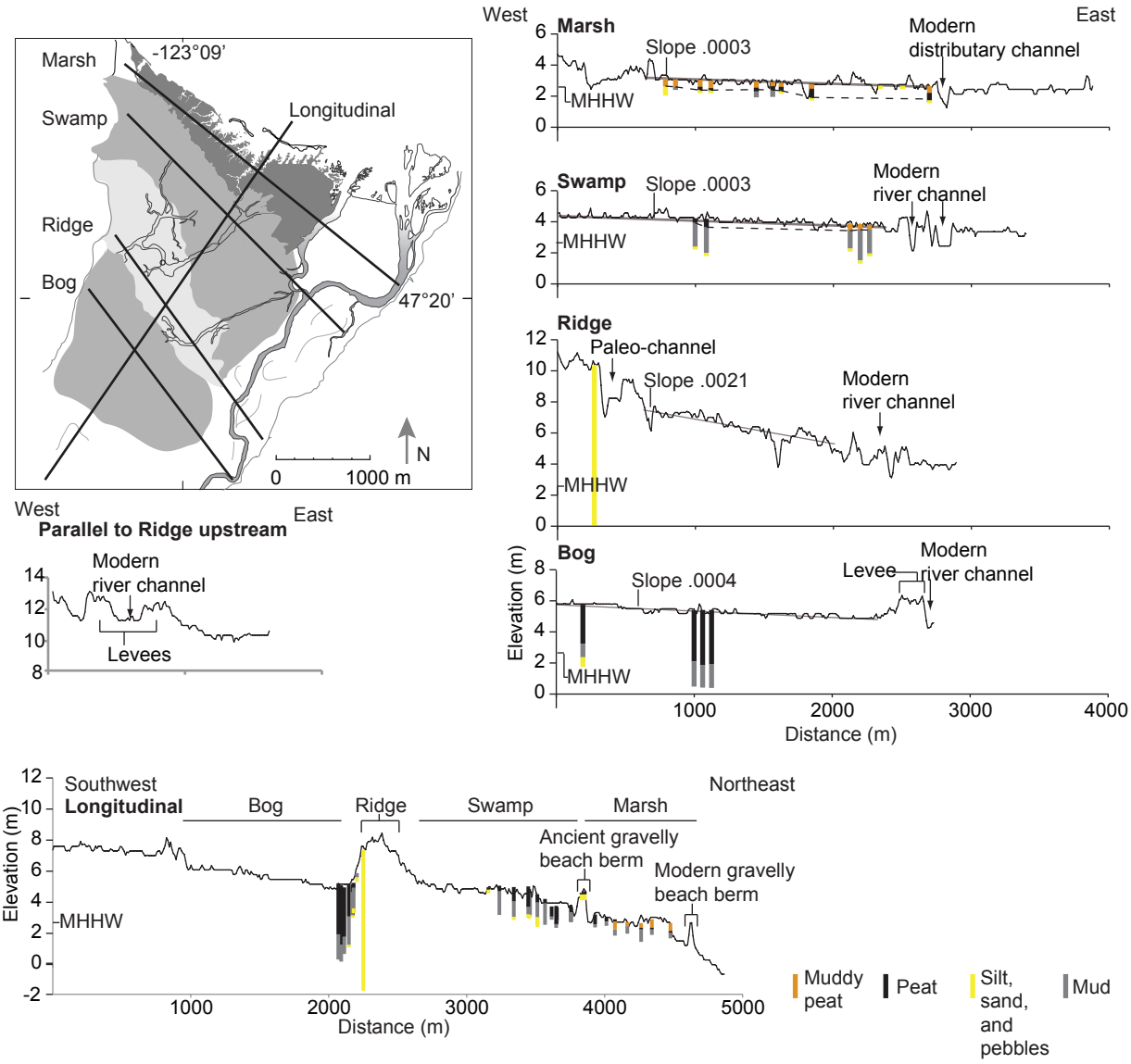

Figure 4.3 Topographic profiles of the Skokomish delta taken from LiDAR data showing a southeastern slope to all areas of the delta. In the profile from upstream the river levees are the highest point of the profile while in the profiles from the study area the northwest end of the profile is always the highest. Stratigraphic sections within 75 m of the profiles are plotted on the profiles. MHHW is Mean Higher High Water at the Union tide gauge. Zero elevation is the NAVD88 datum. Dashed line in the Marsh and Swamp profiles marks the surface uplifted ~1,100 years ago. Upstream profile location on figure 4.2.

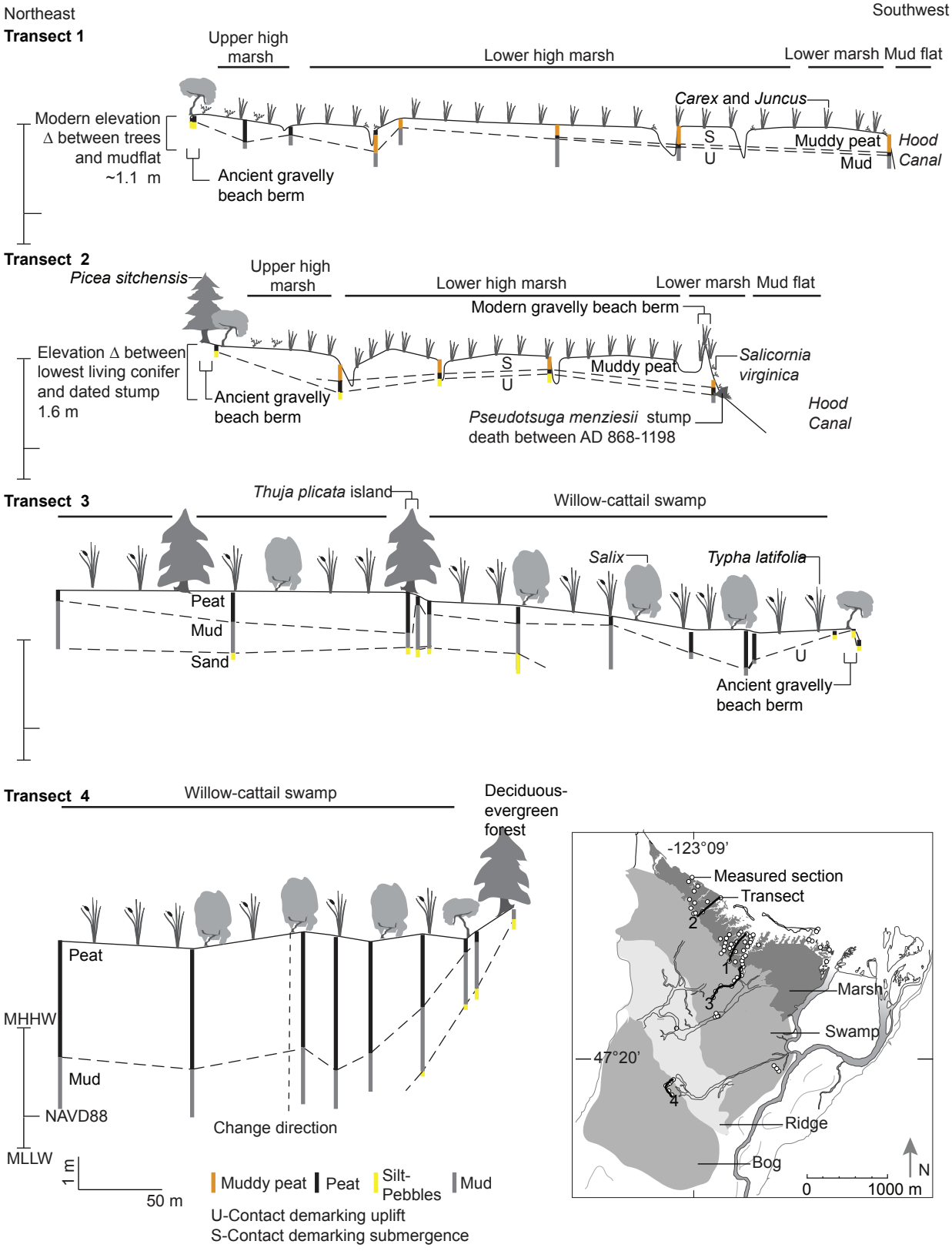

Figure 4.4 Vegetation and stratigraphic transects from the four delta zones indicating uplift and later submergence in the Marsh and Swamp and peat and mud thinning onto the Ridge from the Swamp.

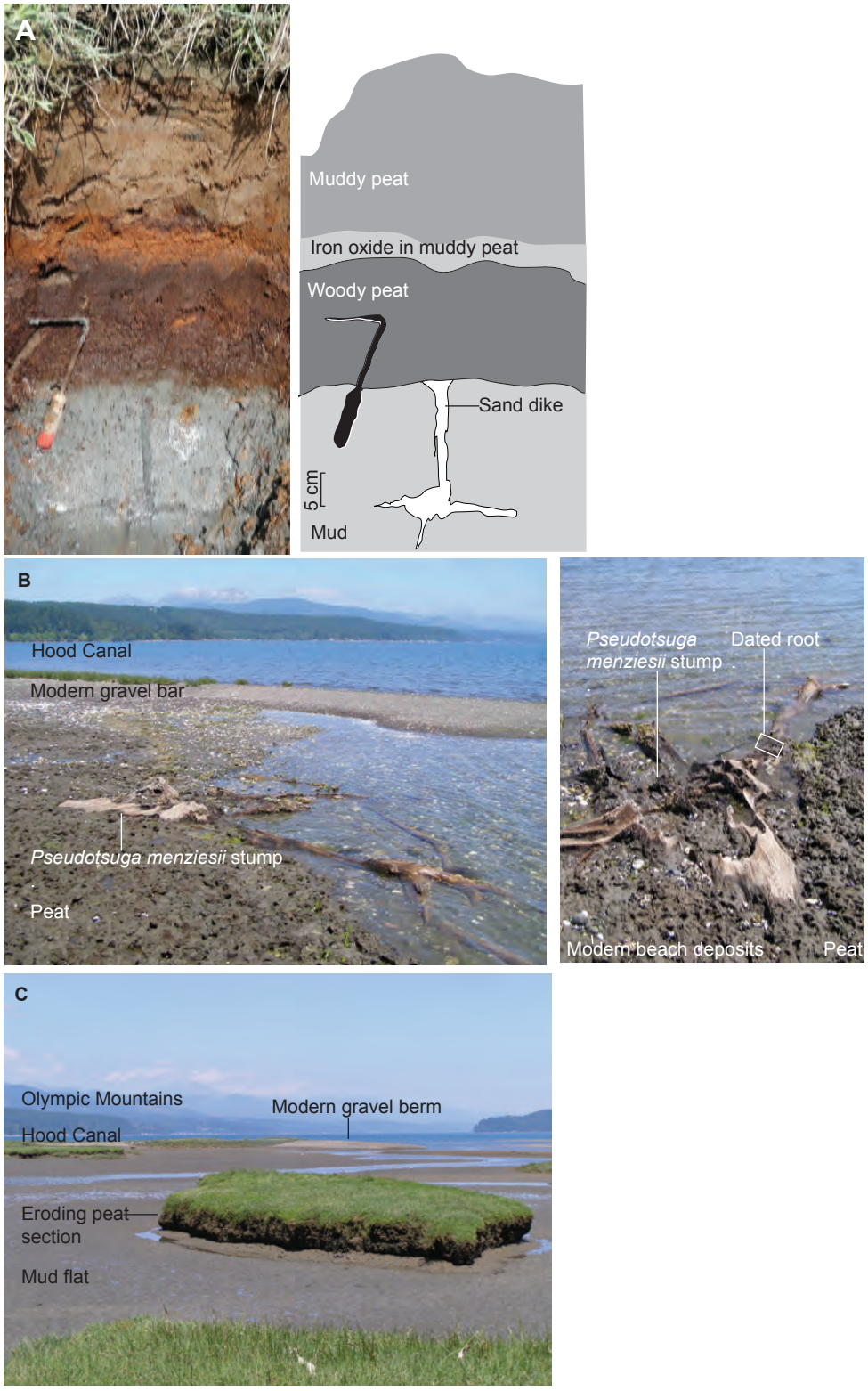

Figure 4.5 Photographs of the Marsh detailing key features indicating uplift and later submergence. A. Photograph of an injected sand dike terminating at the marine mud-woody peat contact. Within 5 m of photograph there is vented sand at the marine mud-woody peat contact. B. Photograph of a Pseudotsuga menziesii stump eroding out of peat in the modern intertidal zone. This stump is at the seaward end of Transect 2 from Figure 2. C. Photograph looking north of intertidal environment of the Marsh and eroding peat facies.

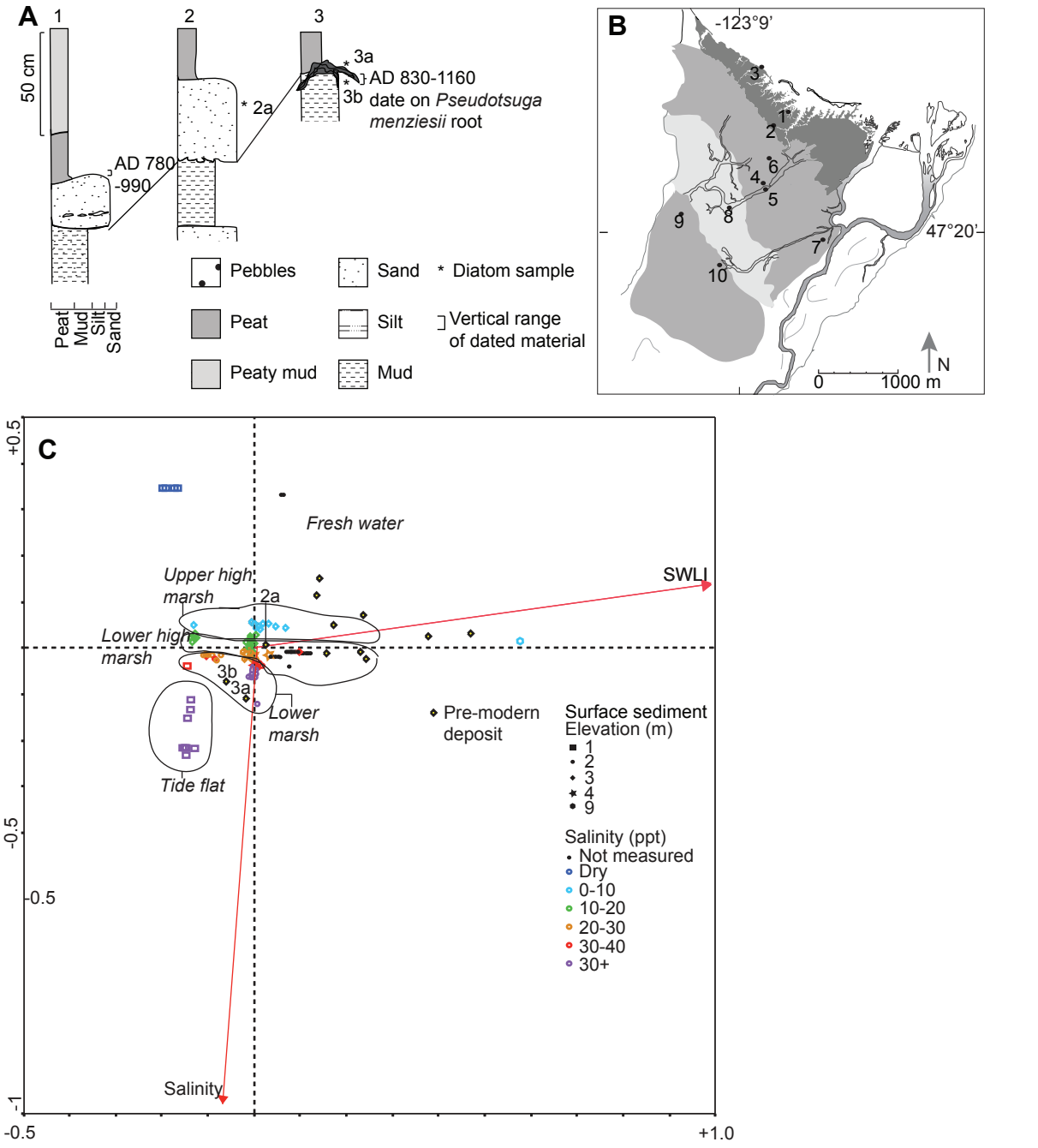

Figure 4.6 Diatom data and stratigraphic sections from the Marsh indicating different elevations of intertidal deposition. A. Stratigraphic sections and dating and diatom sample locations. B. Map of delta with stratigraphic section locations for this figure, Figure 4.7, 4.8 and 4.9. C. Diatom analysis. Samples plotted against modern data, salinity and Standard Water Level Index (SWLI).

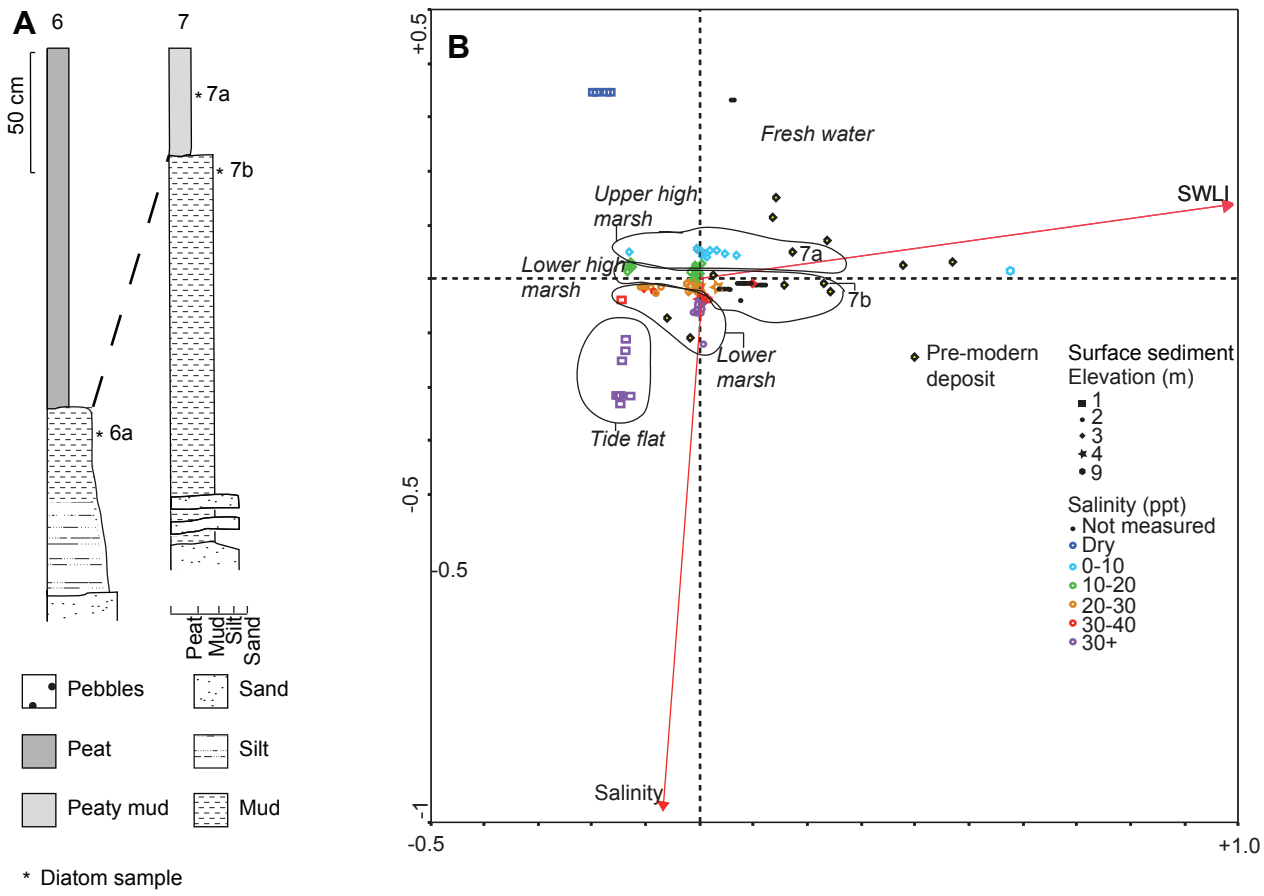

Figure 4.7 Diatom data and stratigraphic sections from the Swamp indicating uplift from lower high marsh to upper high marsh. A. Stratigraphic sections and dating and diatom sample locations. Sample 6a counted by Y. Sawai and was not plotted on the graph. B. Diatom analysis. Samples plotted against modern data, salinity and Standard Water Level Index (SWLI).

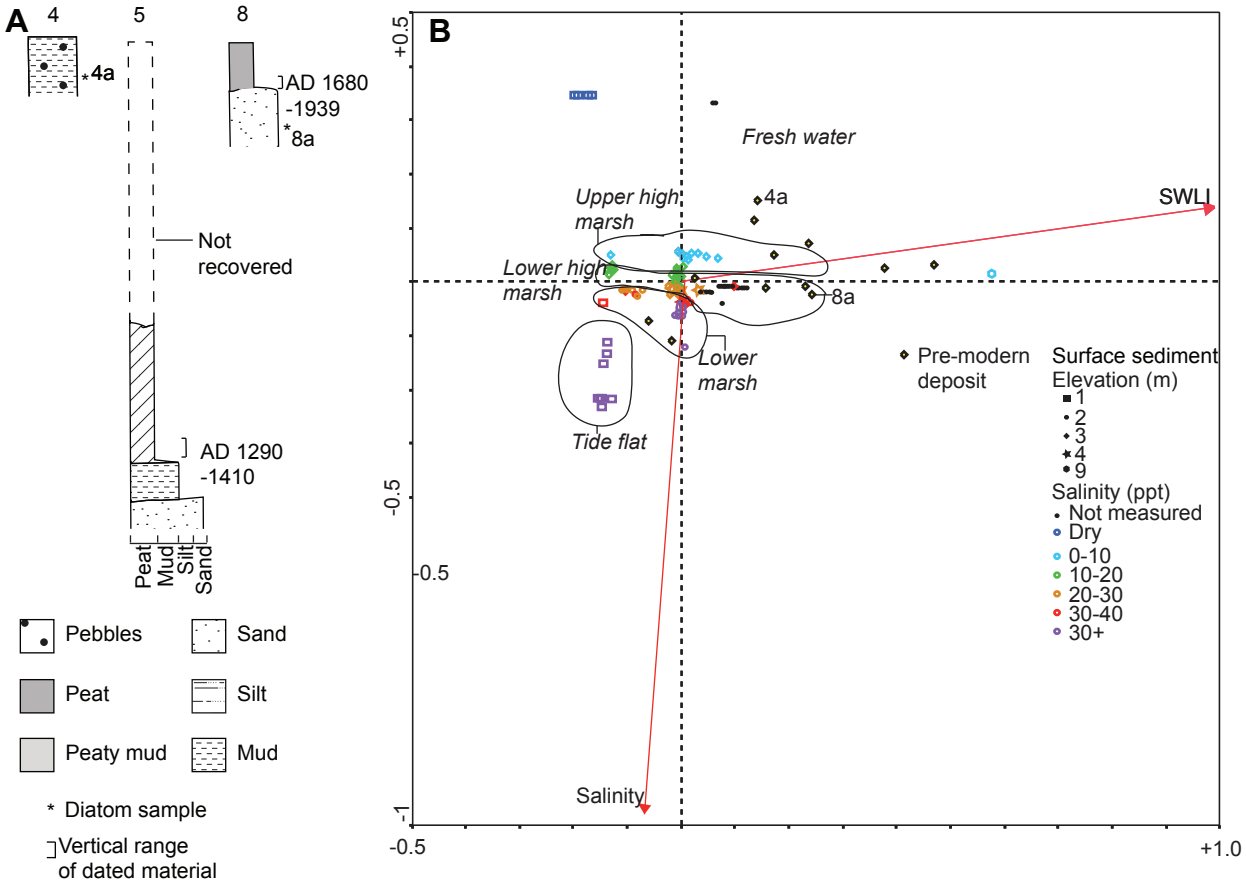

Figure 4.8 Diatom data and stratigraphic sections from the paleochannels indicating mostly fresh water deposition. A. Stratigraphic sections and dating and diatom sample locations. B. Diatom analysis. Samples plotted against modern data, salinity and Standard Water Level Index (SWLI). The sample in core 5 dated *Pseudotsuga menziesii* needles. The date in core 8 is from a *Picea sitchensis* seed.

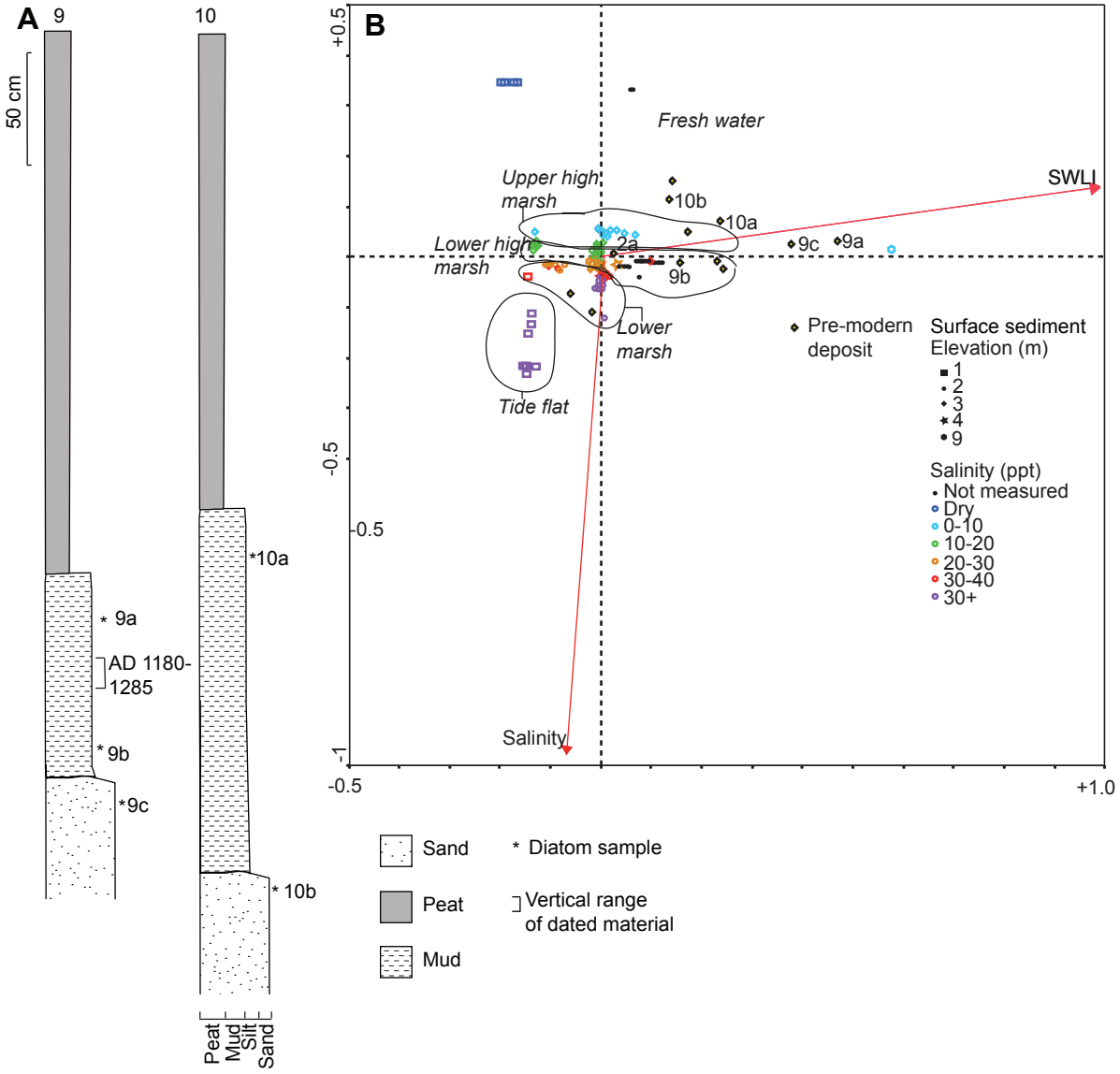

Figure 4.9 Diatom data and stratigraphic sections from the Bog indicating fresh water deposition. A. Stratigraphic sections and dating and diatom sample locations. B. Diatom analysis. Samples plotted against modern data, salinity and Standard Water Level Index (SWLI). The date from core 9 is from plant material.

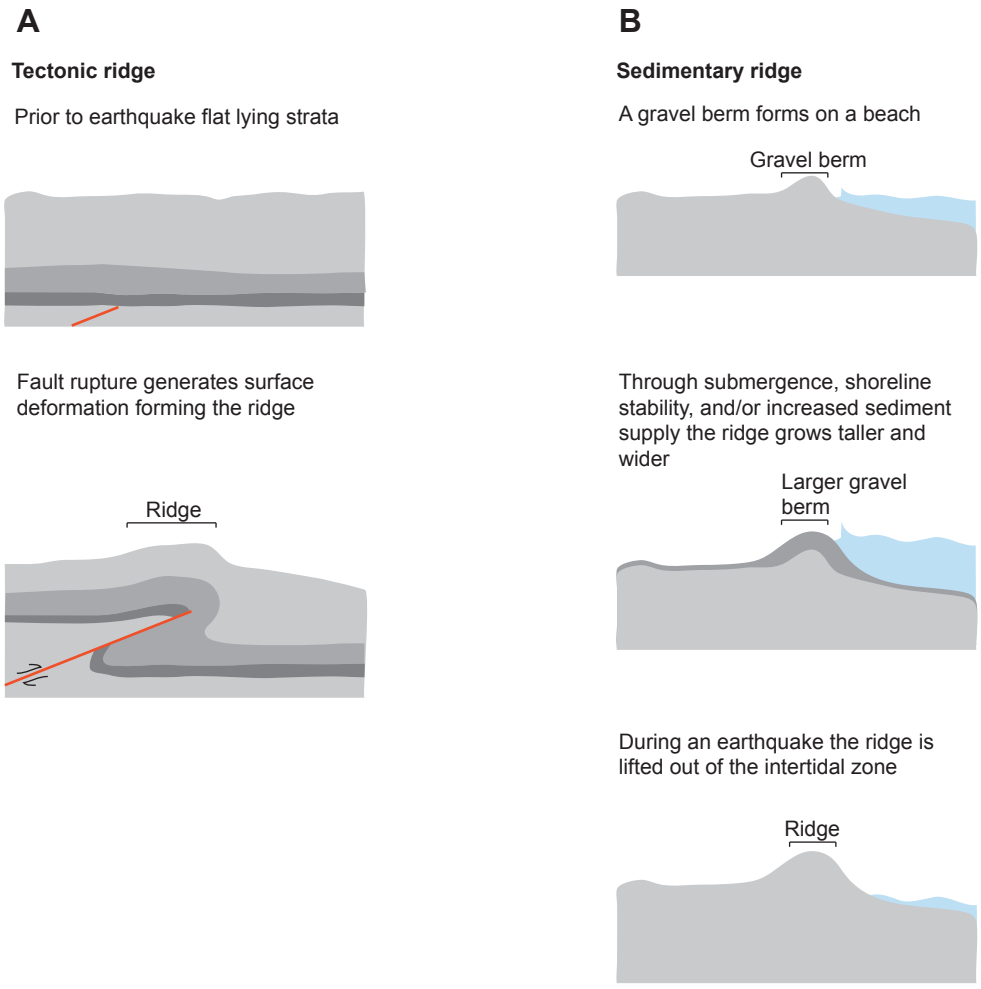

Figure 4.10 Hypotheses for formation of the Ridge by either A. Surface deformation by a blind thrust fault or B. Formation by coastal processes and later uplift out of the intertidal zone by an earthquake.

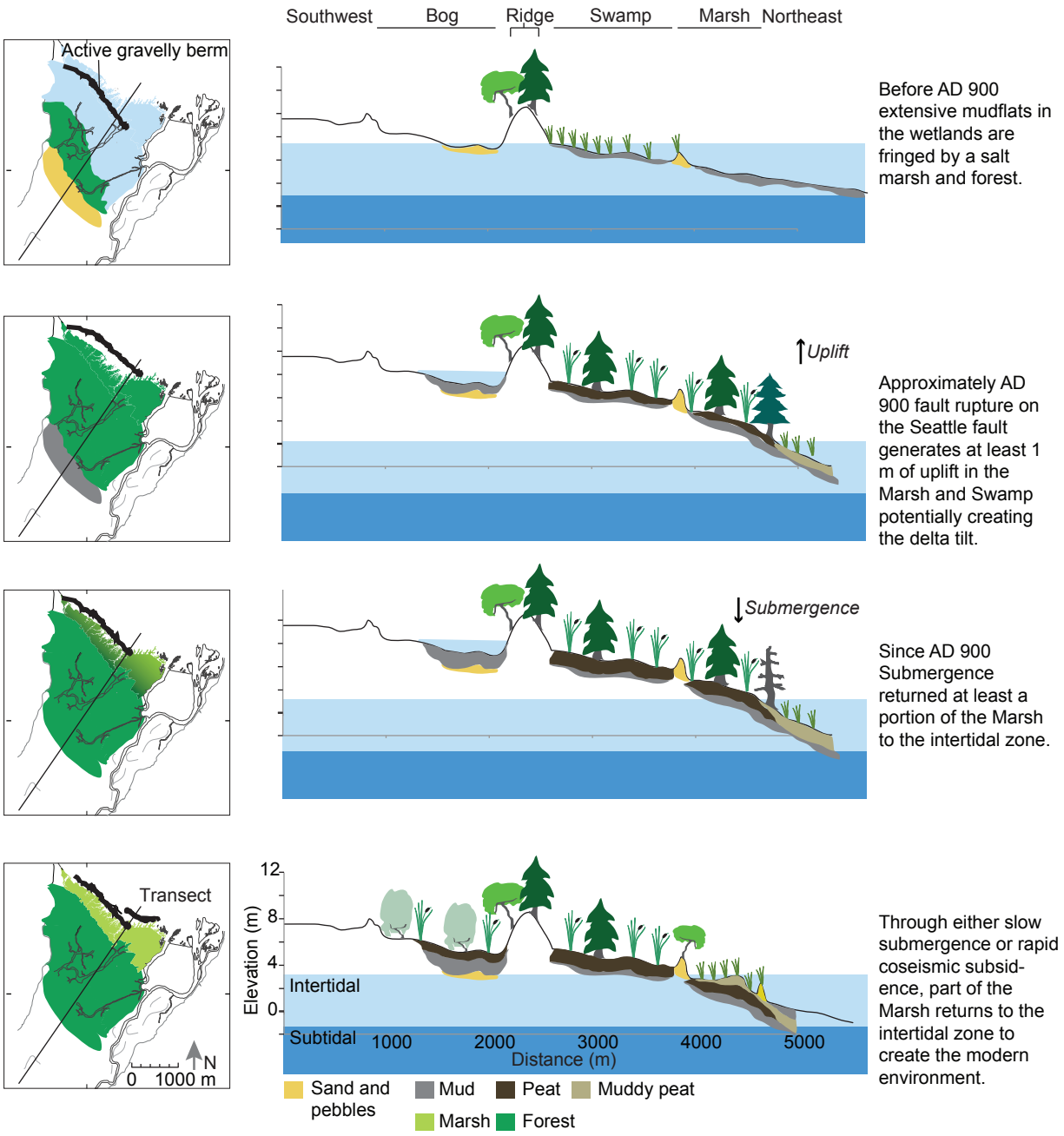

Figure 4.11 Cartoon of delta history showing uplift and later submergence of the delta. A. Pre-earthquake the Ridge was the approximate location of the shoreline. B. Post-earthquake uplifted environments. C. Environments reflecting the return of the front of the delta to intertidal conditions. D. Modern environment.

CHAPTER 5

Conclusions

5.1 REVIEW

This study used detailed sedimentology and stratigraphy in conjunction with modeling to examine the impact of large earthquakes in the Puget Lowland about 1,100 years ago. As part of this study I established characteristics to distinguish between tsunami deposits and vented sediments, the results of which I discussed in Chapter 2. In Chapter 3, using sedimentology, stratigraphy, and tsunami modeling, I examined the impacts of a Seattle fault earthquake in Gorst including uplift, a tsunami and a debris flow. Finally, in Chapter 4, I examined the impacts of tectonics on the stratigraphy and morphology of the Skokomish delta and demonstrated that a tilt to the delta has likely trapped the Skokomish river on one side of the delta since about 1,100 years ago.

In Chapter 2, I discussed the similarities and differences between tsunami and vented-sediment deposits in order to establish characteristics to aid in their distinction. The sandy deposits produced by tsunamis and liquefaction share many sedimentary features but differ in others. The distinctions are important where both can be present in coastal stratigraphy. Such places include wetlands bordering Puget Sound, where a paroxysm about 1,100 years ago caused both tsunami flooding and sediment venting. I analyzed the resulting deposits at Puget Sound, and compared them to tsunami and liquefaction features elsewhere. I found that vented sediments tend to be thicker (though they can be thin), to have more variable thickness at both outcrop and map scale, to be associated with injected dikes, and to contain clasts derived from underlying deposits. Vented sediments also tend to contain a greater

variety of sedimentary structures, and these structures vary laterally over meters. Tsunami deposits tend to be thinner, to fine and thin landward more consistently, to have more uniform thickness on outcrop and map scales, and to have the potential of containing coarser clasts, up to boulders. Foraminifera and diatom assemblages within tsunami deposits and vented sediments can be similar. Of five field localities, there is evidence for vented sediments at four and evidence of tsunami deposition at two. This study indicates a need for more careful analysis and mapping of coastal sediments associated with earthquakes to avoid misidentification of deposits and misevaluation of hazards.

In Chapter 3, I examined a new field locality for evidence of a Seattle fault-zone earthquake, which resulted in extension of the zone of coseismic deformation and tsunami deposition to the south and west. Deposits beside tidewater at Gorst, 20 km west of Seattle, provide evidence for uplift, a tsunami, and sandy debris flows triggered by a large earthquake previously shown to have occurred on the Seattle fault zone AD 900-930. An estimated 3 m or more of uplift changed a shelly tidal flat to a freshwater swamp. This uplift extends, by 3 km, the western limit of documented coseismic deformation along the Seattle fault zone. Now below high-tide level, the elevation of the lowest of the freshwater-swamp deposits indicates at least 1.5 m of relative sea-level rise since all these earthquake-related events took place. This submergence subsequent to the earthquake would indicate even greater uplift on previously mapped marine terraces created by the AD 900-930 earthquake. A sand body between the tidal-flat and swamp deposits contains a basal graded bed, rarely more than 10-cm thick, which was laid down by a tsunami generated by uplift along the Seattle fault. The rest of the sand body, which is commonly 0.5-1.0-m thick, most likely represents debris-flow deposits and the braided streams that reworked them. The debris-flow and braided-stream

deposits extend at least 2 km up Gorst Creek. In a section 1.5 km upstream they include detrital leaves that yielded ages, at two standard deviations, of AD 690-860, 720-940, and 890-990. The tsunami deposits accord with simulations showing that the AD 900-930 earthquake along the Seattle fault zone produced tsunami wave heights of 4.0-5.5 m at Gorst. Tsunami simulations of a similarly aged Tacoma fault rupture produced wave heights of 0.4-0.6 m at Gorst. The sandy debris-flow deposits are the some of the first linked to the AD 900-930 earthquake.

In Chapter 4, I discussed the evidence for recent tectonic activity at the Skokomish delta in the western Puget Lowland. An earthquake about 1,100 years ago generated at least 1 m of coseismic uplift on the delta front, and sand blows accompanied the earthquake. Several active faults are in the vicinity of the delta, but uplift was most likely related to the Saddle Mountain fault zone. This uplift may have been higher on the western side of the delta, causing the abandonment of channels and trapping the mouth of the Skokomish River on the eastern delta. Deposition focused on the eastern side of the delta for the past 1,000 years has resulted in a muddy intertidal zone that is 2 km wider in the east than in the west. An enigmatic, approximately shoreline-parallel ridge crosses the delta and may be the surface expression of a blind thrust fault or a relict, uplifted shoreline. Since the time of the uplift about 1,100 years ago, the delta front has submerged over 1.5 m. This submergence has implications for deformation of the Puget Lowland and for planning for future sea-level rise.

5.2 IMPLICATIONS

Chapter 2 calls to the attention of tsunami geologists the necessity to consider sediment venting as a possible and likely source of deposition associated with earthquakes in

coastal regions. Because these two processes can occur at the same location and during the same earthquake, such as is the case at the Snohomish Delta (Bourgeois and Johnson, 2001), care should be taken in distinguishing the two. Confounding vented-sediment deposits with tsunami deposits could lead researchers to draw incorrect conclusions regarding tsunami run-up and inundation. The differentiation of tsunami deposits and vented sediments is important because the deposits help us understand different processes. Tsunami deposits typically indicate shallow faulting, and with models the distribution of tsunami deposits can be used to test differential slip on faults (e.g. MacInnes et al., 2010) or distinguish the earthquake source when two nearby faults rupture around the same time (Martin et al., 2008; Chapter 3). Vented sediments indicate strong shaking, and the source depth and the distribution of vented sediments can be used to map zones of this strong shaking and to help locate earthquake sources. If the wrong process is inferred, the hazard could be incorrectly assessed.

The study in Chapter 3 indicates a wider band of coseismic deformation during the AD 900-930 Seattle-fault-zone rupture than previous fault interpretations (ten Brink et al., 2006; Kelsey et al., 2008), and this uplift may have implications for the fault structure. My interpreted minimum of 3 m of uplift at Gorst is double the uplift estimated by previous fault models (Koshimura et al., 2002; ten Brink et al., 2006). Higher uplift indicates that the zone of deformation of the Seattle fault may not be as narrow as estimated by the presence of marine terraces, or that there was greater slip on deeper portions of the fault. Different fault structures or slip-distribution patterns determine what areas experience the strongest shaking during earthquakes. Different fault structures will also generate different tsunamis. Though higher displacement at Gorst does not displace significantly more water, a wider band of

deformation in the main stem of Puget Sound would generate a longer-period wave, which would behave differently than waves currently used for hazard analysis.

Chapter 3 and 4 both examine evidence for perplexing submergence in the last 1,100 years. Gorst, Lynch Cove and the Skokomish delta show evidence for 1.5 m or more of submergence in this time, a value greater than the <1 m of relative sea-level rise in the last thousand years calculated by Eronen et al. (1987) but falling within rates of subsidence mapped by Holdahl (1989) and Finnegan et al. (2008). However, submergence rates based on tide gauges such as those used by Holdahl (1989) may not be analogous to long-term rates because eustatic sea-level rise in the last 100 years is occurring at a greater rate than previously (Rahmstorf, 2007). Other workers have attributed this submergence to subsidence related to subduction processes and to formation of the Olympic Mountains (Garrison-Laney, 2003; Holdahl, 1989).

Submergence in the Puget Lowland has three implications. 1) The submergence has likely obscured the uplift record from earthquakes in areas where the amount of uplift was at or about the amount of submergence. For example, at Lynch Cove, Gorst and the Skokomish delta the contact that demarks uplift has returned to the intertidal range in most studied locations where post-earthquake deposition was in freshwater environments. Submergence implies that in areas where bedrock occurs, a marine terrace uplifted 1-2 m during the events ~1,100 years ago would now be within the range of tides and difficult to identify using LiDAR or field methods. 2) Refined submergence rates may have implications for understanding both the impact of subduction-zone earthquakes and behavior of the forearc basin. With additional study, the manner in which rates vary geographically may indicate the

cause of submergence. 3) Submergence rates help refine projections of local effects combined with global sea-level rise.

5.3 FUTURE WORK

As always with science, studying one question leads to many more. This study highlighted several areas of future work.

Chapter 2 highlights the need to distinguish tsunami deposits and vented sediments. Prior to this study, tsunami-deposit researchers rarely gave vented sediments strong consideration when determining the source of sandy layers. It may be important to reexamine key deposits used for tsunami hazard analysis, especially if these sites contain unusually thick deposits.

Further work would also elucidate the differences between tsunami deposits and vented sediments. Most of Chapter 2 relied on using sedimentological features to distinguish the two and concluded that vented sediment deposits are more variable in thickness and internal sedimentary structures. Though not looked at in detail in this study, theoretical and preliminary analyses indicate that microfossil assemblages in vented sediments would be more variable laterally and vertically. In areas where cores are the only viable method of field sampling, microfossil variability may be easier to examine than sedimentary structures and thickness variability. Case histories in other areas would also be useful. I was unable to find thickness vs. elevation transects of vented-sediment deposits that were directly comparable to transects typical in tsunami research. Also, a distinct lack of information on thickness variability in thin (<20-cm thick) vented-sediment deposits makes comparisons with tsunami deposits incomplete. Thin, vented-sediment deposits are at the same scale as

typical tsunami deposits and therefore, the most difficult to distinguish. A detailed study of thin, vented sediment deposits that could be directly compared to studies of tsunami deposits might help refine characteristics to distinguish between the two.

The study of the Skokomish delta (Chapter 4) leaves as many questions as answers. What fault or faults are driving coseismic land-level change at the delta? What is the origin of the Ridge? If the Ridge is fault generated, why does the deformation not extend geomorphologically into the glacially carved upland? Is submergence gradual or punctuated? Many of these questions will not be easy to answer, but more detailed diatom stratigraphy and dating would lead to a better understanding of the uplift and subsidence history of the delta. These results could help elucidate potential sources of land-level change. Detailed geophysical surveys and fault modeling would help us understand which faults influence the relative sea-level history of the delta and the origin of the Ridge. Here also, a better understanding of the extent and behavior of the Olympia and Saddle Mountain fault zones would enable us to put the Skokomish delta into a more regional context.

Chapter 3 and 4 looked at evidence for late Holocene submergence in the Puget Lowland but did not come to conclusions about the cause of submergence. Complex forces interplay to generate submergence in the Puget Lowland. Work by Garrison-Laney (2003) indicated submergence may be related to subduction-zone earthquakes, but historical records indicate gradual submergence (e.g. Holdahl, 1989; Finnegan et al., 2008). Also, it is unclear how historical rates relate to Holocene and longer-term rates. While historical rates indicate submergence, in the areas of this study that experienced uplift about 1,100 years ago, net land-level change is slight uplift or no change. Longer-term rates indicate a series of basins and uplifts in the Puget Lowland. Glacial beveling and post-glacial sea-level rise have

complicated scientists' ability to determine longer-term rates of uplift and submergence. Detailed diatom stratigraphy and dating from marshes across the Puget Lowland would help constrain the timing and rate of submergence.

Chapter 4 summarizes ample evidence for past earthquakes in the Puget Lowland, but the location of faults in the vicinity of the Skokomish delta remains unclear. In general, fault locations in the western Puget Lowland are still not well understood. Geophysical fieldwork in conjunction with fault modeling would greatly aid in answering the questions that remain at the Skokomish delta. The use of LiDAR in conjunction with fault trenches has aided in identifying and illuminating several of the faults in the Puget Lowland (Harding and Berghoff, 2000; Sherrod et al., 2004; Sherrod et al., 2005), and further studies will continue to benefit our understanding of tectonics in the Puget Lowland region. Specifically, the behavior of the east-west-trending faults as they trend toward the Olympic Mountains, and the interaction and relation of these faults with the Saddle Mountain fault zone, have implications for understanding the Skokomish delta and elucidating the tectonic controls on the formation of the Puget Lowland.

References

Adams, J. (1980) Active tilting of the United States midcontinent; geodetic and geomorphic evidence. *Geology,* **8**, 442-446.

Anthony, E.J. (1995) Beach ridge development and sediment supply: examples from West Africa. *Marine Geol.,* **129**, 175-186.

Aspler, L.B., and **Donaldson, J.A**. (1985) Penecontemporaneous sandstone dykes, Nonacho Basin (Early Proterozoic, Northwest Territories): Horizontal injection in vertical, tabular fissures. *Can. J. Earth Sci.*, **23**, 827–838.

Atwater, B.F. (1987) Evidence for great Holocene earthquakes along the outer coast of Washington State. *Science*, **236**, 942-944.

Atwater, B.F. (1992) Geologic evidence for earthquakes during the past 2000 years along the Copalis River, southern coastal Washington. *J. Geophys. Res.*, **97,** 1901-1919.

Atwater, B.F. (1999) Radiocarbon dating of a Seattle earthquake to A.D. 900–930. *Seism. Res. Lett*., **70**, 232.

Atwater, B.F., and **Moore, A.L**. (1992) A tsunami about 1000 Years Ago in Puget Sound, Washington. *Science*, **258**, 1614-1617.

Atwater, B.F. and **Hemphill-Haley, E.** (1997) Recurrence intervals for great earthquakes of the past 3500 years at northeastern Willapa Bay, Washington. *U.S. Geol. Surv.,* **Professional Paper 1576**, 108 pp.

Atwater, B.F., Tuttle, M.P., Schweig, E.S., III, Rubin, C.M., Yamaguchi, D.K., and **Hemphill-Haley, E.** (2004) Earthquake recurrence inferred from paleoseismology. In: *The Quaternary Period in the United States*, (eds., Gillespie, A., Porter, S., and Atwater, B.) Elsevier, Amsterdam, Netherlands, 331-350.

Atwater, B.F., Musumi-Rokkaku, S., Satake, K., Tsuji, Y., Ueda, K., and **Yamaguchi, D.K.** (2005) The orphan tsunami of 1700; Japanese clues to a parent earthquake in North America: *U.S. Geol Surv.,* **Professional Paper 1707** and University of Washington Press, Seattle, 133 pp.

Audemard, F.A., and **de Santis, F**. (1991) Survey of liquefaction structures induced by recent moderate earthquakes. *Bull. Int. Assoc. Eng. Geol*., **44**, 5-16.

Barnhardt, W.A., and **Sherrod, B.L.** (2006) Evolution of a Holocene delta driven by episodic sediment delivery and coseismic deformation, Puget Sound, Washington, USA. *Sedimentology*, **53**, 1211-1228.

Beale, H. (1990) Relative rise in sea-level during the past 5000 years at six salt marshes in northern Puget Sound, Washington. *Shorelines and Coastal Zone Management Program, Washington Department of Ecology*. 55 pp.

Berger, M.J., **George, D.L., LeVeque, R.J.** and **Mandli, K.T.** (in press) The GeoClaw software for depth-averaged flows with adaptive refinement. *Adv. Water Resources.*

Blakely, R.J., Wells, R.E., Weaver, C.S., and **Johnson, S.Y.** (2002) Location, structure, and seismicity of the Seattle fault zone, Washington: Evidence from aeromagnetic anomalies, geologic mapping, and seismic-reflection data. *Geol. Soc. Am. Bull.,* **114**, 169–177.

Blakely, R., Sherrod, B.L., Hughes, J.F., Anderson, M.L., Wells, R.E., and **Weaver, C.S.** (2009) Saddle Mountain fault deformation zone, Olympic Peninsula, Washington: Western boundary of the Seattle uplift. *Geosphere*, **5**, 105-125.

Bondevik, S. (2003) Storegga tsunami sand in peat below the Tapes beach ridge at Haroy, western Norway, and its possible relation to an early Stone Age settlement. *Boreas*, **32**, 476-483.

Booth, D.B., and **Minard, J.P.** (1992) Geological map of the Issaquah 7.5' quadrangle, King County, Washington. *U.S. Geol. Surv. Map,* **MF-2206**.

Booth, D.B. (1994) Glaciofluvial infilling and scour of the Puget Lowland, Washington, during ice-sheet glaciation. *Geology*, **22**, 695-698.

Bountry, J.A., Godaire, J.E., Klinger, R.E., and **Varyu, D.R.** (2009) Geomorphic analysis of the Skokomish River, Mason County, Washington. *U.S. Dept. Interior,* **SRH-2009-22**, 130 pp.

Bourgeois, J. (2009) Geologic effects and records of tsunamis. In: *The Sea Volume 15 (Tsunamis)*, (eds. Robinson, A., and Bernard, E.), Harvard University Press, 55-91.

Bourgeois, J., and **Johnson, S.Y**. (2001) Geologic evidence of earthquakes at the Snohomish delta, Washington, in the past 1200 yr. *Geol. Soc. Am. Bull*., **113**, 482-494.

Bourgeois, J., Pinegina, T., Ponomareva, V., and **Zaretskaia, N**. (2006) Holocene tsunamis in the southwestern Bering Sea, Russian Far East, and their tectonic implications. *Geol. Soc. Am. Bull.*, **118**, 449-463.

Brandon, M.T., Roden-Tice, M.K. and **Garver, J.I.** (1998) Late Cenozoic exhumation of the Cascadia accretionary wedge in the Olympic Mountains, northwest Washington State. *Geol. Soc. Am. Bull*., **110,** 985-1009.

Brocher, T.M., Blakely, R.J., and **Wells, R.E.** (2004) Reinterpretation of the Seattle uplift, Washington, as a passive roof duplex. *Seis. Soc. Am. Bull*., **94**, 1379–1401.

Bucknam, R.C., Hemphill-Haley, E., and **Leopold, E.B.** (1992) Abrupt uplift within the past 1700 years at southern Puget Sound, Washington. *Science*, **258**, 1611-1614.

Cady, W.M. (1975) Tectonic setting of the Tertiary volcanic rocks of the Olympic Peninsula, Washington. *U.S. Geol. Surv. J. Res.*, **3**, 573–582.

Carson, R.J. (1973) First known active fault in Washington, *Wash. Div. Geol. & Earth Resources Newletter* **1**, 1–2.

Carson, R.J. (1976) Preliminary geologic map of north-central Mason County, Washington, *Wash. Div. Geol. & Earth Resources,* **OFR 76-2**.

Cartwright, J., James, D., Huuse, M., Vetel, W., and **Hurst, A.** (2008) The geometry and emplacement of conical sandstone intrusions. *J. Struct. Geol*., **30**, 854–867.

Castilla, R.A. and **Audemard, F.A.** (2007) Sand blows as a potential tool for magnitude estimation of pre-instrumental earthquakes. *J. Seis.*, **11**, 473-487.

Chleborad, A.F. (1994) Modeling and analysis of the 1949 Narrows Landslide, Tacoma, Washington. *Bull. Assoc. Eng. Geol.,* **3**, 305-327.

Choowong, M., Murakoshi, N., Hisada, K., Charusiri, P., Charoentitirat, V., Jankaew, K., Kanjanapayount, P., and **Phantuwongraj, S**. (2008) 2004 Indian Ocean tsunami inflow and outflow at Phuket, Thailand. *Mar. Geol.*, **248**, 179-192.

Cisternas, M., and **Atwater, B.F.** and 13 others, (2006) Predecessors of the giant 1960 Chile earthquake. *Nature*, **437**, 404-407.

Clague, J.J., Harper, J.R., Hebda, R.J. and **Howes, D.E.** (1982) Late Quaternary sea level and crustal movements, coastal British Columbia. *Can. J. Earth Sci.,* **19**, 597-618.

Clague, J.J. and **Bobrowsky, P.T.** (1990) Holocene sea level change and crustal deformation, southwestern British Columbia, In: Geological Survey of Canada, Current research, Part E—Cordillera and Pacific margin: *Geol. Surv. Can.,*

Paper 90-1E, 245-250.

Clague, J.J., Naesgaard, E., and **Sy, A.** (1992) Liquefaction features on the Fraser delta: Evidence for prehistoric earthquakes? *Can. J. Earth Sci.*, **29**, 1734-1745.

Clift, P.D., and **MacLeod, C.J**. (1999) Slow rates of subduction erosion estimated from subsidence and tilting of the Tonga forearc. *Geology*, **27**, 5, 411–414.

Collins, B. D., Montgomery, D.R. and **Sheikh, A.J.** (2003) Reconstructing the historical riverine landscape of the Puget Lowland. In: *Restoration of Puget Sound Rivers*, (eds., Montgomery, D., Bolton, S., Booth, D., and Wall, L.) University of Washington Press, Seattle, 79-128.

Collins, B.D., and **Montgomery, D.R**. (in press) The legacy of Pleistocene glaciation and the organization of lowland alluvial process domains in the Puget Sound region. *Geomorphology*.

Coulbourn, W.T., and **Moberly, R**., (1977) Structural evidence of the evolution of fore-arc basins off South America. *Can. J. Earth Sci*., **14**, 102–116.

Davies, T.R., Phillips, C.J., Pearce, A.J. and **Zhang, X.B.** (1992) Debris flow behavior—an integrated overview. *Proc. Chengdu Symp*. *209,* 217-227.

Dawson, S., Smith, D.E., Ruffman, A., and **Shi, S**. (1996). The diatom biostratigraphy of tsunami sediments: examples from recent and middle Holocene events. *Phys. Chem. Earth,* **21**, 87–92.

Dawson, A. G. and **Shi, S.** (2000) Tsunami deposits. *Pure Appl. Geophys.,* **157**, 875-897.

Dawson, A.G., Lockett, P., and **Shi, S**. (2003) Tsunami hazards in Europe. *Environ. Int.,* **30,** 577-585.

Dragovich, J.D., Pringle, P.T., and **Walsh, T.J.** (1994) Extent and geometry of the mid-Holocene Osceola Mudflow in the Puget Lowland—Implications for Holocene sedimentation and paleogeography. *Wash. Geol.*, **22,** 3–26.

del Moral. R. and **Wood, D.M.** (1993) Early Primary succession on the volcano Mount St. Helens. *J. Veg. Sci***., 4**, 223-234.

Deo, J.N. Stone, J. and **Stein, J**. (2004) Building Confidence in Shell: variations in the marine radiocarbon reservoir correction for the Northwest Coast over the past 3,000 years. *Am. Antiquity*, **69**, 771-786.

Ellicott, E. (1881) Shore topography of Port Orchard, Puget Sound, Washington territory. *U.S. Coast and Geodetic Survey*. Access through the Puget Sound River History Project. http://riverhistory.ess.washington.edu/tsheets

Eronen, M., Kankainen, T., and **Tsukada, M.** (1987) Late Holocene sea-level record in a core from the Puget Lowland, Washington. *Quat. Res*., **27**, 147-159.

Frankel, A.D., Carver, D.L., and **Williams, R.A.** (2002) Nonlinear and linear site response and basin effects in Seattle for the M 6.8 Nisqually, Washington, earthquake. *Bull. Seismol. Soc. Am.*, **92**, 2090-2109.

Finnegan, N.J., Pritchard, M.E., Lohman, R.B., and **Lungren, P.R.** (2008) Constraints on surface deformation in the Seattle, WA, urban corridor from satellite radar interferometry time-series analysis. *Geophys. J. Int.* **174**, 29-31.

Garrison-Laney, C. (2003) Subsidence with in the last 600 years at Puget Sound, Washington. Geol. Soc. Am. *Abstracts with Programs*, **35**, 582.

Geist, E.L., and **Parsons, T.** (2006) Probabilistic analysis of tsunami hazards. *Nat. Haz.*, **37**, 277-314.

Gelfenbaum, G. and **Jaffe**, **B**. (2003) Erosion and sedimentation from the 17 July, 1998 Papua New Guinea tsunami. *Pure Appl. Geophys.*, **160**, 1969-1999.

GeoEngineers, Inc. (2006) Channel migration and avulsion potential analyses, Skokomish River Valley Mason County, Washington. *Mason County Public Works Department*, **2221-026-00**, 17 pp.

Genevois, R., Galgaro, A., and **Teccs, P.R.** (2001) Image Analysis for debris flow properties estimation. *Phys. Chem. Earth*, **26**, 623-631.

Gilbert, J.J. (1884) United States Coast & Geodetic Survey Topographic Sheet, Hoodís Canal, Annas Bay, Washington Territory, **T-1560b.** Accessed through the Puget Sound River History Project.

Goff, J., McFadgen, B.G., and **Chagué-Goff, C**. (2004) Sedimentary differences between the 2002 Easter storm and the 15th-century Okoropunga tsunami, southeastern North Island, New Zealand. *Mar. Geol*., **204**, 235-250.

González, F.I., Sherrod, B.L., Atwater, B.F., Frankel, A.P., Palmer, S.P., Holmes, M.L., Karlin, R.E., Jaffe, B.E., Titov, V.V., Mofjeld, H.O., and **Venturato, A.J.** (2003) Puget Sound Tsunami Sources—2002 Workshop Report. In *A contribution to the Inundation Mapping Project of the U.S. National Tsunami Hazard Mitigation Program, NOAA OAR Special Report, NOAA/OAR/PMEL*, 34 pp.

Goodbred, S.L. and **Kuehl, S.A.** (2000) The significance of large sediment supply, active tectonism, and eustasy on margin sequence development: Late Quaternary stratigraphy and evolution of the Ganges-Brahmaputra delta. *Sed. Geol*., **133**, 227-248.

Gower, H.D., Yount, J.C., and **Crosson, R.S.** (1985) Seismotectonic map of the Puget Sound region, Washington. *U.S. Geol. Surv.*, **Map I-1613**.

Haeussler, P. J., and Clark, K.P. (2000) Geologic map of the Wildcat Lake 7.5' Quadrangle Kitsap and Mason counties, Washington, *U.S. Geol. Surv.,* **OFR 00-356**.

Harding, D.J., and **Berghoff, G.S.** (2000) Fault scarp detection beneath dense vegetation cover: airborne LiDAR mapping of the Seattle fault zone, Bainbridge Island, Washington State. *Proceedings of the American Society of Photogrammetry and Remote Sensing Annual Conference*, Washington, D.C.

Haugerud, R.A. (2009) Preliminary geomorphic map of the Kitsap Peninsula, Washington: *U.S. Geol. Surv.,* **OFR 2009-1033**.

Hemphill-Haley, E., (1996) Diatoms as an aid in identifying late-Holocene tsunami deposits. *The Holocene,* **6**, 439-448.

Highland, L.M. (2003) An *account of preliminary landslide damage and losses resulting* from the February 28, 2001, Nisqually, Washington, Earthquake. *U.S. Geol. Surv.,* **OFR 03-211**, 48 pp.

Higman, B., and **Bourgeois, J.** (2008) Deposits of the 1992 Nicaragua tsunami. In: *Tsunamiites Features and Implications*, (eds., Shiki, T.,Tsuji, Y.,Yamazaki, T., and Minoura, K.,), Elsevier, Amsterdam, Netherlands, 81-102.

Holbrook, J. and **Schumm, S.A.** (1999) Geomorphic and sedimentary response of rivers to tectonic deformation: a brief review and critique of a tool for recognizing subtle epeirogenic deformation in modern and ancient settings. *Tectonophysics*, **385**, 286-306.

Holdahl, S.R., Faucher, **F.** and **Dragert, H.** (1989) Contemporary vertical crustal motion in the Pacific Northwest, In: *Slow deformation and transmission of stress in the earth: American Geophysical Union Monograph* (eds. Cohen, S., and Vanicek, P.) **49**, 17-29.

Holzer, T.L. and **Clark, M.M.** (1993) Sand boils without earthquakes, *Geology,* **21**, 873–876.

Horton, B.P., Edwards, R.J., and **Lloyd, J.M.** (1999) Reconstruction of former sea-levels using a foraminiferal-based transfer function. *J. Foraminiferal Res.,*

29, 117–129.

Hyndman, R.D., and **Wang, K.** (1995) The rupture zone of Cascadia great earthquakes from current deformation and the thermal regime, *J. Geophys. Res.,* **100**, 133–154.

Hughes, J.F. (2005) Meters of synchronous Holocene slip on two strands of a fault in the western Puget Sound lowland, Washington. *Eos,* **86**, S51C-1020.

Iverson, R.M. (1997) The physics of debris flows. *Rev. Geophys.,* **35**, 245-296.

Jacoby, G.C., Williams, P.L., and **Buckley, B.M.** (1992) Tree ring correlation between prehistoric landslides and abrupt tectonic events in Seattle, Washington. *Science*, **258**, 1621-1623.

James, T.S., Clague, J.J., Wang, K. and **Hutchinson, I.** (2000) Postglacial rebound at the northern Cascadia subduction zone. *Quat. Sci. Rev*., **19,** 1527-1541.

Jankaew, K., Atwater, B. F., Sawai, Y., Choowong, M., Charoentitirat, T., Martin, M.E., and **Pendergast, A.** (2008) Medieval precursor to the 2004 tsunami in Thailand. *Nature*, **455**, 1228-1231.

Jay, D.A. and **Simenstad, C.A.** (1996) Downstream effects of water withdrawal in a small, high-gradient basin: Erosion and deposition on the Skokomish River delta. *Estuaries*, **19**, 501-517.

Johnston, A.C. and **Schweig, E.S.** (1996) The enigma of the New Madrid Earthquakes of 1811-1812. *Ann. Rev. Earth Planet. Sci*., **24**, 339-384.

Johnson, S. Y., Potter, C.J., Armentrout, J.M., Miller, J.J. Finn, C. and **Weaver, C. S.** (1996) The southern Whidbey Island fault, an active structure in the Puget Lowland, Washington. *Geol. Soc. Am. Bull*., **108**, 334–354.

Johnson, S.Y., Dadisman, S.V., Childs, J.R., and **Stanley, W.D.** (1999) Active tectonics of the Seattle Fault and central Puget Sound, Washington: implications for earthquake hazards. *Geol. Soc. Am. Bull.,* **111**, 1042-1053.

Johnson, S.Y., Blakely, R.J., Stephenson, W.J., Dadisman, S.V., and **Fisher, M.A.** (2004) Active shortening in the Cascadia forearc and implications for seismic hazards of the Puget Lowland. *Tectonics*, **23**, TC1011.

Jovanelly, T.J. (2006) Tsunami origin for an ~1100 year old enigmatic sand sheet in Lynch Cove, Puget Sound, Washington. *Kent State University, Dissertation*, 98 pp.

Jovanelly, T.J., and **Moore, A.L**. (2009) Sedimentological analysis of an ancient

sand sheet of multiple origins at Lynch Cove, Puget Sound, Washington. *J. Coast. Res.,* **25**, 294-304.

Kang, Z., and **Zhang, S.** (1980) A preliminary analysis of the characteristics of debris flow. *Proc. Int. Symp. River Sed*., Engl. Sum., Chinese Society for Hydraulic Engineering, Beijing, China, 225-226.

Karlin, R.E., and **Abella, S.E.B.** (1992) Paleoearthquakes in the Puget Sound region recorded in sediments from Lake Washington, U.S.A. *Science,* **258**, 1617-1620.

Kelsey, H.M., Sherrod, B.L., Nelson, A.R., and **Brocher, T.M.** (2008) Earthquakes generated from bedding plane-parallel reverse faults above an active wedge thrust, Seattle fault zone. *Geol. Soc. Am. Bull*., **120**, 1581–1597.

Kim, W., Sheets, B.A. and **Paola, C.** (2010) Steering of experimental channels by lateral basin tilting. *Basin Res.*, **22**, 286-301.

Kobayashi, K. (1995) Role of subducted lithospheric slab in uplift and subsidence of the northwestern Pacific margins. *Marine Geol*., **127**, 119–144.

Komatsubara, J., Fujiwara, O., Takada, K., Sawai, Y., Than Tin Aung, and **Kamataki, T**. (2008) Historical tsunamis and storms recorded in a coastal lowland, Shizuoka Prefecture, along the Pacific Coast of Japan. *Sedimentology*, **55**, 1703-1716.

Koshimura, S., Mofjeld, H.O., Gonzalez, F.I., and **Moore, A.L.** (2002) Modeling the 1100 bp paleotsunami in Puget Sound, Washington. *Geophys. Res. Lett.*, **29**, 1948, doi: 10.1029/2002GL015170.

Kozloff, E. (1983) *Seashore Life of the Northern Pacific Coast, An Illustrated Guide to Northern California, Oregon, Washington & British Columbia*. University of Washington Press, Seattle, Wa., 370 pp.

Kramer, S.L (2009) Evaluation of liquefaction hazards in Washington State. *Washington Department of Transportation Report* **WA-RD 668.1**, 328 pp.

Karel, P., and **Liberty, L.M.** (2008) The western extension of the Seattle fault: new insights from seismic reflection data. *Eos,* **89.,** T21B-1951.

Lajoie, K.R. (1986) Coastal tectonics. In: Active tectonics: Impact on society: National Academy Press, Studies in Geophysics, 95–124.

LeVeque R.J., and **George D.L.** (2008). High resolution finite volume methods for the shallow water equations with bathymetry and dry states. *Adv. Numer. Mod.*, **10**, 43-73.

LeVeque, R.L., George. D.L. and **Berger, M.J.** (in press) Tsunami modeling with adaptively refined finite volume methods. *Acta Numerica* **20**.

Liberty, L.M., and **Pratt, T.L.** (2008) Structure of the eastern Seattle fault zone, Washington State: New insights from seismic reflection data, *Bull. Seismol. Soc. Am.,* **98**, 1681–1695.

Logan, R.L. Schuster, R.L., Pringle, P., Walsh, T., and **Palmer, S.P.** (1998) Radiocarbon ages of probable coseismic features from the Olympic Peninsula and Lake Sammamish, Washington. *J. Wash. Geol.*, **26**, 59-67.

Long, A.J. and **Shennan, I.** (1998) Models of rapid relative sea-level change in Washington and Oregon, USA. *The Holocene,* **8**, 129-142.

Lowe, D.R. (1975) Water escape structures in coarse-grained sediment. *Sedimentology*, **22**, 157-204.

Ludwin, R.S., Weaver, C.S. and **Crosson, R.S.** (1991) Seismicity of Washington and Oregon. In: *Neotectonics of North America*. (eds. Slemmons, D., Engdahl, E., and Blackwell, D.) *Geol. Soc. Am.,* 77-98.

MacInnes, B.T., Bourgeois, J., Pinegina, T.K., and **Kravchunovskaya, E.A.** (2009) Tsunami geomorphology: Erosion and deposition from the 15 November 2006 Kuril Island tsunami. *Geology,* **37**, 995-998.

MacInnes, B.T., Weiss, R., Bourgeois, J., and **Pinegina, T.K.** (2010) Slip distribution of the 1952 Kamchatka great earthquake based on near-field tsunami deposits and historical records. *Bull. Seismol. Soc. Am*., **100**, 1695-1709.

Major, J.J. (1997) Depositional processes in large-scale debris-flow experiments, *J. Geol*., **105,** 345–366.

Martin, M.E., Weiss, R., Bourgeois, J., Pinegina, T., Houston, H., and **Titov, V.** (2008) Combining constraints from tsunami modeling and sedimentology to untangle the 1969 Ozernoi and 1971 Kamchatskii tsunamis. *Geophys. Res. Lett.*, **35**. L01610, doi:10.1029/2007GL032349.

Mathewes, R.W. and **Clague**, **J.J.** (1994) Detection of large prehistoric earthquakes in the Pacific Northwest by microfossil analysis. *Science*, **264**, 688-691.

Matsumoto, D., Naruse, H., Fujino, S., **Surphawajruksakul, A., Jarupongsakul, T., Sakakura, N.,** and **Murayama, M.** (2008) Truncated flame structures within a deposit of the Indian Ocean Tsunami: evidence of syn-sedimentary deformation. *Sedimentology*, **55**, 1559-1570.

Mazzotti, S., Dragert, H., Hyndman, R.D., Miller, M.M., and **Henton, J.A.** (2002) GPS deformation in a region of high crustal seismicity: N. Cascadia forearc: *Earth Planet. Sci. Lett.*, **198**, 41–48.

McCaffrey, R., Qamar, A., King, R.W., Wells, R.E., Khazaradze, G., Williams, C.A., Stevens, C.W., Vollick, J.J., and **Zwick, P.C**. (2007) Fault locking, block rotation and crustal deformation in the Pacific Northwest: *Geophys. J. Int*., **169**, 1315–1340.

McCaffrey, W. Kneller, B., Peakall, J., Capart, H., Young, D.-L., and **Zech, Y**. (2009) Dam-break induced debris flow. In: *Particulate gravity currents*, (eds., McCaffrey, W.m Kneller, B., and Peakall, J.) Blackwell Publishing Ltd., Oxford, 149-158.

McCalpin, J.P., ed. (2009) *Paleoseismology*, 2nd edition. Academic Press, San Diego, 629 pp.

Meyers, R.A., Smith, D.G., Jol, H.M., and **Peterson, C.D.** (1996) Evidence for eight great earthquake-subsidence events detected with ground penetrating radar, Willapa Barrier, Washington. *Geology*, **24**, 99-102.

Minard, J.P. (1985) Geological map of the Marysville quadrangle, Snohomish County, Washington. *U.S. Geol. Surv.*, **MF-1743**.

Mitchell, C.E., Vincent, P., Weldon, R.J., and **Richards, M.A.** (1994) Present-day vertical deformation of the Cascadia margin, Pacific Northwest, United States. *J. Geophys. Res.,* **99**, 257-278.

Mofjeld, H.O., Venturato, A.J., Titov, V.V., Gonzalez, F.I., and **Newman, J.C.** (2002) Tidal datum distributions in Puget Sound, Washington, based on a tidal model. *NOAA Tech. Memo.* **OAR PMEL-122,** 35 pp**.**

Moore, A.L. (1994) Evidence for a tsunami in Puget Sound ~1000 years ago. *University of Washington, Unpublished Master's paper*, 37 pp.

Morton, R.A., Gelfenbaum, G., and **Jaffe, B.E.** (2007) Physical criteria for distinguishing sandy tsunami and storm deposits using modern examples. *Sed. Geol.,* **200**, 184-207.

Murty, T.S. (1977) Seismic sea waves: tsunamis. *Bull. Fish. Res. Board Can.,* **198**, 337 pp.

Nanson, G.C. (1980), Point bar and floodplain formation of the meandering Beatton River, northeastern British Columbia, Canada. *Sedimentology*, **27**, 3–29.

Nelson, A.R., Johnson, S. Y., Kelsey, H.M., Wells. R.E., Sherrod, B.L., Pezzopane, S.K., Bradley, L., Koehler, R.D., and **Bucknam, R.C.** (2003) Late Holocene earthquakes on the Toe Jam Hill fault, Seattle fault zone, Bainbridge Island, Washington. *Geol. Soc. Am. Bull.*, **115**, 1368–1403.

Nisqually Clearinghouse (accessed 29 March 2010) http://www.ce.washington.edu/~nisqually/index.html

Obermeier, S.F. (1989) The New Madrid earthquakes; An engineering-geologic interpretation of relict liquefaction features. *U.S. Geol. Surv.,* **Professional Paper 1336-B**, 114 pp.

Obermeier, S.F. (1996) Use of liquefaction-induced features for paleoseismic analysis- An overview of how seismic liquefaction features can be distinguished from other features and how their regional distribution and properties of source sediment can be used to infer the location and strength of Holocene paleo-earthquakes. *Engin. Geol.*, **44**, 1-76.

Obermeier, S.F. and **Dickenson, S.E.** (2000) Liquefaction evidence for the strength of ground motions resulting from late Holocene Cascadia subduction earthquakes, with emphasis on the event of 1700 AD. *Bull. Seismol. Soc. Am.*, **90**, 876-896.

Okada, R. (1985). Surface deformation due to shear and tensile faults in a half-space. *Bull. Seismol. Soc. Am*., **75**, 1135-1154.

Ota, Y., Odagiri, S., Sasaki, H., and **Mukoyama, S.** (2006) Late Holocene deformation as deduced from the former shoreline height of marine terraces above the Seattle fault zone, Washington State. *Jishin*, **58**, 385-399.

Pan, W., Wang, S., and **Cai, S**. (2010) Numerical simulations of the coastal effects of tsunami waves caused by the 1993 Hokkaido-Nansei-Oki earthquake. *Chinese J. Ocean. Lim*., **28**, 1029-1039.

Paris R., Lavigne F., Wassmer P., and **Sartohadi J.** (2007) Coastal sedimentation associated with the December 26, 2004 tsunami in Lhok Nga, west Banda Aceh (Sumatra, Indonesia). *Mar. Geol.* **238**, 93-106.

Pierson, T.C. and **Scott, K.M.** (1985) Downstream dilution of a lahar: Transition from debris flow to hyperconcentrated streamflow, *Water Resour. Res*., **21**, 1511–1524.

Pinegina, T.K., Bourgeois, J., Bazanova, L.I., Melekestsev, I.V., and **Braitseva, O.A. (**2003) A millennial-scale record of Holocene tsunamis on the Kronotsky Bay coast, Kamchatka, Russia: *Quat. Res.*, **59**, 36-47.

Polenz, M., Alldritt, K., Hehemann, N.J. Sarikhan, I.Y., and **Logan, R.L**. (2009) Geologic Map of the Belfair 7.5-minute Quadrangle, Mason, Kitsap, and Pierce Counties. *Washington State Department of Natural Resources,* **OFR 2009-7**.

Polenz, M., Czajkowski, J., Legorreta, G., Contreras, T., Miller, B., Martin, M.E., Logan, R.L., Carson, R.J., Johnson, C.N., Skov, R.H., Mahan, S., and **Cohan, C.R.** (2010) Geologic Map of the Skokomish Valley and Union 7.5-minute Quadrangles, Mason County. *Washington State Department of Natural Resources Open File Report,* **2010-3**.

Pratt, T.L., Johnson, S.Y., Potter, C.J., Stephenson, W.J., and **Finn, C.A.** (1997) Seismic reflection images beneath Puget Sound, western Washington State; The Puget Lowland thrust sheet hypothesis. *J. Geophys. Res.,* **102**, 469–489.

Prunier, C.S. (1998) Holocene faulting and landsliding in Lake Sammamish related to the Seattle fault. *University of Nevada Reno, Master's Thesis,* 166 pp.

Puget Sound LiDAR Consortium (2005) PSLC 2002 - Bare Earth LiDAR DEM raster digital data, www.pugetsoundlidar.org

Puget Sound River History Project (Accessed 9 December 2010) Skokomish River Areal Photographs. http://riverhistory.ess.washington.edu/ims/

Rahmstorf, S. (2007) A semi-empirical approach to projecting future sea-level rise. *Science*, **315**, 368-370.

Reimer, P.J., Baillie, M.G.L., Bard, E., Bayliss, A., Beck, J.W., Blackwell, P.G., Bronk Ramsey , C., Buck, C.E., Burr, G.S., Edwards, R.L., Friedrich, M., Grootes, P.M., Guilderson, T.P., Hajdas, I., Heaton, T.J., Hogg, A.G., Hughen, K.A., Kaiser, K.F., Kromer, B., McCormac, F.G., Manning, S.W., Reimer, R.W., Richards, D.A., Southon, J.R., Talamo, S., Turney, C.S.M., van der Plicht, J. and **Weyhenmeyer, C.E.** (2009) INTCAL 09 and MARINE09 Radiocarbon age calibration curves, 0-50,000 years Cal BP. *Radiocarbon*, **51**, 1111-1150.

Reinhart, M.A. (1991) Sedimentological analysis of postulated tsunami generated deposits from Cascadia great-subduction earthquakes along southern coastal Washington. *University of Washington, Unpublished Masters paper*, 132 pp.

Reilinger, R. and **Adams, J.** (1982) Geodetic evidence for active landward tilting of the Oregon and Washington coastal ranges: *Geophys. Res. Lett*., **9**, 401-403.

Sarikhan, I., Walsh, T., and **Cakir, R.,** (2007) Morphology of the Alderwood landslide; a probable origin for tsunami in Lynch Cove, Puget Sound, Washington. *Geol. Soc. Am., Cordilleran Section - 103rd Annual Meeting*. 18-5.

Saucier, R.T. (1989) Evidence for episodic sand-blow activity during the 1811-12 New Madrid (Missouri) earthquake series, *Geology* **17**, 103-106.

Sawai, Y., Horton, B.P. and **Nagumo**, **T.** (2004a) Diatom-based elevation transfer function along the Pacific coast of eastern Hokkaido, northern Japan -an aid in paleo-seismic study along the coasts near Kurile subduction zone. *Quat. Sci. Rev.* **23**, 2467-2483.

Sawai, Y., Satake, K., Kamataki, T., Nasu, H., Shishikura, M., Atwater, B.F., Horton, B.P. Kelsey, H.K., Nagumo, T., Yamaguchi, M. (2004b) Transient uplift after a 17th-century earthquake along the Kuril Subduction Zone. *Science,* **306**, 1918.

Sawai, Y., Takanobu, K., Shihsikua, M., Nasu, H., Okamura, Y., **Satake, K., Thompson, K. H., Matsumoto, D., Fujii, Y., Komatsubura, J.,** and **Aung, T. T.** (2009), Aperiodic recurrence of geologically recorded tsunamis during the past 5500 years in eastern Hokkaido, Japan, *J. Geophys. Res.*, **114,** doi:10.1029/2007JB005503.

Scott, K.M. (1988) Origins, behavior, and sedimentology of lahars and lahar-runout flows in the Toutle-Cowlitz system. *U.S. Geol. Surv.,* **Professional Paper 1447-A**, 1-74.

Scott, K.M., Pringle, P.T., and **Vallane, J.W**. (1995) Sedimentology, behavior, and hazard of debris flows at Mount Rainier, Washington. *U.S. Geol. Surv.,* **OFR 90-385**, 106 pp.

Schuster, R.L., Logan, R.L., and **Pringle, P.T. (**1992) Prehistoric rock avalanches in the Olympic Mountains, Washington: *Science*, **258**, 1620–1621.

Shennan, I., Long, A.J., Rutherford, M.M., Green, F.M., Innes, J.B., Lloyd, J.M., Zong, Y., and **Walker, K.J.** (1996) Tidal marsh stratigraphy, sea-level change and large earthquakes, I: A 5000 year record in Washington, U.S.A. *Quat. Sci. Rev*., **15**, 1023–1059.

Seed, H. (1979) Soil liquefaction and cyclic mobility evaluation for level round during earthquakes. *J. Geotech. Engin. Div.-ASCE,* **105**, 201-255.

Seed, H.B. and **Idriss, L.M.** (1982) *Ground Motions and Soil Liquefaction during Earthquakes*, Earthquake Engineering Research Institute, Berkeley, Ca, 134 pp.

Sherrod, B.L. (1999) Gradient analysis of diatom assemblages in a Puget Sound salt marsh—Can such assemblages be used for quantitative paleoecological reconstructions? *Palaeogeography, Palaeoclimatology, Palaeoecology*, **149**, 213–226.

Sherrod, B.L. (2001) Evidence for earthquake-induced subsidence about 1100 yr ago in coastal marshes of southern Puget Sound, Washington. *Geol. Soc. Am. Bull.*, **113**, 1299-1311.

Sherrod, B.L. (2002) Late Quaternary surface rupture along the Seattle fault zone near Bellevue, Washington. *Eos*, **83**, S21C-12.

Sherrod, B.L., Brocher, T.M., Weaver, C.S., Bucknam, R.C., Blakely, R.J., Kelsey, H.M., Nelson, A.R., and **Haugerud, R.** (2004) Holocene fault scarps near Tacoma, Washington, USA. *Geology*, **32**, 9-12.

Shipman, H. (1989) Vertical Land Movements in Coastal Washington: Implications for Sea Level Change. Shorelands and Coastal Zone Management Program, Washington State Department of Ecology, 41 pp.

Shipman, H. (2001) Coastal landsliding on Puget Sound: A review of landslides occurring between 1996 and 1999. Washington State Department of Ecology, Report #**01-06-019**, 101 pp.

Sims, J.D. and **C.D. Garvin** (1995). Recurrent liquefaction at Soda Lake, California, induced by the 1989 Loma Prieta earthquake, and 1990 and 1991 aftershocks: Implications for paleoseismicity studies, *Bull. Seismol. Soc. Am.* **85**, 51-65.

Smith, G.R., Montgomery, D.R., and Peterson, N.P., Crowley, B., and **Goedert, J.** (2007) Spawning sockeye salmon fossils in Pleistocene of Skokomish Valley, Washington, *Quat. Res.,* **68**, 227-238.

Stover, S.C. and **Montgomery, D.R.** (2001) Channel change and flooding, Skokomish River, Washington. *J. Hydrology*, **243**, 272-286.

Switzer, A.D. Pucillo, K., Haredy, R.A., Jones B.G., and **Bryant E.A.** (2005) Sea level, storm, or tsunami: Enigmatic sand sheet deposits in a sheltered coastal embayment from southeastern New South Wales, Australia. *J. Coast. Res.*, **21**, 655-663.

Tabor, R.W., and **Cady, W.M**. (1978a) The structure of the Olympic Mountains, Washington—Analysis of a subduction zone. *U.S. Geol. Surv.,* **Professional Paper 1033**, 25 pp.

Tabor, R.W., and **Cady, W.M.** (1978b) Geologic map of the Olympic Peninsula, Washington. *U.S. Geol. Surv.,* **MIS I-994**.

Takada, K., and **Atwater, B.F.** (2004) Evidence for liquefaction identified in peeled slices of Holocene deposits along the lower Columbia River, Washington. *Bull.*

Seismol. Soc. Am., **94**, 550-575.

Takahashi, T. (1981) Debris flow. *Annu. Rev. Fluid Mech*., ***13*****,** 57–77.

Taylor, M. and **Stone, G.W.** (1996) Beach ridges: a review. *J. Coast. Res.* **12**, 612-621.

Ter Braak, C.J.F. (1987–1992) CANOCO — a FORTRAN program for Canonical Community Ordination. Microcomputer Power, Ithaca, New York, USA.

ten Brink, U.S., Song, J., and **Bucknam, R.C**. (2006) Rupture models for the A.D. 900-930 Seattle fault earthquake from uplifted shorelines, *Geology*, **34**, 585-588.

Titov V.V, and **Synolakis C.E.** (1997) Extreme inundation flows during the Hokkaido-Nansei-Oki tsunami. *Geophys. Res. Lett.*, **24**, 315-318.

Titus, J.H., Titus, P.J. and **del Moral, R.** (1998) Wetland development in primary and secondary successional substrates fourteen years after the eruption of Mount St. Helens, Washington, USA. *Northwest Sci.,* **73**, 186-204.

Thorsen, G.W. (1989) Landslide provinces in Washington. *Engin. Geol. Washington.* **78,** 71-89.

Thorson, R.M. (1980) Ice-sheet glaciation of the Puget Lowland, Washington, during the Vashon Stade (Late Pleistocene). *Quat. Res*., **13**, 303-321.

Thorson, R.M. (1989) Glacio-isostatic response of the Puget Sound area, Washington. *Geo. Soc. Am. Bull*., **101**, 1163-1174.

Tuttle, M., Law, K.T., Seeber, L., and **Jacob, K.** (1990) Liquefaction and ground failure induced by the 1988 Saguenay, Quebec, earthquake. *Can. Geotec. J.,* **27**, 580-589.

Tuttle, M.P. (1999) Late Holocene earthquakes and their implications for earthquake potential of the New Madrid seismic zone, central United States. *University of Maryland Dissertation* 250 pp.

Tuttle, M.P. (2001) The use of liquefaction features in paleoseismology: Lessons learned in the New Madrid seismic zone, central United States, *J. Seismol.*, **5**, 361-380.

Tuttle, M.P., and **Schweig, E.S.** (1996) Recognizing and dating prehistoric liquefaction features: Lessons learned in the New Madrid seismic zone, central United States. *J. Geophys. Res.*, **101,** 6171-6178.

Tuttle, M.P., **Schweig, E.S., Sims, J.D., Lafferty, R.H., Wolf, L.W.,** and **Haynes, M.L.** (2002) The earthquake potential of the New Madrid seismic zone, *Bull. Seismol. Soc. Am.*, **92**, 2080-2089.

Tuttle, M. P., Ruffman, A., Anderson, T., and **Jeter, H.** (2004) Distinguishing tsunami from storm deposits in eastern North America; the 1929 Grand Banks tsunami versus the 1991 Halloween storm. *Seismol. Res. Lett.*, **75**, 117-131.

Varnes, D.J. (1978) Slope movement types and processes. In: R.L. Schuster and R.J. Kfizek (Editors), *Trans. Res. Board Special Rep.,* **176**, 11-33.

Venturato, A., Arcas, D., Titov, V., Mofjeld, H., Chamberlin, C., and **González, F.** (2007) Tacoma, Washington, Tsunami Hazard Mapping Project: modeling tsunami inundation from Tacoma and Seattle fault earthquakes. *NOAA Technical Memorandum OAR PMEL*, **132**, 27 pp.

Verdonck, D. (2006) Contemporary vertical crustal deformation in Cascadia. *Tectonophysics*. **417**, 221-230.

Walsh, T.J., Combellick, R.A., and **Black, G.L.,** (1995) Liquefaction features from a subduction zone earthquake: Preserved examples from the 1964 Alaska earthquake. *Washington Division of Geology and Earth Resources,* **Report of Investigations 32**, 80 pp.

Wang, C., Wong, A., Dreger, D.S., and **Manga, M.** (2006) Liquefaction limits during earthquakes and underground explosions: implications on ground motion attenuation. *Bull. Seismol. Soc. Am*., **96**, 355–363.

Washington Economic Steering Committee (WESC) (1996) Impacts of Climate change on Washington's economy. *Washington State Department of Ecology*, **07-01-010**, 25 pp.

Wells, R.E., Weaver, C.S., and **Blakely, R.J**., (1998) Forearc migration in Cascadia and its neotectonic significance: *Geology*, **26**, 759–762.

Whistler, J.E., Atwater, B.F., and **Montgomery, D.R.** (2002) Holocene liquefaction near the Seattle fault at the Issaquah Creek delta. *Eos*, S22B-1036.

Williams, H.F.L. and **Roberts, M.C.** (1989) Holocene sea-level change and delta growth—Fraser River delta, British Columbia. *Can. J. Earth Sci.,* **26,** 1657-1666.

Williams, H.F.L., and **Hutchinson, I.** (2000) Stratigraphic and microfossil evidence for late Holocene tsunamis at Swantown Marsh, Whidbey Island, Washington. *Quat. Res.*, **54**, 218-227.

Williams, H.F.L., Hutchinson, I., and **Nelson, A.R.** (2005) Multiple sources for late-Holocene tsunamis at Discovery Bay, Washington State, USA. *The Holocene*, **15**, 60-73.

Wilson, J.R., Bartholomew, J.R., and **Carson, R.J.** (1979) Late Quaternary faults and their relationship to tectonism in the Olympic Peninsula, Washington. *Geology*, **7**, 235-239.

Witter, R.C., Givler, R.W., and **Carson, R.J.** (2008) Two post-glacial earthquakes on the Saddle Mountain West fault, southeastern Olympic Peninsula, Washington. *Bull. Seismol. Soc. Am.*, **98,** 2894–2917.

Wood, S. H., Wurts, C., Lane, T., Ballenger, N., Shaleen, **M.,** and **Totorica, D.** (1985) Hydrologic effects, in The Borah Peak, Idaho Earthquake of October 23, 1983. *Earthquake Spectra***, 2**, 127-150.

Xie, X. and **Heller, P.L.** (2009) Plate tectonics and basin subsidence history. *Geol. Soc. Am. Bull.***, 121**, 55-64.

Zehfuss, **P.H**., (2005) Distal records of sandy Holocene lahars from Mount Rainier, Washington. *University of Washington Dissertation*, 141 pp.

Appendix 1 Lynch Cove GPS points for field sites and stratigraphic information

Date	Site	Latitude	Longitude	core or outcrop	sand thickness in cm, ls =landslide	dike y=yes	peat thickness in cm	peat/peat contact s=sharp, g=gradational	Grain size in paleomud flat s=sand, m=mud, si=silt
6-May-08	184	47.44234	-122.84449	outcrop	50		52		
6-May-08	185	47.443	-122.84387	outcrop	42		68		
6-May-08	186	47.43653	-122.84373	outcrop	0		69		
6-May-08	187	47.43701	-122.84234	outcrop	0		?		
6-Aug-08	238	47.445083	-122.840583	outcrop	16		55		
6-Aug-08	239	47.444889	-122.843500	outcrop	45		20		
6-Aug-08	240	47.441778	-122.849111	core	25		150		
6-Aug-08	241	47.439722	-122.839417	outcrop	0		10		
6-Aug-08	242	47.440056	-122.839972	outcrop	0		90		
6-Aug-08	243	47.441750	-122.849667	outcrop	15		?		
26-Aug-08	285	47.437611	-122.841556	outcrop	10		?		
26-Aug-08	286	47.438306	-122.843417	outcrop	20		100		
26-Aug-08	288	47.437778	-122.843750	outcrop	13	y	100		
26-Aug-08	289	47.439111	-122.838833	outcrop	ls		10		
27-Aug-08	288b	47.437833	-122.843750	outcrop	35		100		
27-Aug-08	286b	47.438250	-122.843417	outcrop	25		100		
27-Aug-08	291	47.438111	-122.843028	outcrop	12		100		
4-Jan-09	335	47.437639	-122.841472	outcrop	29.5		35	s	sm
4-Jan-09	335 b	47.437639	-122.841500	outcrop	27		37	s	sm
9-Apr-09	341	47.436583	-122.842861	outcrop	6	y	60	g	si m
9-Apr-09	343	47.436333	-122.842806	outcrop	10	y	51	s	m
9-Apr-09	344	47.436222	-122.842889	outcrop	18		84	s	m
9-Apr-09	345	47.435778	-122.841972	outcrop	0		47		m fs
9-Apr-09	346	47.435722	-122.841750	outcrop	0		32		m fs
9-Apr-09	347	47.435306	-122.842194	outcrop	0		57		si m
9-Apr-09	348	47.435083	-122.842417	outcrop	0		75		m
9-Apr-09	349	47.434778	-122.842583	outcrop	0		83		m
9-Apr-09	350	47.434444	-122.842778	outcrop	0		78	g	m
9-Apr-09	351	47.434111	-122.843194	outcrop	0		65	g	si m
9-Apr-09	352	47.434028	-122.842861	outcrop	0		80	g	m
9-Apr-09	353	47.434472	-122.842472	outcrop	0		80	g	m
9-Apr-09	354	47.434667	-122.842028	outcrop	0		70	g	m
9-Apr-09	355	47.435083	-122.841722	outcrop	0		76	g	si m
9-Apr-09	356	47.435222	-122.843861	outcrop	?		137	g	m
9-Apr-09	357			outcrop	?				
13-Apr-09	364	47.440556	-122.841778	outcrop	0		40	s	m
13-Apr-09	365	47.440639	-122.842167	outcrop	0		49	s	m

Appendix 1 continued

Date	Site	Latitude	Longitude	core or outcrop	sand thickness in cm, ls =landslide	dike y=yes	peat thickness in cm	peat/peat contact s=sharp, g=gradational	Grain size in paleomud flat s=sand, m=mud, si=silt
13-Apr-09	366	47.441028	-122.842694	outcrop	21		46	s	m
13-Apr-09	367	47.441083	-122.842833	outcrop	0		63	s	m
13-Apr-09	368	47.440972	-122.842667	outcrop	33		31	s	m
13-Apr-09	369	47.441306	-122.843639	outcrop	0		60	s	m fs
13-Apr-09	369 - 3	47.441306	-122.843639	outcrop	0		44		fs m
13-Apr-09	369 + 7	47.441306	-122.843639	outcrop	0		45		m
13-Apr-09	370	47.441389	-122.844139	outcrop	0		48		s m
13-Apr-09	371	47.441583	-122.844222	outcrop	0		93		m
13-Apr-09	372	47.441556	-122.845750	outcrop	0		89	g	
13-Apr-09	373	47.441139	-122.845889	outcrop	0		77	g	sm
13-Apr-09	374	47.441028	-122.845944	outcrop	8		74	g	sm
13-Apr-09	375	47.440722	-122.846278	outcrop	37		46	s	si m
14-Apr-09	376	47.437500	-122.840417	core	0		10		g
14-Apr-09	377	47.437306	-122.840639	core	ls		10		g
14-Apr-09	378	47.437000	-122.841528	core	ls		14		g
14-Apr-09	379	47.437028	-122.841750	core	ls		11		sm
14-Apr-09	380	47.437500	-122.840972	core	ls		13		g s
14-Apr-09	381	47.434778	-122.841056	core	ls		20		gm
14-Apr-09	382	47.437861	-122.840556	core	ls		18		
14-Apr-09	383	47.437917	-122.840750	core	ls		12		
14-Apr-09	384	47.439194	-122.839639	core	y		10		
14-Apr-09	385	47.439361	-122.839639	core	y		24		
14-Apr-09	386	47.441778	-122.841417	core	7		0		m
14-Apr-09	387	47.441944	-122.841306	core	7		0		m
14-Apr-09	388	47.442083	-122.841222	core	0		0		si m
14-Apr-09	389	47.442306	-122.841028	core	0		0		m si
14-Apr-09	390	47.442556	-122.840861	core	0		0		m
14-Apr-09	391	47.442917	-122.840639	core	0		0		m si
14-Apr-09	392	47.443056	-122.841000	core	0		0		m si
14-Apr-09	393	47.443000	-122.842361	core	0		0		m si
14-Apr-09	394	47.443056	-122.842556	core	0		0		sm
14-Apr-09	395	47.443139	-122.842806	core	20		15		si m
14-Apr-09	396	47.440472	-122.846194	outcrop	25		80	s	si m
28-Apr-09	404	47.437222	-122.841806	outcrop	0		43	g	si m
28-Apr-09	405	47.437111	-122.843639	outcrop	0		50	g	gsm
28-Apr-09	406	47.437028	-122.842333	outcrop	21	y	52	g	m

Appendix 1 continued

Date	Site	Latitude	Longitude	core or outcrop	sand thickness in cm, ls =landslide	dike y=yes	peat thickness in cm	peat/peat contact s=sharp, g=gradational	Grain size in paleomud flat s=sand, m=mud, si=silt
28-Apr-09	406b	47.437028	-122.842361	outcrop	45	y	30	s	m
28-Apr-09	407	47.436944	-122.842444	outcrop	10	y	52	g	m
28-Apr-09	408	47.434333	-122.842167	outcrop	0		57	g	si m
28-Apr-09	409	47.434000	-122.842056	outcrop	0		50		si m
28-Apr-09	410	47.433833	-122.842194	outcrop	0		76	g	si m
28-Apr-09	411	47.433222	-122.842250	outcrop	0		45		m
28-Apr-09	412	47.433250	-122.841972	outcrop	0	?	19		
28-Apr-09	413	47.432972	-122.842472	outcrop	0		42	g	ms
28-Apr-09	414	47.433167	-122.842972	outcrop	0		61		si m
28-Apr-09	415	47.433333	-122.842972	outcrop	0		69	s	m
28-Apr-09	416	47.433500	-122.843222	outcrop	0		85	g	si m
28-Apr-09	417	47.435194	-122.844167	outcrop	16		136	g	m
28-Apr-09	418	47.435250	-122.844306	outcrop	n/a		0		
28-Apr-09	419	47.435639	-122.843667	outcrop	6		136	g	si m
28-Apr-09	420	47.435667	-122.844306	outcrop	0		180	s	m
28-Apr-09	421	47.436000	-122.844500	outcrop	0		130		m
28-Apr-09	422	47.435917	-122.844028	outcrop	0		145	g	sm
28-Apr-09	423	47.436917	-122.843917	outcrop	0		85	g	sm
28-Apr-09	424	47.436944	-122.844111	outcrop	12		128	s	m
28-Apr-09	425	47.437056	-122.844639	outcrop	1		10		m
28-Apr-09	426	47.437056	-122.844444	outcrop	0		133		m
28-Apr-09	427	47.437556	-122.844861	outcrop	22	y	80		m
19-May-09	431	47.439361	-122.841528	core					
19-May-09	432	47.439417	-122.841556	outcrop	20		33	g	m
25-May-09	433	47.449917	-122.842222	core	0		34	g	sm
25-May-09	434	47.432528	-122.843528	outcrop	0		44	s	sm
25-May-09	435	47.432667	-122.843833	outcrop			42	g	m
25-May-09	436	47.432639	-122.844278	outcrop	0		40	s	m
25-May-09	437	47.432444	-122.844528	outcrop	0		41	g	m
25-May-09	438	47.432417	-122.845000	outcrop	0		34		m
25-May-09	439	47.432250	-122.845306	outcrop	0		39		m
25-May-09	440	47.43221	-122.84575	outcrop	0		45		sm
25-May-09	441	47.4321	-122.84611	outcrop	0		29	g	m
25-May-09	442	47.43193	-122.84624	outcrop	9	y	28		m
25-May-09	443	47.43203	-122.84649	outcrop	20		30	s	si m
25-May-09	444	47.43215	-122.84675	outcrop	25		50	s	si m

Appendix 1 continued

Date	Site	Latitude	Longitude	core or outcrop	sand thickness in cm, ls =landslide	dike y=yes	peat thickness in cm	peat/peat contact s=sharp, g=gradational	Grain size in paleomud flat s=sand, m=mud, si=silt
25-May-09	446	47.43301	-122.84669	core	25		63	g	m
25-May-09	447	47.43312	-122.84653	core	0		67		m
25-May-09	448	47.43321	-122.84638	core	0		85		m
25-May-09	449	47.43349	-122.84639	core	0		122	g	m
25-May-09	450	47.43347	-122.84674	core	0		87	g	m
25-May-09	451	47.43343	-122.84719	core	0		62	g	si m
25-May-09	452	47.43347	-122.84673	core	0		33		g
25-May-09	453	47.43334	-122.84483	core	0		2		g
25-May-09	454	47.43324	-122.84483	core	0		91	g	m
25-May-09	455	47.4331	-122.84517	outcrop	0		84	g	m
25-May-09	456	47.43302	-122.84539	outcrop	0		71	g	m
27-May-09	457	47.44075	-122.85622	core	0		122	s	m fs
27-May-09	458	47.44082	-122.85677	core	0		82	s	sm
27-May-09	459	47.4409	-122.85709	core	0		32		m s
27-May-09	460	47.44109	-122.85737	core	0		21	g	m fs
27-May-09	461	47.44118	-122.85763	core	0		56		sm
27-May-09	462	47.44136	-122.85784	core	0		81		m si
27-May-09	463	47.44047	-122.85503	core	0		21		g
27-May-09	464	47.44073	-122.85383	core	0		101	g	ms
27-May-09	465	47.44117	-122.85332	core	0		149	g	ms
27-May-09	466	47.44143	-122.85281	core	0		127	g	ms
27-May-09	467	47.44169	-122.85199	outcrop	0		120	g	sm
27-May-09	468	47.44202	-122.85177	outcrop	10		74	g	mfs
27-May-09	469	47.44207	-122.85178	outcrop	12		85	g	sm
27-May-09	470	47.4422	-122.85172	outcrop	6		82	g	m fs
29-May-09	471	47.43962	-122.83924	core	45		25		g
29-May-09	472	47.43947	-122.83886	core	41		25		g
29-May-09	473	47.4394	-122.83864	core	ls		0		g
29-May-09	474	47.43912	-122.83857	core	LS		30		g
29-May-09	475	47.43917	-122.83856	core	ls		30		g
29-May-09	476	47.43726	-122.83886	core	0		29		g
29-May-09	477	47.43725	-122.83926	core	1		42		ms
29-May-09	478	47.43763	-122.84389	outcrop	1		132		m fs
29-May-09	479	47.43766	-122.84416	outcrop	34		103		m fs
29-May-09	480	47.43779	-122.84445	outcrop	0		85		m fs
29-May-09	481	47.43775	-122.84479	outcrop	5	y	112		m

Appendix 1 continued

Date	Site	Latitude	Longitude	core or outcrop	sand thickness in cm, ls =landslide	dike y=yes	peat thickness in cm	peat/peat contact s=sharp, g=gradational	Grain size in paleomud flat s=sand, m=mud, si=silt
29-May-09	482	47.43772	-122.84503	outcrop	1	y	130	g	m
29-May-09	483	47.43702	-122.84569	outcrop	29		165		m
29-May-09	484	47.43761	-122.84597	outcrop	31	y	169	g	m
29-May-09	485	47.43791	-122.84631	outcrop	0		187	g	m
29-May-09	486	47.43823	-122.84659	outcrop	0	y	130	g	si m
29-May-09	487	47.43872	-122.84748	outcrop	0		121	g	m si
29-May-09	488	47.43903	-122.84749	outcrop	0		78	g	m si
29-May-09	489	47.43964	-122.84792	outcrop	0		89	g	m si
29-May-09	490	47.43982	-122.8475	outcrop	0		95	g	m si
29-May-09	491	47.44018	-122.84741	outcrop	13		77	m	m fs
29-May-09	492	47.44009	-122.84679	outcrop	27		87		m si
29-May-09	493	47.43985	-122.84653	outcrop	0		106		s I m
8-Jun-09	495	47.43947	-122.84194	outcrop	31	y	33	s	m
8-Jun-09	496	47.43966	-122.84228	outcrop	11		51	s	m
8-Jun-09	497	47.43969	-122.84218	outcrop	9	y	64	g	m
8-Jun-09	498	47.43976	-122.84210	outcrop	7		55		m si
8-Jun-09	499	47.43995	-122.84224	outcrop	5		53	g	m
8-Jun-09	500	47.4395	-122.84230	outcrop	6		63		m
8-Jun-09	501	47.43923	-122.84248	outcrop	7		65		si m
8-Jun-09	502	47.43922	-122.84289	outcrop	31	y	63	g	m
8-Jun-09	503	47.43879	-122.84319	outcrop	23	y	114	s	m
8-Jun-09	504	47.43875	-122.84335	outcrop	8	y	91	s	m
8-Jun-09	505	47.43821	-122.84251	outcrop	8	y	69	s	si m
8-Jun-09	532	47 26 19.2	-122 50 35.9	outcrop	19		109	s	si m
8-Jun-09	538	47.43849	-122.84250	core/endli	0		45		m
8-Jun-09	539	47.43849	-122.84250	core/midline			0		m
8-Jun-09	540	47.44141	-122.83938	gouge cor	48		0		m
8-Jun-09	541	47.44177	-122.83926	gouge cor	36		0		m
8-Jun-09	542	47.44192	-122.83907	gouge cor	58		0		sm
8-Jun-09	543	47.44235	-122.83901	gouge cor	83		0		sm
8-Jun-09	544	47.44257	-122.83903	gouge cor	86		0		sm
8-Jun-09	545	47.44279	-122.83895	gouge cor	30		0		sm
8-Jun-09	546	47.44301	-122.83887	gouge cor	40		0		ms
8-Jun-09	547	47.44332	-122.83879	gouge cor	40		0		ms
8-Jun-09	548	47.44329	-122.83956	gouge cor	40		0		ms
8-Jun-09	549	47.44307	-122.83968	gouge cor	65		0		ms

Appendix 1 continued

Date	Site	Latitude	Longitude	core or outcrop	sand thickness in cm, ls =landslide	dike y=yes	peat thickness in cm	peat/peat contact s=sharp, g=gradational	Grain size in paleomud flat s=sand, m=mud, si=silt
8-Jun-09	550	47.44283	-122.83981	gouge cor	40		0		ms
8-Jun-09	551	47.44257	-122.83992	gouge cor	10		0		ms
8-Jun-09	552	47.44235	-122.84006	gouge cor	30		0		ms
8-Jun-09	553	47.44209	-122.84021	gouge cor	21		0		sm
8-Jun-09	554	47.44181	-122.84033	gouge cor	20		0		m
8-Jun-09	555	47.44165	-122.84038	gouge cor	27		0		m
8-Jun-09	556	47.44197	-122.83975	gouge cor	65		0		m
8-Jun-09	557	47.43902	-122.8441	outcrop			128		
8-Jun-09	558	47.34902	-122.84410	excavation	8		164	164	m
8-Jun-09	560	47.43768	-122.84074	end of profile					
20-Aug-09	1180	47.43706	-122.84227	ex	10	y	107		
25-Aug-09	1190	47.43691	-122.84251	outcrop	11	y	52		
25-Aug-09	1200	47.43655	-122.84289	outcrop		y	100		
3-Sep-09	1250	47.43925	-122.84280	outcrop					
3-Sep-09	1260	47.43892	-122.84317	outcrop					
19-Sep-09	1310	47.43937	-122.84132	outcrop	18				
19-Sep-09	1320	47.43991	-122.84342	outcrop	0		73	s	si m
19-Sep-09	1330	47.43991	-122.84347	outcrop	0		91	s	si m
19-Sep-09	1340A	47.43947	-122.84365	outcrop	0		79	s	si m
19-Sep-09	1340b	48.43947	-122.84366	outcrop	0		72	S	SI M
19-Sep-09	1350	47.43939	-122.84391	outcrop	0		83	s	si m
19-Sep-09	1370	47.43954	-122.84419	outcrop	0		57	s	si m
19-Sep-09	1380	47.43944	-122.84447	outcrop	0		68	s	si m

Appendix 2: Gorst GPS locations and stratigraphic information

Date	Site	Latitude	Longitude	Core/ Excavation	Tsunami thickness in cm	Total sand thickness in cm
25-Apr-07	Gorst 1/ 162	47.52678	-122.69600	Excavation		
25-Apr-07	Gorst 2	47.526444	-122.692000	Excavation		
6-Jun-07	core 2/ 163	47.526444	-122.692000	core		
6-Jun-07	Gorst 6 163 or 5	47.526444	-122.692000	core		
6-Jun-07	core 3/165	47.526361	-122.692111	core		
6-Jun-07	core 4	47.525833	-122.691861	core		
6-Jun-07	core 5			core		
14-Jun-07	pt 167	47.526861	-122.698111	core		
14-Jun-07	g2-0/517	48.273611	-125.346667	Excavation		10
14-Jun-07	g2-1			Excavation		10
14-Jun-07	g2-2			Excavation		18
14-Jun-07	g2-3	47.527361	-122.695583	Excavation	8.5	19
14-Jun-07	g2-4			Excavation		
14-Jun-07	g2-5			Excavation		
14-Jun-07	g3	48.261944	-125.378056	Excavation	11	50
14-Jun-07	otto 1			Excavation		
14-Jun-07	otto 2			Excavation		
9-Aug-07	g2-6	47.527306	-122.695611	Excavation	6	30
9-Aug-07	g2-7	47.527278	-122.684514	Excavation	4	50
9-Aug-07	g2-5			Excavation		35
9-Aug-07	g2-8			Excavation		20
9-Aug-07	g2-9			Excavation		50
9-Aug-07	g2-10			Excavation		30
9-Aug-07	g2-11			Excavation		35
9-Aug-07	g2-12			Excavation		24
9-Aug-07	g2-13			Excavation		10
9-Aug-07	g2-14			Excavation		8
9-Aug-07	g2-15			Excavation		3
10-Aug-07	g2-16			Excavation		4
10-Aug-07	g3-b	47.52683	-122.69703	Excavation	2	50
10-Aug-07	g3-c	48.52683	-122.69702	Excavation	1	44
23-Aug-07	169/core 1	47.527333	-122.692611	core		150
25-Aug-07	core2 trimarsh	47.527250	-122.692556	core		57
25-Aug-07	core14 trimarsh/171?	47.526750	-122.692417	core		115
25-Aug-07	core8 trimarsh/171	47.526528	-122.692889	core		60
25-Aug-07	core 19 trimarsh/172	47.526889	-122.691944	ex/core		75
25-Aug-07	core 24			core	6	69

Appendix 2 continued

Date	Site	Latitude	Longitude	Core/ Excavation	Tsunami thickness in cm	Total sand thickness in cm
27-Aug-07	pt174	47.528111	-122.682556	Excavation		0
27-Aug-07	pt 175	47.528444	-122.682111	Excavation		0
27-Aug-07	pt176	47.528306	-122.681306	core		0
27-Aug-07	pt177	47.528222	-122.682000	core		0
27-Aug-07	pt178	47.528111	-122.682278	core		0
28-Aug-07	pt179 core 1	47.525861	-122.691833	core		20
28-Aug-07	pt179 core2			core		36
28-Aug-07	pt 179 core3			core		32
1-Sep-07	180-1	47.526611	-122.697861	core		50
1-Sep-07	181	47.526667	-122.698444	core		27
3-Sep-07	1-Jul			Excavation		20
23-Nov-07	G2			Excavation		
3-Apr-08				ross creek		
22-Aug-08				Pit for Radiocarbon		
2-Oct-08	trench 1			Trenches		25
3-Oct-08	trench 2	47.530485	-122.708573	Trenches		30
3-Oct-08	trench3			Trenches		50
8-Nov-10	310	47.530722	-122.696472	data point		
8-Nov-10	311	47.530111	-122.684556	Excavation		
8-Nov-10	312	47.529611	-122.685444	Excavation		
8-Nov-10	313	47.528972	-122.688306	Excavation		
8-Nov-10	314	47.529056	-122.693500	Excavation		
8-Nov-10	316	47.528333	-122.699500	Excavation		
10-Apr-09	358	47.525861	-122.692139	Excavation	eroded?	
10-Apr-09	359	47.526861	-122.695583	Excavation		
10-Apr-09	360	47.526750	-122.695583	Excavation		
10-Apr-09	361	47.526528	-122.695500	Excavation	eroded?	
10-Apr-09	362	47.526583	-122.695611	Excavation		
10-Apr-09	363	47.526472	-122.696417	Excavation		18
29-Apr-09	428	47.526222	-122.692306	vibra core		
29-Apr-09	429	47.526556	-122.692472	vibra core		
29-Apr-09	430	47.527000	-122.692667	vibra core		
26-Aug-08	290	47.530056	-122.708194	core		
10-Jun-09	506	47.52655	-122.69600	outcrop		
10-Jun-09	507	47.52629	-122.69642	outcrop		22
10-Jun-09	G1/508	47.52678	-122.69600	Excavation		
10-Jun-09	509	47.52685	-122.69701	upstream of g3		

Appendix 2 continued

Date	Site	Latitude	Longitude	Core/ Excavation	Tsunami thickness in cm	Total sand thickness in cm
10-Jun-09	510	47.52683	-122.69701	G3		
10-Jun-09	517	47.52725	-122.69588	G2		
10-Jun-09	511	47.52709	-122.69650	Excavation		
10-Jun-09	514	47.52704	-122.69635	Excavation		
10-Jun-09	515	47.52683	-122.69615	Excavation		
10-Jun-09	516	47.52668	-122.69633	Excavation		
10-Jun-09	512	47.52699	-122.69606	Excavation		
10-Jun-09	518	47.52685	-122.69298	Excavation		
14-Sep-09	1270	47.52586	-122.69186	core/profile end		
14-Sep-09	pt 20			core		
14-Sep-09	pt 22			core		
14-Sep-09	pt 24			core		
14-Sep-09	1280	47.52599	-122.69109	core		0
14-Sep-09	1290	47.52591	-122.69117	core		0
14-Sep-09	1330	47.52576	-122.69127	core		17
28-Sep-09	1410	47.53124	-122.71583	Excavation		0
28-Sep-09	1420	47.52964	-122.71875	Excavation		30
28-Sep-09	1430	47.52971	-122.71917	Excavation		94
28-Sep-09	1440	47.52988	-122.71923	Excavation		35
28-Sep-09	1450	47.52995	-122.71935	core		0
28-Sep-09	1460	47.52999	-122.71933	core		0
28-Sep-09	1470	47.53012	-122.71934	core		0
28-Sep-09	1480	47.53012	-122.71989	core		0
28-Sep-09	1490	47.53035	-122.71930	core		0
28-Sep-09	1500	47.53096	-122.71713	core/profile end		0
28-Sep-09	1510	47.52803	-122.70661	Excavation		0
28-Sep-09	1520	47.52733	-122.70621	core		80
4-May-10	1650	47.53316	-122.72072	glacial outcrops		
4-May-10	1660	47.53277	-122.72255	glacial outcrops		
4-May-10	1670	47.53277	-122.72637	glacial outcrops		
4-May-10	1680	47.53172	-122.73297	glacial outcrops		
4-May-10	1690	47.53055	-122.73513	glacial outcrops		
4-May-10	1700	47.52901	-122.73708	glacial outcrops		
4-May-10	1710	47.52825	-122.73719	glacial outcrops		
4-May-10	1720	47.52739	-122.74	glacial outcrops		
4-May-10	1730	47.52739	-122.742	glacial outcrops		
4-May-10	1740	47.5266	-122.742	glacial outcrops		
4-May-10	1750	47.52617	-122.74305	glacial outcrops		

Appendix 2 continued

Date	Site	Latitude	Longitude	Core/ Excavation	Tsunami thickness in cm	Total sand thickness in cm
4-May-10	1760	47.52572	-122.74391	glacial outcrops		
4-May-10	1770	47.52438	-122.74563	glacial outcrops		
4-May-10	1780	47.52564	-122.74042	glacial outcrops		
4-May-10	1790	47.52713	-122.73491	glacial outcrops		
4-May-10	1800	47.52717	-122.7271	glacial outcrops		
8-May-10	1810	47.52507	-122.70793	sewer excavations		
28-Jun-10	2010	47.52663	-122.70251	sewer excavations		
28-Jun-10	2020	47.52954	-122.697	sewer excavations		
29-Jun-10	2030	47.52958	-122.69833	sewer excavations		
29-Jun-10	2040	47.52675	-122.70383	sewer excavations		
7-Jul-10	2140	47.52692	-122.69618	Excavation		3
7-Jul-10	2150	47.5301	-122.69599	sewer excavations		
7-Jul-10	2160	47.52524	-122.7023	sewer excavations		
12-Jul-10	2170	47.53038	-122.69587	sewer excavations		
12-Jul-10	2180	47.52528	-122.70324	sewer excavations		

Appendix 3: Skokomish GPS locations and stratigraphic information

Date	Site	Latitude	Longitude	Core/ excavation	Total peat thickness in cm	Basal unit	Notes
9-Jul-08	198	47.341183	-123.139733	excavation			
9-Jul-08	199	47.340067	-123.141883	excavation	94	pebbly sand	
9-Jul-08	205	47.341972	-123.146083	excavation	37	mud	
9-Jul-08	208	47.346083	-123.148222	excavation	62	pebbly mud	
9-Jul-08	209	47.346611	-123.146028	excavation			
9-Jul-08	20x	47.342694	-123.142806	excavation	84	sandy mud	vented sand
9-Jul-08	218	47.342333	-123.140667	excavation			
9-Jul-08	219	47.342194	-123.141139	core	66		
9-Jul-08	220	47.341500	-123.141889	core	53	sandy mud	
9-Jul-08	221	47.341500	-123.143250	core	54	mud	
14-Jul-08	222	47.343333	-123.146361	excavation	121	pebbly sand	
14-Jul-08	223	47.342611	-123.146750	excavation	71	pebbly mud	
14-Jul-08	224	47.341806	-123.147944	excavation	99	muddy sand	
14-Jul-08	225	47.341639	-123.147472	excavation	89	muddy sand	
14-Jul-08	226	47.340889	-123.145861	excavation	104	pebbly mud	
14-Jul-08	227	47.340611	-123.144417	excavation	142	sandy mud	
14-Jul-08	228	47.339222	-123.144972	excavation		muddy sand	
8-Aug-08	244	47.338778	-123.142500	excavation	62	muddy sand	
8-Aug-08	245	47.338389	-123.142556	excavation	22	pebbly mud	
8-Aug-08	245b	47.338361	-123.142528	excavation	5	pebbly mud	
8-Aug-08	246	47.337694	-123.142528	excavation	10	pebbly mud	
8-Aug-08	246b	47.337667	-123.142528	core	90	pebbly mud	
8-Aug-08	247	47.337500	-123.143167	core	134	sandy mud	
8-Aug-08	248	47.337139	-123.143611	core	70	sandy mud	
8-Aug-08	249	47.336583	-123.144139	core	63	mud	
8-Aug-08	250	47.336583	-123.146000	core	65	mud	
8-Aug-08	251	47.336583	-123.146000	core	50	mud	
8-Aug-08	252	47.336611	-123.146583	core	30	mud	
8-Aug-08	253	47.336000	-123.146861	core	150	mud	
8-Aug-08	254	47.335222	-123.147417	core	100+	mud	
8-Aug-08	255			core	30	mud	
12-Aug-10	256	47.339694	-123.142389	excavation	87	pebble mud	
12-Aug-10	257	47.339333	-123.142444	excavation	40	mud	
12-Aug-10	258	47.339083	-123.142444	excavation	70	sand	
12-Aug-10	259	47.338639	-123.142111	excavation	50	sand	
12-Aug-10	260	47.339333	-123.143528	excavation	25	mud	
12-Aug-10	261	47.340278	-123.145833	core	70	sandy mud	
12-Aug-10	262	47.340556	-123.145556	core	30	sandy mud	

Appendix 3 continued

Date	Site	Latitude	Longitude	Core/ excavation	Total peat thickness in cm	Basal unit	Notes
12-Aug-10	262 b	47.340583	-123.145583	core	18	mud	
12-Aug-10	263	47.341028	-123.145444	excavation	22	mud	vented sand
12-Aug-10	264	47.341389	-123.145250	excavation	45	mud	
12-Aug-10	265	47.341833	-123.145000	excavation	45	mud	
12-Aug-10	266	47.342333	-123.144639	excavation	65	mud	
12-Aug-10	267	47.344972	-123.149222	excavation	12	sandy mud	
12-Aug-10	268	47.344861	-123.150361	core	31	mud	
12-Aug-10	269	47.344806	-123.150611	core	35	pebbly mud	
12-Aug-10	270	47.345500	-123.150944	core	5	pebbly mud	
12-Aug-10	271	47.346333	-123.151167	core	51	mud	
19-Aug-08	276	47.349167	-123.150194				
19-Aug-08	277	47.348667	-123.150944	excavation		pebbles	
19-Aug-08	278	47.348000	-123.149944	excavation		pebbles	
19-Aug-08	279	47.347361	-123.150472	excavation		pebbles	
19-Aug-08	280	47.346000	-123.150333	excavation		pebbles	
11-Jun-09	519	47.3405	-123.14394	core	35	mud	
11-Jun-09	520	47.34085	-123.14378	cre	22	mud	
11-Jun-09	521	47.34139	-123.14374	core	43	mud	
11-Jun-09	522	47.34126	-123.14417	core	35	mud	
11-Jun-09	523	47.34081	-123.1444	core	23	mud	
11-Jun-09	524	47.3405	-123.14356	core	13	mud	
11-Jun-09	525	47.34028	-123.14401	core	68	mud	
11-Jun-09	526	47.33944	-123.14444	core	10	mud	
11-Jun-09	pt 2			core	15	mud	
11-Jun-09	pt 4			core	60	mud	
11-Jun-09	pt 8			core	30	mud	
11-Jun-09	pt 13			core	58	mud	
11-Jun-09	pt 14			core	28	mud	
11-Jun-09	pt 16			core	44	mud	
11-Jun-09	pt 21			core	75	mud	
11-Jun-09	pt 25			core	106	mud	
11-Jun-09	527/pt 28	47.34244	-123.14154	core	109	sandy mud	
11-Jun-09	528	47 20 32.8	-123 08 35.5	excavation	57	sandy mud	
11-Jun-09	529	47 20 33.6	-123 08 34.2	excavation	61	sandy mud	
15-Sep-09		47.34691667	-123.1616944	excavation			
30-Mar-10	1590	47.34734	-123.14603	end of profile		mud	
30-Mar-10	1600	47.34601	-123.14794	excavation	54	pebbles	
30-Mar-10	1610	47.3456	-123.14854	excavation	68	pebbles	

Appendix 3 continued

Date	Site	Latitude	Longitude	Core/ excavation	Total peat thickness in cm	Basal unit	Notes
30-Mar-10	1630	47.34526	-123.14899	excavation	85	pebbles	
30-Mar-10	1640	47.3449	-123.14985	ex, end of profi	25	gravel	
21-Jun-10	1900	47.33295	-123.1466	core	177	gravel	
21-Jun-10	1910	47.33246	-123.14722	core	153	gravel	
21-Jun-10	1920	47.33245	-123.14718	core	121	gravel	
21-Jun-10	1930	47.33241	-123.14724	core	145	gravel	
21-Jun-10	1940	47.33263	-123.14744	core	170	gravel	
21-Jun-10	1950	47.33241	-123.14777	core	178	gravel	
21-Jun-10	1960	47.33271	-123.14669	core	188	gravel	
21-Jun-10	1970	47.33314	-123.14675	core	29	gravel	
21-Jun-10	1980	47.32682	-123.13531	core	35	mud	
21-Jun-10	1990	47.32699	-123.13564	core	37	mud	
21-Jun-10	2000	47.32729	-123.1362	core	47	mud	
21-Jun-10	2005	47.33119	-123.153067	4 cores	6	sandy mud	gps from google earth
2-Jul-10	2050	47.32373	-123.15341	core		mud	
2-Jul-10	2060	47.32424	-123.15423	core		mud	
2-Jul-10	2070	47.32467	-123.15489	core		mud	
2-Jul-10	2080	47.32483	-123.15489	core		mud	
2-Jul-10	2090	47.32498	-123.15464	core		mud	
2-Jul-10	2100	47.32525	-123.15449	core		mud	
2-Jul-10	2110	47.32542	-123.15425	core		mud	
2-Jul-10	2120	47.32544	-123.15422	core		mud	
2-Jul-10	2130	47.32558	-123.15396	core		mud	
DNR		47.34875	-123.1583333	core			hood canal school

Appendix 4: Issaquah Creek GPS locations and stratigraphic information

Date	Site	Latitude	Longitude	core/outcrop	sand thickness (cm)	notes
19-Aug-09	1150	47.55781	-122.05976	outcrop		Jon Whistler's big outcrop
19-Aug-09	1160	47.5577	-122.05843	outcrop	9	
19-Aug-09	1170	47.55703	-122.05735	outcrop	72	tree stumps
19-Aug-09	1210	47.55742	-122.05522	outcrop	0	
19-Aug-09	1220	47.55742	-122.05522	outcrop	0	
19-Aug-09	1230	47.55842	-122.06043	outcrop	24	
19-Aug-09	1240	47.5577	-122.05885	outcrop	15	
11-Sep-09	1160-4			outcrop	2	
11-Sep-09	1160-3			outcrop	12	
11-Sep-09	1160-2			outcrop	116	
11-Sep-09	1160-7			outcrop	35	
11-Sep-09	1160-6			outcrop	0	
11-Sep-09	1160-5			outcrop	70	

APPENDIX 7 x-ray defraction of fine-grained sediments

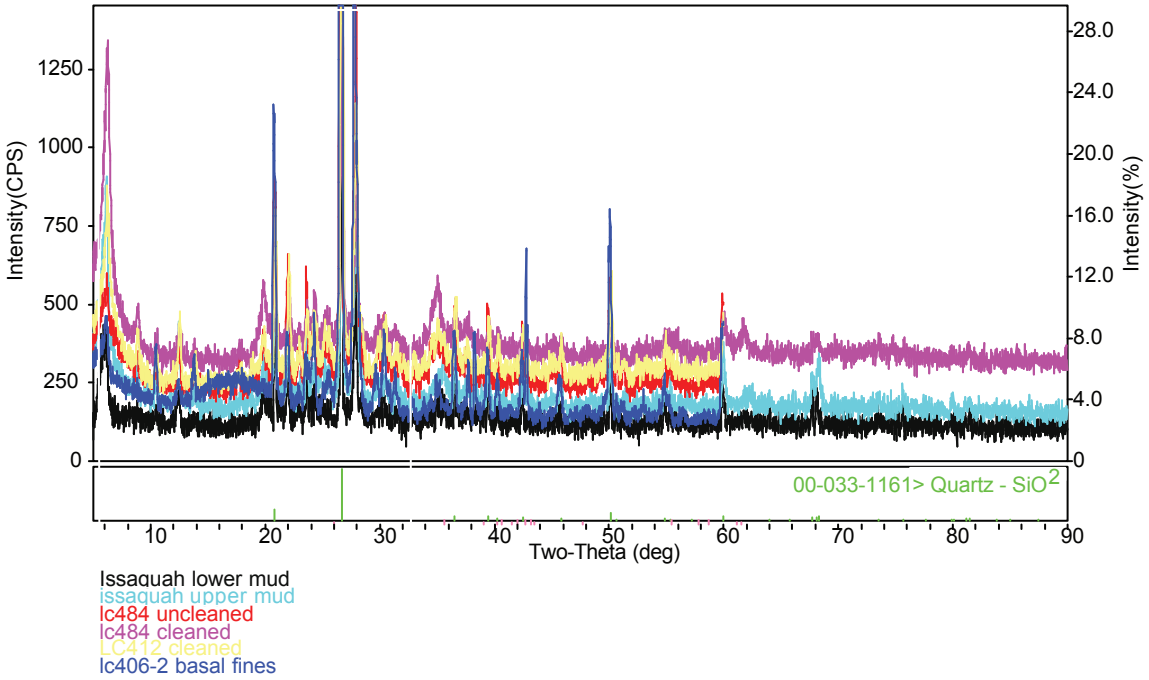

Appendix 1: X-ray defraction of fine grained sediments from chapter 2. Issaquah samples are of the mud above and below the vented sand. LC 484 is a gray intraclast from LynchCove. The cleaned sample was cleaned with 30% hydrogen peroxide dand then rinsed. The uncleaned sample was not processed in any way. LC412 is from the glacial mud outcrop. LC406-2 is the paleomudflat deposit. In all samples the quartz peak obscured less prominant minerals. Other likely minerals present included clays and sheet silicates. The location and relative intensity of quartz is included for reference.

Appendix 6 Hood Canal tsunami simulations

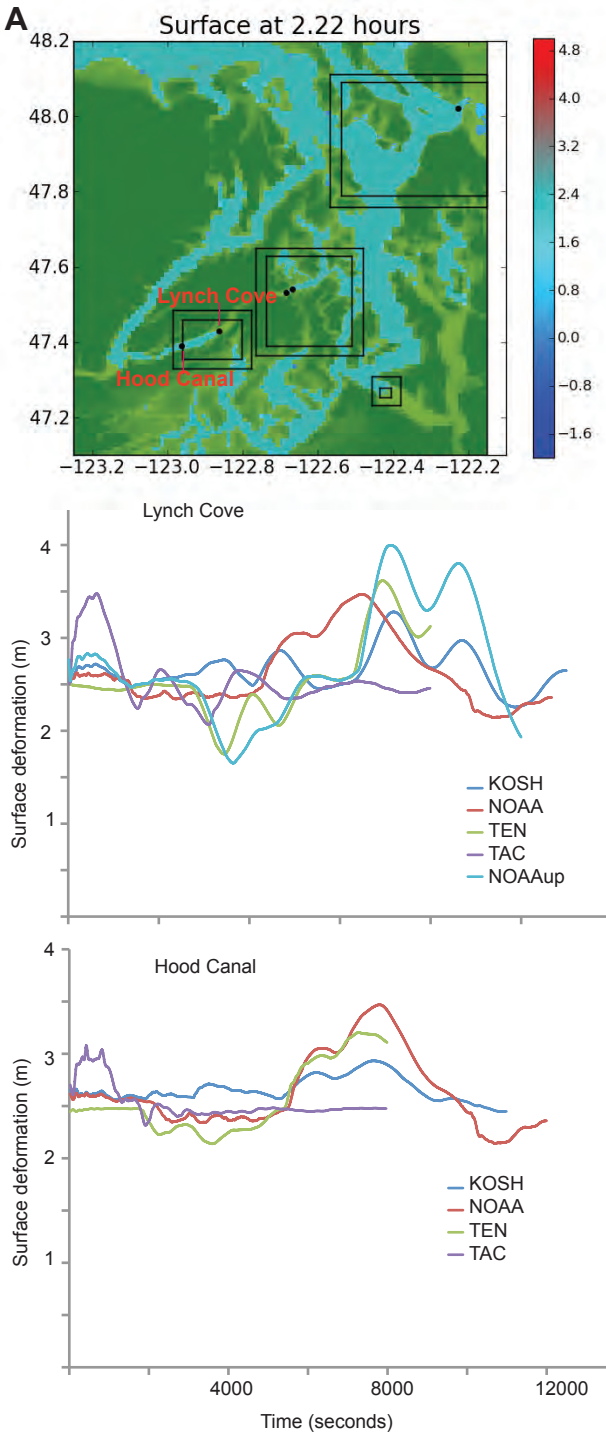

Appendix 6 Simulations of Seattle and Tacoma fault earthquakes generated tsunamis in Hood Canal. Model parameters in chapter 3 all simulations were made at +2.5 m water level, approximately modern high tide. A. Simulation snap shot showind “tide gauge” laocations.Synthetic “tide gauge” records from Hood Canal show Seattle fault earthquake generate ~1 m wave height in Hood Canal. Despite uplift at the terminus of Hood Canal from a Tacoma fault rupture, the simulated tsunami from the Tacoma fault has a wave height of approximately 0.5 m. These simulations support the conclusion from chapter 2 that it is unlikely that a Seattle or Tacoma fault generated tsunami deposited the sand deposit in Lynch Cove. The deposit in Lynch Cove is on average 20 cm thick.

VITA

Maria Elizabeth Martin was born in Tucson, Arizona. She attended Arizona State University and received a Bachelor of Science in Geological Sciences in 2003. She attended the University of Washington for graduate school in Geological Sciences receiving her Master's degree in 2006 and her Doctor of Philosophy in 2011.